Integration of fMRI data in radiosurgery treatment planning of benign pathologies

Carlos Miguel Figueiredo de Carvalho

Medical Physics

Department of Physics and Astronomy

2019

Supervisor

Sofia Silva, PhD, Instituto Português de Oncologia do Porto FG, EPE

Co-supervisor

Sara Pinto, MsC, Instituto Português de Oncologia do Porto FG, EPE

U.PORTO

FACULDADE DE CIÊNCIAS
UNIVERSIDADE DO PORTO

Todas as correções determinadas pelo júri, e só essas, foram efetuadas.

O Presidente do Júri,

Porto, _____/_____/_____

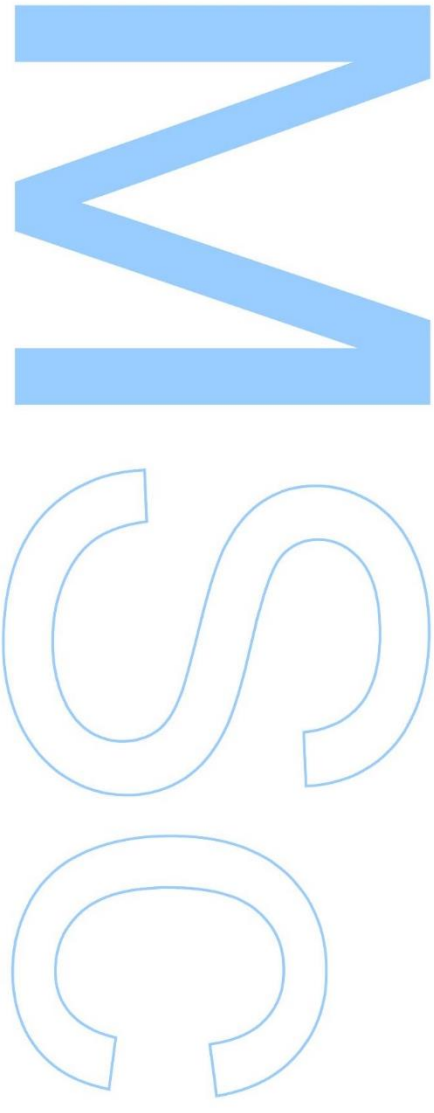

Acknowledgements

Firstly, I would like to thank my supervisor, Professor Sofia Silva, and co-supervisor, Professor Sara Pinto, for their dedication, counseling and availability to help during the course of all of the dissertation.

I am also very grateful of PhD student Firas Ghareeb for his availability and help in the creation of the code for the final image conversion.

I thank dosimetrist Teresa Viterbo and physicist Joana Lencart from the department of Medical Physics of Instituto Português de Oncologia do Porto for their contribution in the creation of all the treatment plans for the patients and volunteers that were analyzed in this dissertation.

I am also very grateful of dosimetrist Mª Fátima Borges for her help in the registration of the converted images onto the CTs in the Eclipse Treatment System.

I would like to thank neuroradiologists Dr. Mavilde Arantes and Dr. Eduarda Carneiro for their availability and help in the analysis and determination of the proper Z-threshold value to be used in the processing of the fMRI data for each patient and volunteer.

I want also to thank the radiology technicians Pedro Conde and Emanuel Machado for their constant availability to perform the MRI and fMRI exams to all the patients and volunteers that participated in this study.

Finally, an enormous thanks to my family for their constant support and patience during the course of the dissertation. They helped me maintain optimistic and believed in me during these long months of work.

Resumo

O objetivo da dissertação presente era a integração da neuroimagem funcional no planeamento de radiocirurgia com LINAC para patologias benignas, tais como meningiomas e adenomas da hipófise, no departamento de radioterapia do Instituto Português de Oncologia do Porto, e tirar conclusões nos seus potenciais benefícios para a conservação de regiões funcionais do cérebro em pacientes de radiocirurgia, bem como a criação de um protocolo com os passos necessários para o processamento da informação da fMRI usando o FSL.

Ao longo da dissertação, três pacientes e quinze voluntários participaram neste estudo. O paradigma selecionado para a fMRI foi uma tarefa motora que consistia no movimento repetitivo de abertura e fecho da mão, direita ou esquerda, dependendo da localização da patologia em questão. Antes da integração da informação da fMRI no processo de planeamento, as imagens foram convertidas usando o *mricron*, processadas com a ferramenta FSL e reconvertidas usando o MATLAB. A informação da fMRI foi então, de seguida, importada para o Eclipse Treatment Planning System e usada na delineação de novos OARs funcionais, subsequentemente usados para optimização.

Apesar de alguns planos de tratamento não terem sido sujeitos a reoptimização, ou cuja optimização não teve impacto na redução de dose pretendida devido à distância dos fOARs delineados à patologia a ser tratada, os novos planos reoptimizados a partir da integração da informação das imagens funcionais exibiram uma redução na dose média nos fOARs sem afetar a viabilidade do tratamento radiocirurgico. Os resultados obtidos no presente estudo estão dentro dos intervalos reportados por outros estudos em tópicos semelhantes.

Foi concluído que a integração de informação BOLD-fMRI no planeamento de tratamento radiocirurgico com LINAC permite uma redução na dose de radiação nos órgãos funcionais em risco, demostrando-se potencialmente benéfico para os pacientes. A simplicidade da integração da informação de neuroimagem funcional no processo de planeamento justifica uma investigação futura na implementação, em novas aplicações em outras patologias e em possíveis melhorias do processo.

Palavras chave: fMRI, BOLD, FSL, Benign pathologies, Radiosurgery, LINAC

Abstract

The purpose of the present dissertation was the integration of functional neuroimaging in LINAC radiosurgery treatment planning for benign pathologies, such as meningiomas and pituitary adenomas, in the radiotherapy department of Instituto Português de Oncologia do Porto and to take conclusions on its potential benefits in the sparing of functional brain regions of radiosurgical patients, as well as the creation of guidelines with all the necessary steps for processing of the fMRI data using FSL.

During the course of the dissertation, three patients and fifteen volunteers participated in this study. The paradigm selected for the fMRI performed was a motor task consisting of repetitive opening and closing movement of the hand, either right or left, depending on the location of the pathology. Before the integration of the fMRI information in the planning process, images were converted using *mricron,* processed with FSL tool and reconverted with MATLAB. The fMRI data was imported into Eclipse Treatment Planning System and used in the delineation of new functional OARs, subsequently used for optimization.

Although some treatment plans were not reoptimized or the reoptimization had no impact on dose reduction due to the distance of the fOARs from the lesion to be treated, the new reoptimized plans created from the integration of the fMRI data exhibited a reduction of mean dose in the fOARs without affecting the viability of the radiosurgical treatment. The obtained results were within the reduction range reported by other studies in similar topics.

It is concluded that the integration of BOLD-fMRI data into LINAC radiosurgical treatment planning allows a reduction in radiation doses to functional organs at risk, proving to be potentially beneficial for the patients. The simplicity of the integration of functional neuroimaging into the planning process justifies further research in implementation, new applications for other pathologies and improvements to the procedure.

Keywords: fMRI, BOLD, FSL, Benign pathologies, Radiosurgery, LINAC

Index

Figure Index

Table Index

Acronym List

BET	Brain Extraction Tool
BOLD	Blood Oxygen Level Dependent
DOF	Degrees of Freedom
EPI	Echo Planar Imaging
FEAT	FMRI Expert Analysis Tool
FID	Free Induction Decay
fMRI	functional Magnetic Resonance Imaging
fOAR	functional Organ at Risk
FOV	Field of View
FWHM	Full Width Half Maximum
GE-EPI	Gradient Echo – Echo Planar Imaging
ID	Identification Number
IR-EPI	Inversion Recovery – Echo Planar Imaging
MRI	Magnetic Resonance Imaging
NMR	Nuclear Magnetic Resonance
OAR	Organ at Risk
RF	Radio Frequency
SE-EPI	Spin Echo – Echo Planar Imaging
SRS	Stereotactic Radiosurgery
SRT	Stereotactic Radiotherapy
TE	Echo Time
TPS	Treatment planning System
TR	Repetition Time

1 – Introduction

1.1- State of the Art

In 1936, Pauling and Coryell[1] observed that the magnetization level of hemoglobin depends on its levels of oxygenation. By subjecting deoxyhemoglobin and oxyhemoglobin to a magnetic field they observed that the prior was strongly attracted by the field and the latter repelled by it. Later, in 1990, the work of Ogawa et al[2] referred for the first time the blood oxygenation level-dependent (BOLD) technique as a contrast technique/agent for magnetic resonance imaging (MRI). Using gradient-echo sequences with high fields, changes on the magnetic susceptibility of the blood were observed, allowing the demonstration of *in vivo* images of rat's brain microvasculature[2].

Functional MRI (fMRI) was first introduced by the works of J.W. Belliveau et al[3] in 1991. Their study used dynamic susceptibility contrast to measure the changes in cerebral blood volume following neural activation caused by visual stimulation, aiming to create a functional magnetic resonance map of human task activation. In 1992, Ogawa et al[4] published a new study demonstrating intrinsic magnetic susceptibility changes in the human brain caused by neuronal activation after visual stimulation using the BOLD contrast technique. In that same year, Kwong KK et al[5] applied the BOLD contrast technique to fMRI, obtaining noninvasive tomographic maps of human brain activity by using motor and visual paradigms and measuring blood oxygenation changes of the brain.

The observations on the studies of fMRI and BOLD technique showed correlation between the magnetic susceptibility observed in the images and neuronal activation. This led to the beginning of multiple studies in the application of fMRI in radiosurgery, a technique first introduced by Lars Leksel[6,7] in 1949 and created as a method for noninvasive destruction of intracranial target volumes with minimization of its effects on the surrounding tissues. In 1996, Thomas Witt et al[8] utilized functional MRI in three patients to identify with precision the localization of important cortical areas associated with decrease of deoxyhemoglobin during a performance task. The reception of radiation on these areas was restricted to reduce the morbidity of the radiosurgery treatment.

Before thinking about the application of the fMRI into radiosurgery treatment planning it was necessary to study the feasibility and repeatability of using fMRI to delineate functional organs at risk (fOARs). In 2006, Roberto Garcia-Alvarez et al[9] studied the variability of motor cortex activations of both hemispheres in fifteen subjects, establishing a margin for the creation of fOARs. In the study, subjects underwent three different fMRI acquisitions, in which they were asked to perform a self-paced finger-thumb motion with alternate hands to acquire data in both hemispheres. Through the analysis of the fMRI data acquired, it was concluded that the activation areas were consistent in volume, shape and location, and it was possible to compute uncertainty margins in order to give a 90% confidence in the delineation of a true fOAR. These margins were determined to be 2.9 mm and 2.2 mm for the right and left primary motor cortex activation, respectively.

In the more recent years, many studies surfaced regarding the feasibility and advantages of the integration of fMRI in radiosurgery. Some authors of those studies are Joseph Stancanello et al[10], Evaggelos Pantelis et al[11], Árpád Kovács et al[12], Alfredo Conti et al[13], Minglei Wang et al[14], Lun Sun et al[15] and De Martin E et al[16]. These studies had the goal of proposing and validating a method that proves feasibility of the integration of fMRI information in the delineation of fOARs in radiosurgery using CyberKnife system to decrease the morbidity associated with the technique. The image processing and statistical analysis of the raw data acquired from the fMRI that the patients were subjected to was performed by software tools such as statistical parametric mapping (SPM99[10] or SPM5[12]), Matlab workstation[14], SPSS[15] (version 17.0; SPSS Inc, Chicago, Illinois) or BrainVoyager QX[15] (Brain Innovation, Maastricht, the Netherlands). Using a treatment planning system (TPS), the resulting image from the fusion of the MR image processed with the CT is utilized to delineate the new fOARs and create new treatment plans with reduced doses given to those regions. The previous studies reported reductions between 12% and 32% in the dose to the functional areas delineated and reductions between 12.5% and 63% in the mean dose to the motor cortex. All these studies commonly concluded that it was feasible and beneficial to incorporate functional MRI in the treatment planning of radiosurgery with CyberKnife system.

The study for this dissertation arises from the rising interest and need of a Radiotherapy department performing routine SRS treatments to integrate the fMRI tool in the pre-treatment planning improvement of SRS and SRT of benign pathologies such as meningiomas and pituitary adenomas. It also aims to fill the literature gap concerning the integration of fMRI in radiosurgery performed with LINAC systems and also to supply a

Radiotherapy department with a customized user guide with explanation of the steps taken and parameters utilized in the processing of the fMRI data with FSL (FMRIB Software Library, Oxford, UK).

1.2 – Dissertation Structure

The present dissertation is divided into nine chapters, along which the study performed will be thoroughly explained and described for a better comprehension of it.

Chapter 2 has a description of the important concepts for this study. For a better understanding of magnetic resonance imaging, its fundamental principles are here succinctly explained. In the same chapter, functional MRI technique along with BOLD technique is explained, for a better comprehension of the functionalities behind this medical imaging technique. Lastly, important concepts for functional image acquisition of this study such as image acquisition sequence and paradigms are also described.

The description of the brain anatomy with identification of the different lobes, their location and functionalities to comprehend the importance of their preservation is made in chapter 3.

For a better understanding of the characteristics of benign pathologies pertinent for this study, a complete chapter (chapter 4) was dedicated to the description of their characteristics and classification.

Another important concept for this study is the radiosurgery technique. In chapter 5 this technique is succinctly described along with the fundamental principles behind it, more specifically about LINAC radiosurgery treatment.

The experimental methodology (chapter 6) contains a detailed description of the volunteers and patients who participated in this study and the paradigm selected for image acquisition. This chapter also briefly describes the image processing steps prior to fMRI data integration into the planning process, including conversion steps, FSL guidelines for image processing and reconversion steps for a better comprehension of what was developed during the course of this dissertation. Lastly, later in this chapter, the integration of fMRI data and the treatment planning process are described in detail for a better understanding of our results.

Chapter 7 reports the experimental results obtained during the study of the treatment plans created for each of the 18 subjects who participated in the study. It exhibits the doses achieved in the treatment plan created with and without the fMRI data integration as well as the differences between them.

In chapter 8, the parameters selected for the conversion and processing of the images are discussed in detail, as well as the analysis of the results obtained and their comparison with the results from other studies on the same topic. Additionally, the limitations encountered in the course of this study in the processing of the images, in the paradigm selected and fMRI data integration procedure are identified and explained. Lastly, perspectives for future research on the topic of this study are described.

In the last chapter (chapter 9), final conclusions about the results obtained and the goal set for this dissertation are presented.

2 – Magnetic Resonance Imaging

In 1946, a technique called Nuclear Magnetic Resonance (NMR) which consisted in the measurement of the absorption and emission of radiofrequency by an atomic nucleus while in the presence of a strong magnetic field, was discovered independently by Bloch et al. and Purcell et al.[17,18]

A few years later, in 1973, Magnetic Resonance Imaging (MRI) was first described by Lauterbur and Mansfield[17,18]. The significant advances, over the past decades, in MRI techniques allowed to explore a whole new field of evaluating regions of neural activity based on focal metabolic changes.[19] Its high spatial resolution and contrast as well as not requiring the use of ionizing radiation during imaging, makes MRI one of the best and most clinically useful technique in the preoperative planning for neurosurgery of brain tumors and other pathologies[20,21,22].

2.1 – Physics principles behind Magnetic Resonance imaging

A fundamental property of nuclei with odd atomic numbers, such as the nucleus of the hydrogen atom that has only has one proton, is that they possess angular momentum ***J***, often called spin.[23]

A magnetic field is created around nuclei with nonzero angular momentum ($J \neq 0$). Physically, this magnetic field is represented by a vector quantity **μ**, called nuclear magnetic dipole or magnetic moment. The relationship between spin angular momentum and magnetic moment is one of the fundamental relationships of particle physics, given by the following equation:

$$\mu = \gamma \mathbf{J} \tag{2.1}$$

where γ is a physical constant known as gyromagnetic ratio. Its value depends on the atomic species; for protons, $\gamma = 42.58\ MHz/T$.[23]

To be able to uniquely define the magnetic moment, its magnitude and orientation must be known. Based on the theory of quantum mechanics, the magnitude of μ is given by:

$$\mu = \gamma \hbar \sqrt{I(I+1)} \tag{2.2}$$

where ħ relates to Planck's constant *h* ($\hbar = h/2\pi$) and I is the nuclear spin quantum number. Nuclei with an even mass number and even charge number have null spin ($I =$

0) while nuclei with an odd charge number and/or odd mass number have nonzero spin ($I \neq 0$).The direction of μ, unlike its constant magnitude, depends on the existence of an external magnetic field. In its absence, its direction will be completely random due to random thermal motion of the nuclei, resulting in null total magnetization of the medium. To activate the macroscopic magnetism of a system, it is necessary to expose it to a strong external magnetic field. Assuming an external magnetic field of strength B_0 applied in the z-direction, the direction of μ aligns with the field and its magnitude is given by the following expression[23]:

$$\mu_z = \lambda m_I \hbar \tag{2.3}$$

where m_I is the magnetic quantum number. For nucleus with nuclear spin of 1/2, m_I takes the values of ±1/2, meaning that μ_z will have two possible orientations in relation to the applied external magnetic field: parallel orientation (↑) if positive m_I or anti-parallel (↓) if negative m_I (Figure 1). Spins in different orientations have different energy of interaction with the external magnetic field. According to quantum theory, that energy is given by:

$$E = -\mu \,.\, \boldsymbol{B}_0 = \, -\mu_z \,.\, B_0 = \, -\gamma \hbar m_I B_0 \tag{2.4}$$

which means for the different spins:

$$\begin{aligned} E\left(m_I = {}^1/_2\right) &= \, -\gamma \hbar B_0/2 \\ E\left(m_I = -{}^1/_2\right) &= \, \gamma \hbar B_0/2 \end{aligned} \tag{2.5}$$

The energy values given by equation (2.5) indicate that the parallel orientation state is the state of lower energy while the anti-parallel orientation state is the state of higher energy. The energy difference between both states is given by:

$$\Delta E = E_\downarrow - E_\uparrow = \gamma \hbar B_0 \tag{2.6}$$

This difference between the energy of the different levels is also known as the Zeeman effect. The population of the different spin states is related to this energy difference through the well-known Boltzmann distribution[23]:

$$\frac{n_\uparrow}{n_\downarrow} = e^{\frac{\Delta E}{KT}} \tag{2.7}$$

where T is the absolute temperature (in kelvin) of the spin system and K is the Boltzmann constant ($k \approx 1{,}38x10^{-23}J/K$).

The sum of all microscopic magnetic moments of a system is denominated as net magnetization vector **M**, described by three components: M_z known as longitudinal magnetization, and M_x and M_y that combine into $\mathbf{M_{xy}}$ known as transverse magnetization. At equilibrium, the longitudinal magnetization reaches its maximum due to a small population difference between the two spin states caused by spins being more likely to take the lower energy state than the higher one, which, even though small, generates an observable macroscopic magnetization in the longitudinal component known as equilibrium magnetization M_0 [23,24]. Since the spins do not rotate in phase, the sum of all the microscopic transverse magnetization of the spins results in a null macroscopic transverse magnetization.
The nuclei will emit magnetic resonance signals (necessary to measure the spin magnetization) when transitioning to equilibrium from an excited state. This excited state is achieved by applying a radiofrequency (RF) pulse with a frequency equal to the natural resonance frequency of the spin system called Larmor frequency (or precession frequency) ω_0, given by the following equation[23]:

$$\omega_0 = \gamma B_0 \tag{2.8}$$

From the expression above we can see that the Larmor frequency is proportional to the applied external magnetization field and will vary with the atomic species used because the value of the gyromagnetic constant is nucleus dependent.[23]

For convenience, a rotating frame is used to facilitate the analysis of the excitation effect of an RF pulse in the spin system. The rotating frame is a spinning axis system whose transverse plane is rotating clock-wise at an angular velocity equal to the Larmor frequency, where the spins appear to be stationary when they rotate at that same frequency[23,24]. The net magnetization vector will have a spiral movement in the direction of the xy plane, with an inclination angle α that depends on the intensity and duration of the RF pulse[8], as seen in Figure 2.

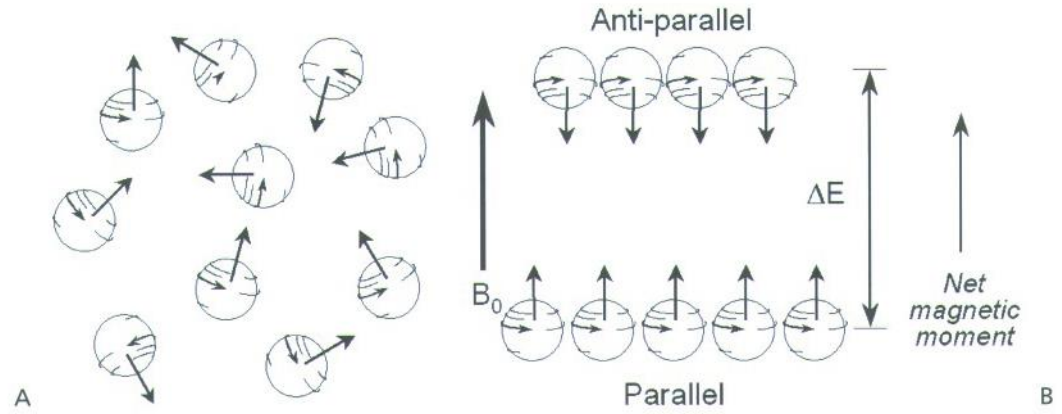

Fig. 1 – A) In the absence of an external magnetic field the spins have random orientation and produces a null total net magnetic moment. B) In the presence of an external magnetic field the spins will align in two possible orientations: parallel and antiparallel according to its magnetic quantum number, resulting in a measurable net magnetic moment (adapted from [24]).

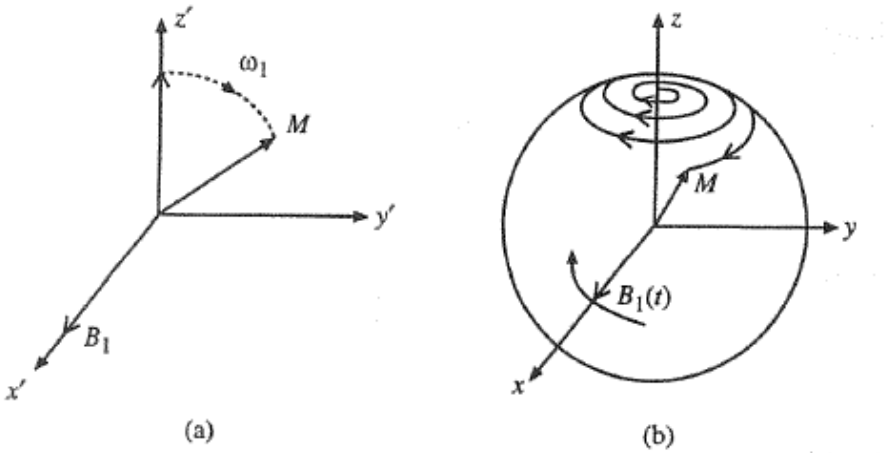

Fig. 2 – Motion of the bulk magnetization vector in the presence of a rotating RF field observed in the (a) rotating frame, and (b) the laboratory frame (adapted from[23]).

As a result of the excitation, the bulk magnetization is tipped away from the direction of $\mathbf{B}_0$ reducing the longitudinal magnetization and creating a measurable transverse magnetization[23]. The transverse magnetization will be maximum when the inclination angle of the RF pulse is 90º and null if the inclination angle is 180º[24].

When the perturbation elicited by the RF pulse finishes, the spin system will return to its equilibrium state. This process is characterized by the recovery of the longitudinal magnetization and the destruction of the transverse magnetization and it is denominated as relaxation[23]. During the relaxation process protons will emit the electromagnetic energy of their excited states in the form of a nuclear magnetic signal known as the free induction decay (FID) signal[24].

2.1.1 – T1 and T2 Relaxation times

Longitudinal relaxation time T1

Longitudinal relaxation consists in returning of the excited magnetization to equilibrium state and releasing the energy of the excited spins into the local tissue. This regrowth of the longitudinal magnetization is also denominated by spin-lattice relaxation and is characterized by the time constant T1, which is the time needed for M_z to recover 63% of its equilibrium value. The recovery of the longitudinal magnetization can be expressed mathematically by[24]:

$$M_z = M_z^0 \left(1 - e^{-\frac{t}{T1}}\right) + M_{z'}(0_+) e^{-\frac{t}{T1}} \tag{2.9}$$

where $M_{z'}(0+)$ is the longitudinal magnetization right after the RF pulse is applied and M_z^0 is the equilibrium value of the longitudinal magnetization, assuming an instantaneous RF pulse.

The time constant T1 depends on multiple parameters such as the magnetic field strength, the physical characteristics of the medium, the presence of proteins or paramagnetic ions, and the nuclei that originated the signal[24].

Transverse relaxation time T2

The transverse relaxation consists in the loss of phase coherence of the individual spins caused by magnetic field variation. This will lead to the destruction of the transverse magnetization, also denominated by spin-spin interaction, and is characterized by the time constant T2, which is the time needed for M_{xy} to decay to 37% of its peak level. The decay of the transverse magnetization can be expressed mathematically by[24]:

$$M_{xy} = M_{xy0} e^{-\frac{t}{T2}} \tag{2.10}$$

where M_{xy0} is the transverse magnetization right after the RF pulse is applied (the peak level of M_{xy}).

The time constant T2, just like T1, also depends on multiple parameters such as the molecular structure of the sample, the magnetic field strength, or the presence of ferromagnetic or paramagnetic objects.

Transverse relaxation time T2*

When a tissue is exposed to a RF pulse, it becomes "magnetized". The ability of a tissue to become magnetized is denominated as magnetic susceptibility. In tissue boundaries we can often see a susceptibility gradient that can cause local inhomogeneities of the magnetic field[25]. Due to these inhomogeneities the spins will suffer a rapid dephasing, accelerating the decay of the FID signal. This decay will be characterized by a new relaxation time T2* translated mathematically by the following expression[25,26]:

$$\frac{1}{T_2^*} = \frac{1}{T_2} + \frac{1}{T_{2_{inhomog}}} \tag{2.11}$$

2.2 – Functional Magnetic Resonance imaging

The technique that allows us to observe neural activity with MRI during specific tasks is called functional magnetic resonance imaging (fMRI). This imaging technique reveals short-term physiological changes associated with active brain function, allowing the identification of the different parts of the brain where those particular mental processes occur, and characterize the patterns of activation associated with those processes. Through the identification of the position of eloquent brain areas related to different intracranial pathologies, fMRI has gained an increasing role in preoperative planning[19,21].

The fMRI technique was first described in the 1980s by John Belliveau[22]. In 1990, the work and studies presented by Ogawa et al[2] introduced a new noninvasive technique for the evaluation of the blood flow in cortical areas that replaces the paramagnetic contrast agents with the blood oxygenation levels. This specific fMRI technique is called blood oxygenation level dependent (BOLD) technique which allows functional images by exploiting the magnetic susceptibility variations produced by the different local concentrations of oxygenated and deoxygenated blood, triggered by neuronal activity. There are different techniques for fMRI but currently the most commonly used is the BOLD technique due to its good spatial resolution and direct correlation to surface anatomy[19,22].

2.2.1 – Blood Oxygenation Level Dependent technique

The BOLD technique exploits properties of cerebral hemodynamics resulting from neuronal activity[19,20,22], such as the magnetic properties of hemoglobin[2,19,22]. When hemoglobin carries oxygen, it is designated as oxyhemoglobin (HbO_2) and it is diamagnetic[1], while when it does not carry oxygen it is designated as deoxyhemoglobin (dHb) and it is paramagnetic[1]. During neuronal activity, local oxygen consumption by neurons increases, leading to a local blood flow increment (called hemodynamic response), that restores the local oxygen level. The hemodynamic response will allow a local oxy-hemoglobin concentration greater than what is needed to provide oxygen to neurons, leading to a reduction of the concentration of deoxyhemoglobin by flushing it away from the capillary bed. The paramagnetic properties of dHb distort the magnetic field and create magnetic field inhomogeneities that lead to a rapid dephasing of excited spins during signal acquisition, resulting in a low MRI signal. When its concentration is reduced, since the HbO_2 diamagnetic properties will not substantially distort the local magnetic field, excited spins dephase slower resulting in a strong MRI signal[19,20,21,22] (Figure 3).

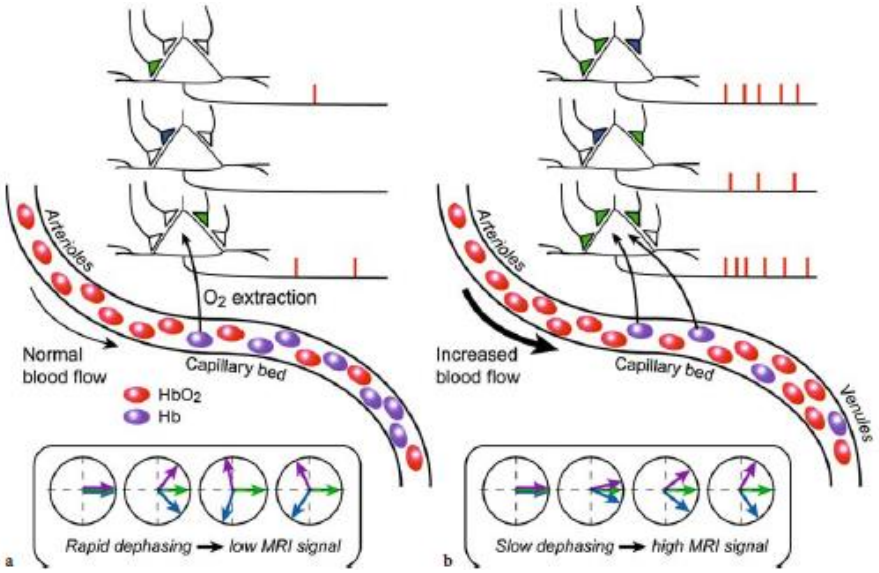

Fig. 3 a) Neural baseline state (resting state) with small HbO2/dHb ratio resulting in low MRI signal. b) Neural activated state with oversupply of HbO2 increasing the HbO2/dHb ratio resulting in high MRI signal (adapted from [22]).

Once the neural activity from the stimulus is over and it returns to the resting state the HbO_2/dHb ratio will return to its small value resulting once again in low MRI signal. The changes in the local HbO_2/dHb ratio and its association to the change in magnetic field homogeneity act as a marker of neural activity[22].

2.3 – Acquisition Sequence

The most utilized image acquisition sequence in fMRI is the Echo-Planar Imaging (EPI). This sequence fills the entire k-space by rapidly changing spatial gradients in a single electromagnetic pulse. Since EPI is fundamentally a spatial encoding scheme, it allows images with different contrast behaviors such as Spin-echo EPI (SE-EPI), Gradient-echo EPI (GE-EPI) and Inversion-Recovery EPI (IR-EPI)[28,29]. The acquisition sequence utilized in this study is GE-EPI, as can be seen in Figure 4.

Echo-planar Imaging has numerous advantages over conventional MR imaging, but it also has some disadvantages. The advantages include reduced imaging time due to its fast acquisition which leads to a good temporal resolution, decreased sensibility to motion artifacts and ability to image rapid physiologic processes of the human body[30]. The disadvantages of EPI are artifacts resulting from imperfections in the magnetic field and geometric distortions due to field inhomogeneities in the boundaries between brain tissues and other nearby tissues or air-filled cavities[28].

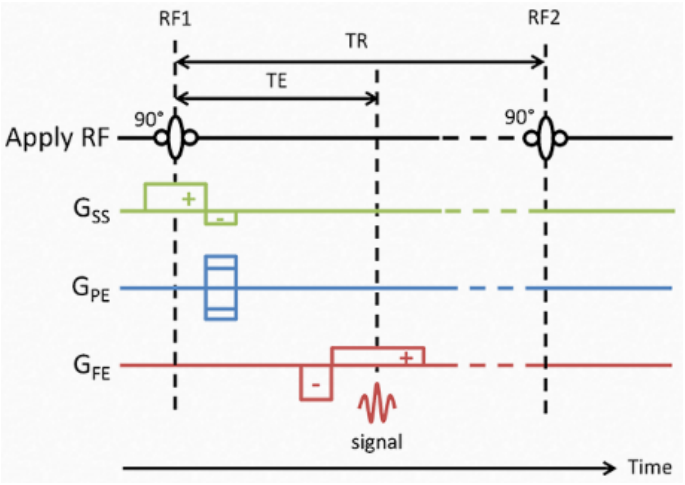

Fig. 4 Acquisition sequence Gradient-echo Echo-planar imaging utilized in the study for the acquisition of fMRI images (adapted from [30]). In the image, acquisition sequence parameters such as echo time (TE), repetition time (TR) and the 90º flip angle are represented.

2.4 – Paradigms

The BOLD technique relies on a close relation between neural activity and cerebral blood flow within the brain. Despite the advances in fMRI, its temporal resolution is limited because its signal temporal evolution is an order of magnitude poorer than the evolution of neural activity itself, at least for brief events, which can lead to temporal blurring between the response and the underlying neuronal activity[31] (Figure 5). To ensure the relationship needed to acquire precise BOLD responses in the area of interest, a

paradigm needs to be designed and used. A paradigm is a temporal allocation of stimuli or events that will evoke hemodynamic responses and brain activation in the subject[32].

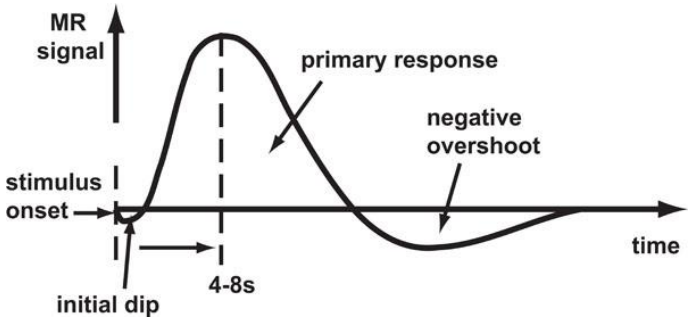

Fig. 5 Schematic of a signal produced by the BOLD technique. The initial dip refers to the increase in the concentration of dHb as the oxygen is used by the neurons. The primary response shows the influx of HbO_2 and the negative overshoot happens after the end of neural activity where there is a decrease of HbO_2 (adapted from [33]).

There are two types of paradigms: blocked task paradigm and event-related paradigm. The most commonly used experimental paradigm in fMRI is the blocked task paradigm. This paradigm will consist in alternating blocks of temporal periods of activity, where the patient will either perform a designated task or be subject to a selected stimulus, and temporal periods of rest to ensure contrast of fMRI signals between task blocks. The signal acquired during a blocked condition will be compared to the other successive blocks[27,31], and the delay in the hemodynamic response considered in the design of the paradigms. If the blocks' length is too short (less than 10 seconds) there will be no difference between the BOLD signal amplitude of the different blocks because the hemodynamic response cannot return to the its baseline, making long block intervals better for maximizing BOLD amplitude between the conditions. Typical paradigms last from 16 seconds to one minute (Figure 6).[27,31]

The event-related paradigm differs from the blocked paradigm in that, instead of analyzing the signal of continuous stimulus from a specific task, different trial events are measured. In an event-related paradigm two separate trial types might be done in rapid succession and then the separate signal contributions of the different trials will be compared directly.[31]

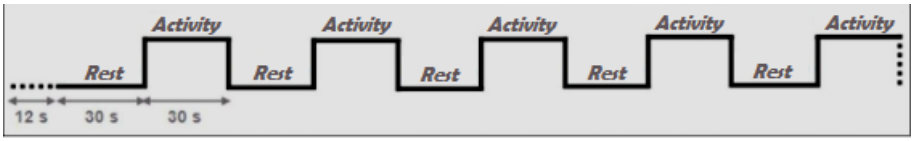

Fig. 6 Schematic example of a blocked paradigm design with an initial 12 seconds baseline and then alternating 30 seconds of activity and rest periods.

3 – Brain Anatomy

The human brain is one of the largest and most complex organs of our body, acting as a control center for many voluntary and involuntary actions, being also responsible for more complex tasks such as logical thinking, learning, emotion, speech and memory. The entire human brain weighs about 1.5 kg and its surface is strongly folded.[34,35]

3.1 – Cerebral Hemispheres – Structure and Functions

The brain is divided into two cerebral hemispheres by a *longitudinal sulcus* and interconnected by the *corpus callosum* [34,35,36,37]. Overall, each hemisphere controls the opposite side of the body, the right hemisphere being responsible for the left side of the body and vice versa[38]. Despite the hemispheres working together as a whole, not all functions are shared between them. The left hemisphere is usually associated with speech, arithmetic calculations, reasoning and writing, while the right hemisphere excels in visual perception, spatial ability and creativity[38]. Each cerebral hemisphere is divided into 6 lobes via sulci and fissures: frontal, parietal, temporal, occipital, central (insular cortex) and limbic lobes[36,37], represented in Figure 7.

The parietal lobe comprises the primary somatosensory cortex, responsible for the reception of body sensations (tact, pressure, temperature and pain), as well as projections of the visual field and auditory spectrums[36,37], making it responsible for the reaction to these complex stimuli. This lobe is also responsible for mimicking or copying.[36] Damage to the parietal lobe may produce loss of general sensations on the opposite side of the body. It may also affect the ability to read or comprehend written words, as well as impair spatial orientation[36].

The temporal lobe contains the primary auditory cortex, responsible for receiving and processing auditive information. It is also responsible for some aspects of learning and memory[36,37]. Damage to the temporal lobe can lead to inability to comprehend spoken language, memory impairment as well as orientation impairment[36].

The occipital lobe is formed by the primary visual cortex, responsible for receiving and processing visual information and interpretation of the visual world[3,4]. Damage to the occipital lobe will lead to vision impairment and disabilities[36,37].
The central lobe (or insular cortex) receives input from its connections to the primary and secondary somatosensory cortex, orbitofrontal cortex and inferior parietal lobule, being

suggested that it plays an important role in the perception and recognition of fine touch and auditory impulses, and is thought to be associated with language function[36,37].

The limbic lobe is formed by the hippocampus, septum, amygdala and olfactory bulb. This lobe is associated with emotions and motivation as well as aggressive behavior[36,37].

Finally, the frontal lobe contains the primary motor cortex, the supplementary motor area, the premotor cortex, the prefrontal cortex and Broca's motor speech center[36,37], being responsible for movement control and for memory, motivation, emotion, reasoning, speech and language[35,36,37]. The motor cortex is connected with the supplementary motor area and premotor cortex through frontal lobe association fibers and these pathways are suspected to be responsible for modulation of motor cortical activity related to preparation, guidance and temporal organization of movement[37]. Damage to the frontal lobe may cause motor aphasia, memory impairment, changes in personality or behavior and inability to plan and execute tasks[36,37].

Besides the frontal lobe, two other brain structures have movement related functions: basal ganglia and the cerebellum.[36,37]

The basal ganglia are responsible for the control and planning of stereotyped movements, regulation of posture and muscle tone adjustment. It influences the motor activity by sending impulses through the thalamus to the cerebral motor and premotor cortex[36,37].

The cerebellum plays a major role in planning, initiating and organizing the movement[39,40]. The cerebellum connects with the motor cortex and receives input through two fibers: mossy and climbing fibers[37]. This connection will work to coordinate movement as the cerebellum provides movement corrections. This function is critical in motor learning and reflex modification[37,39,40]. The output of the cerebellum will be directed through the fibers to the thalamus and from there to the motor cortex[37].

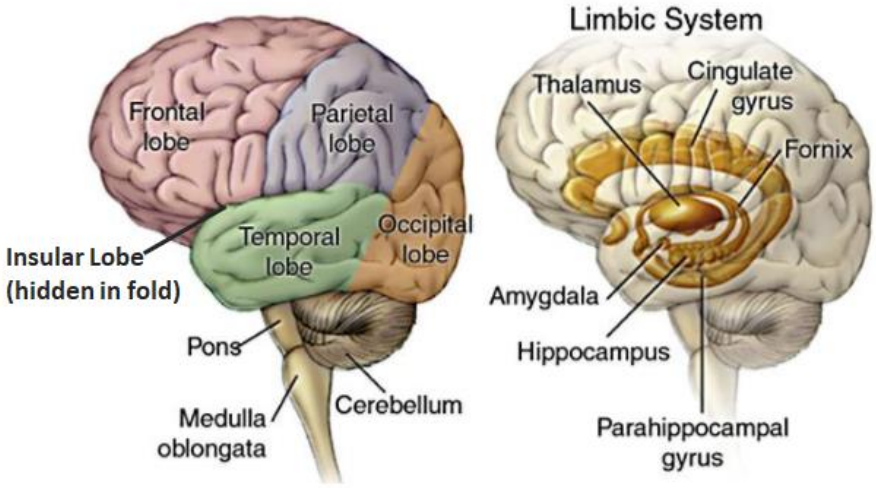

Fig. 7 Representation of the six lobes of the cerebrum and other important structures such as the cerebellum and medulla oblongata (adapted from [41]).

4 – Pathologies

4.1 – Meningiomas

Meningiomas arise from clonal outgrowth of meningothelial cells of the arachnoid layer that forms the external lining of the brain. They may occur primarily at the base of the skull in the parasellar regions, over the cerebral convexities as well as within the ventricular system, where they arise from the stromal arachnoid cells of the choroid plexus[41,42,43,44]. These neoplasms are usually rounded masses that compress the underlying brain. The mass is usually encapsulated by thin, fibrous tissue and can also grow in a sheet-like fashion along the surface of the dura[44].

Meningiomas have three major categories: benign (the most predominant type >90%), atypical (5%) and malignant (3-5%). Within the benign category the meningiomas have several subtypes:[41,44]

- Syncytial**:** Described by the whorled clusters of cells that sit in tight groups without visible cell membranes.
- Fibroblastic**:** Described by elongated cells and abundant collagen deposition between them.
- Transitional: Whose cells share the features of the syncytial and fibroblastic types.
- Psammomatous: This psammoma bodies result from the calcification of the syncytial nests of meningothelial cells.
- Secretory: These cells contain PAS-positive intracytoplasmic droplets and intracellular lumens that can be identified by electron microscopy.
- Microcystic: Described by a loose, spongy appearance.

There are several established risk factors associated with the development of meningiomas. One of the factors is the deletion and inactivation of the neurofibromatosis type 2 gene (NF2) on chromosome 22. This gene is a tumor suppressor gene acting via its product, the protein merlin, whose function is to build a link between the cell membrane and the actin cytoskeleton. The malfunction of this gene is a predominant feature in the occurrence of multiple sporadic meningiomas, schwannonmas and gliomas. Other factors include exposure to ionizing radiation, head injuries, hormonal receptors or association with other diseases, for example breast cancer[41,42,43].

4.2 – Pituitary adenomas

Pituitary adenomas are non-metastasizing neoplasms that arise from clonal outgrowth of adenohypophysial cells (composing a complex gland responsible to produce many hormones). These neoplasms are soft and well-circumscribed, usually small lesions confined to the sella turcica, but as they grow at a slow pace, enlarging by expansion, they can frequently erode the sella turcica and anterior clinoid processes. Larger lesions can extend superiorly through the diaphragm sella into the suprasellar region and compress the optic chiasm or other adjacent cranial nerves or structures[44,45,46]. Despite their distinct borders, adenomas are not encapsulated but are surrounded by compressed adenohypophysial cells and condensed reticulin fiber network of the adjacent nontumorous anterior lobe[45].

Pituitary adenomas have a functional classification which defines the tumor based on hormonal inactivity or activity in vivo. This type of classification is commonly used by endocrinologists. The tumor can be classified functionally as:[45,46]

- Endocrinologically inactive adenomas: The largest group of adenomas, produce no hormones and are usually undetected clinically due to the lack of symptoms.
- GH-cell adenoma: Associated with acromegaly or gigantism, including adenomas causing hyperprolactinemia and its clinical sequela.
- ACTH-cell adenoma: Associated with Cushing's or Nelson's syndromes.
- TSH-cell adenoma: Rare clinically detectable gonadotroph adenomas.

5 – Stereotactic Radiosurgery

The bases of stereotactic radiosurgery (SRS) were first introduced by Lars Leksel in 1949[48]. The SRS technique is a treatment modality that delivers single or up to five large dose fractions of radiation to a specific intracranial target while sparing surrounding tissue[48,49]. This modality utilizes stereotactic localization techniques to focus multiple small photon beams in a defined intracranial target, leading to a highly conformal dose delivery with steep dose gradients to normal tissues along the path of the beams[48,49,50]. The stereotactic techniques may include rigid frames or masks, image-guidance techniques or other positioning tools[3]. In a stereotactic radiosurgery the dose per fraction can be higher than the one delivered using conventional radiation therapy in a similar situation, depending on the tumor size. Stereotactic radiation therapy (SRT) has the same number of fractions used on conventional radiation therapy but, unlike conventional radiation therapy, it uses stereotactic localization in the treatment.[50]

Currently there are three types of equipment that allow us to perform SRS: Gamma Knife, CyberKnife and linear accelerator (linac) whose collimated X-ray beam will focus on a stereotatically identified intracranial target[48]. During the procedure on a linac the gantry rotates around the patient, producing one or more radiation beams focused on the intended target[48].

To optimize treatment delivery using a linac, a radiation technique called volumetric modulated arc therapy (VMAT) can be used[51]. VMAT differs from standard intensity-modulated radiotherapy (IMRT) and three-dimensional conformal radiotherapy by delivering dose through the use of dynamic arcs[49]. During this technique, radiation is delivered with a 360º degree rotational movement of the gantry and, unlike other IMRT treatments where the machine only delivers dose at a small number of gantry positions and at each position must reset all beam parameters, VMAT can apply the prescribed dose fraction to the target continuously and in a single rotation[49,51,52,53]. The patient couch can also be rotated to allow the execution of multiple non-coplanar arcs that will intersect at the target volume[1]. By varying dynamic parameters such as gantry rotation speed, delivery dose rate and multileaf collimator (MLC) aperture shape, VMAT allows for a conformal dose distribution along the planning target volume while minimizing the dose to organs at risk (OAR) and normal tissue[49,51,53].

5.1 – Treatment planning for Stereotactic Radiosurgery

The main technique for treatment planning of SRS is sphere packing. This technique creates a point in space, known as isocenter, where a set of beams approach it through unique paths, providing both geometric accuracy and high-dose gradient. The resultant dose distribution will be approximately spherical, allowing it to be used in plans for spherical targets[48]. The sphere packing technique defines the initial dose sphere inside the target volume and is usually selected to be the largest sphere that the system can produce inside the target volume. The remaining volume that isn't covered will be then filled with spheres of equal or smaller diameter until the whole volume is adequately covered. Nevertheless, this technique is used only when radiosurgery cones are available to irradiate exclusively spherical lesions. When PTV is irregular (not spherical), a combination of cones of different diameters and several isocenters must be used in the treatment planning.

Because SRS treatment involves the delivery of high radiation dose in a small number of fractions, a high degree of dose conformity and accurate patient positioning is mandatory. These goals are achieved with accurate stereotactic localization through radiotherapy masks worn by the patient on the day of the procedure, ensuring that the patient cannot move during the dose delivery.[48]

Before proceeding to the treatment planning, MRI, CT and planar angiography images (in case of arteriovenous malformations) of the patient are acquired. MRI is an excellent modality for imaging soft tissue contrast. However, due to not providing tissue attenuation coefficients, it must be fused with the CT images to allow for appropriate heterogeneities corrections in the dose calculation[48].
In the frameless technique used at IPO-Porto, the CT scan is performed with the patient in an ExacTrac tracking surface[54] to ensure that the patient's anatomy is in conformity with the stereotactic coordinates. In the planning system the nonstereotactic MRI scan will be mapped into stereotactic space through registration of the MRI data set with the CT data set.

After registration is done, the clinician can proceed with the contouring of the desired structures such as OARs and target volume, as well as setting the dose prescription[48].

The dosimetric characteristics of the treatment plan will vary from one delivery approach to another. In SRS, the prescribed dose is usually defined according to ICRU Report 91 (95% of prescribed dose to 98% of the planning target volume[50]) or according to other international recommendations. During planning the goal is more to achieve maximum normal tissue sparing rather than maximum target dose uniformity, as the main concern is the dose to the normal tissue outside the target volume[48]. During planning, neurosurgeon, radiation oncologist and physicist or dosimetrist will work together as a team to create the optimal treatment plan[48].

For dose calculation in radiotherapy there are two planning approaches: forward planning and inverse planning. In forward planning, a treatment plan is created through an iterative trial and error approach, in which the planner attempts to determine a set of parameters until no other change will make noticeable improvements to the plan quality[48]. In inverse planning, the dosimetrist outlines the target and other sensitive structures, defines the treatment goal and includes one or more constraints before an optimization algorithm determines the plan parameters that best satisfy the set goals. In complex radiotherapy planning (IMRT, VMAT and SRS), only the latter method is used[48].

On every treatment session, the patient will be positioned with the radiotherapy mask fixed on the same frameless (for example, ExacTrac) tracking surface. The machine will identify patient positioning through infrared scans and perform x-rays to the patient for monitoring, allowing the radiation oncologist, alongside the radiation therapy technicians (RTTs), to do real-time internal anatomy verification at any couch position or gantry angle and perform any shift or position correction, if necessary.

6 – Experimental methodology

6.1 – Data acquisition

6.1.1 – Sample description

In this study participated 3 patients, 2 women and 1 man, with a range of age between 36 and 43 years old, selected from the group of patients that were to be subjected to stereotactic radiosurgery (SRS) or to stereotactic radiotherapy (SRT) treatment at the Instituto Português de Oncologia do Porto (IPO-Porto). The selection criterion for the patients in this study was that they had benign lesions that are either pituitary adenomas or meningiomas located in the frontal cortex. The criterion used ensures that the lesion does not impair the patient's capability to follow instructions properly while having lesions in desirable locations for the paradigms used in this study.

In addition to the selected patients, to increase the data available in the study, 15 volunteers from a healthy group, 8 women and 7 men, with a range of age between 21 and 57 years old, also participated in the study. An imaginary benign tumor was delineated in their CT-converted MRI images, in regions and sizes similar to other existing patients of the institute, to quantify and analyze the data from the different plans as if they were affected by the imaginary benign tumor.

In table 1 there are all the general information of each patient and volunteer that participated in this study as well as some individual information used in image acquisition and processing, such as the activation threshold (Z-score) chosen for each participant.

Table 1 General information of patients and volunteers that participated in this study

	#	Gender	Age (years)	Pathology	Dominant hand	Hand used in image acquisition	Minimum activation threshold (Z-score) on fMRI processing
Patients	1	Female	36	Meningioma in the frontal lobe	Right hand	Right hand	6.0
	2	Female	43	Meningioma in the frontal lobe	Right hand	Right hand	6.5
	3	Male	38	Pituitary Adenoma	Right hand	Right hand	5.5
Volunteers	1	Female	57	Meningioma near the Cerebellum	Right hand	Right hand	10.5
	2	Male	34	Meningioma in the frontal lobe	Right hand	Right hand	9.0
	3	Male	35	Meningioma in the frontal lobe	Left hand	Left hand	11.0
	4	Female	27	Meningioma in the frontal lobe	Right hand	Right hand	8.5
	5	Male	21	Meningioma in the frontal lobe	Right hand	Left hand	9.0
	6	Female	27	Meningioma in the frontal lobe	Right hand	Right hand	8.0
	7	Female	33	Meningioma in the frontal lobe	Right hand	Left hand	13.5
	8	Female	28	Meningioma in the frontal lobe	Left hand	Left hand	13.0
	9	Male	24	Meningioma in the frontal lobe	Right hand	Right hand	6.0
	10	Male	34	Meningioma in the frontal lobe	Right hand	Right hand	9.0
	11	Male	34	Meningioma near the Cerebellum	Right hand	Right hand	9.0
	12	Female	37	Meningioma in the frontal lobe	Right hand	Right hand	9.0
	13	Male	34	Meningioma in the frontal lobe	Right hand	Right hand	9.0
	14	Female	57	Meningioma in the frontal lobe	Right hand	Right hand	10.5
	15	Female	45	Meningioma in the cavernous sinus	Right hand	Left hand	8.5

6.1.2 – Equipment utilized in image acquisition

For this study, every exam was performed on a MRI machine Signa HDxt 3T (GE Healthcare) (Figure 8). All MRI and fMRI images were acquired during the development of the present dissertation, with the support and collaboration of medical professionals, radiologists and technicians of IPO.

Fig. 8 MRI machine Signa HDxt 3T – GE healthcare (adapted from [55]).

6.1.3 – fMRI acquisition sequence parameters

Patient and volunteer BOLD fMRI data were obtained using GE-EPI acquisition sequence described by the following parameters: magnetic field B_0 of 3 T; slice thickness of 3 mm; echo time (TE) of 35 ms; repetition time (TR) of 3000 ms; acquisition matrix of 64 x 64 pixels; field of view (FOV) of 288 x 288 mm^2; flip angle of 90º.

6.1.4 – Selected Paradigm and Motor Task

Before the fMRI exam, patients and volunteers were instructed on the motor task and the paradigm methodology to ensure activations on the desirable area. The selected motor task consisted of repetitive opening and closing movements of the hand, either right or left, depending on the location of the lesion. The participants also answered a specific questionnaire about the realization of the MR imaging.

The paradigm consisted of performing motor activity followed by a rest time period of equal duration (30 s), for a total of 5 minutes (Figure 6). The shift between activity and rest periods was made through the illumination of the MRI room. The participants were instructed to initiate the hand movement when the lights of the room were dimmed and to return to rest state when the light in the room returned to normal. With this method we were able to control the alternation between activity and rest period of the paradigm while reducing possible “undesirable activations” in the image caused by visual stimulation caused by the resonance room lighting.

6.2 – Image processing

The processing of acquired fMRI images must be done prior to their use in the treatment planning system (TPS). This processing includes the removal of any noise in the image and the fusion of the results with the structural MRI image, to achieve correct anatomical localization. This processing was performed using the FMRIB Software Library (FSL 6.0.1)[2]. FSL is a comprehensive library that includes tools specialized in the analysis and processing of fMRI, MRI and DTI brain imaging data and was developed in Oxford, UK by members of the Analysis Group[56,57].

6.2.1 – Imaging processing using FSL

The acquired images are exported from the MRI machine in DICOM format which is incompatible with FSL. The conversion of DICOM images to NIFTI (FSL input image format) was performed using the *dcm2niigui* tool provided by the neuroimaging visualization program *mricron.* This program not only converts images to the proper NIFTI format but also reorients them for proper visualization in FSL.

After importing the images to FSL, the first step is to use the Brain Extraction Tool (BET) to remove the scalp and the bones of the skull from the structural MRI (Figure 9). This step generates an image that has only the brain, which will be used for the registration and fusion with fMRI data. The step of scalp and skull removal requires manipulating the values of the *"fractional intensity threshold"* and *"threshold gradient"* (BET parameters) to achieve a good estimate of the brain outline.

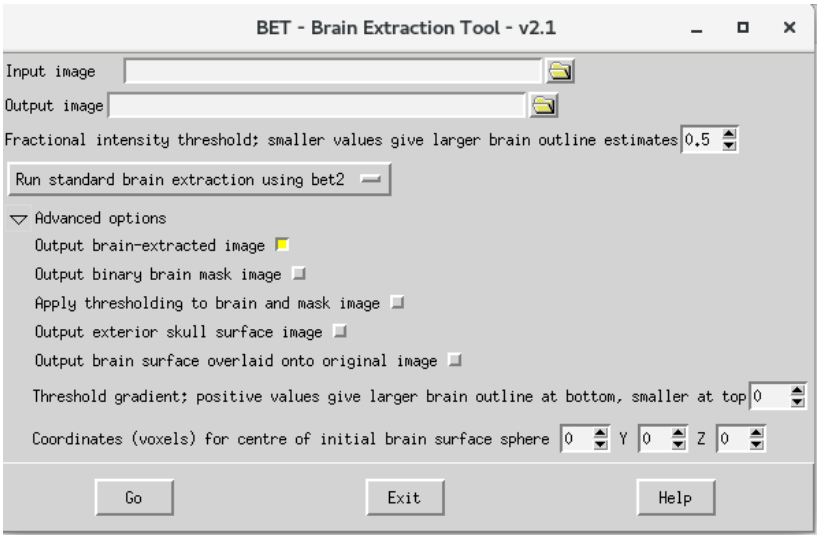

Fig. 9 Brain Extraction Tool menu.

The second step is to use the FMRI Expert Analysis Tool (FEAT) to analyze the fMRI data (Figure 10). This tool is responsible for pre-processing, registration and post-processing of the image. After importing the fMRI data into FEAT, the tool automatically displays some image parameters such as total volumes and repetition time (TR).

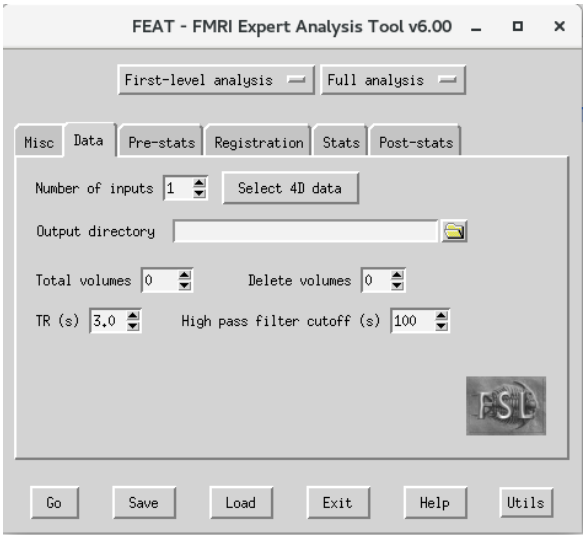

Fig. 10 FEAT Data import tab.

After that, it is necessary to define the image pre-processing parameters responsible for the image motion correction, slice timing correction (if needed) and spatial smoothing (Figure 11). Motion correction is an important step to remove artifacts caused by any patient movement during image acquisition. The correction used was the MCFLIRT (Motion Correction FMRIB's Linear Image Registration Tool) which is an effective tool for motion correction and linear image co-registration.

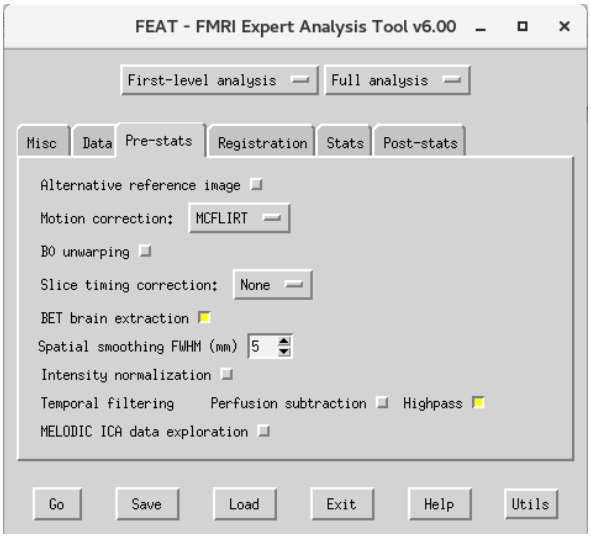

Fig. 11 FEAT Pre-stats tab.

The next step in FEAT is the registration of the fMRI image with the structural MRI to ensure proper anatomical localization of the fMRI results. In this step we defined the main structural image as the image obtained by the BET and the registration as *Normal*

search with 6 degrees of freedom (DOF). For the standard space, FSL already has a default standard space image with defined *normal search* of 12 DOF (Figure 12).

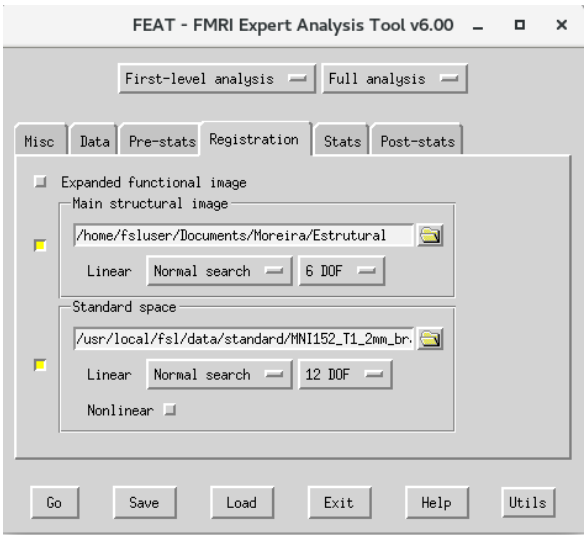

Fig. 12 FEAT Registration tab.

Afterwards the clinician must define a model setup that describes the paradigm model used (Figure 13). The paradigm used was a blocked paradigm that allows the use of the "*model setup wizard"* (Figure 14) to automatically obtain the model that best fits our paradigm and use it in the image processing (Figure 15).

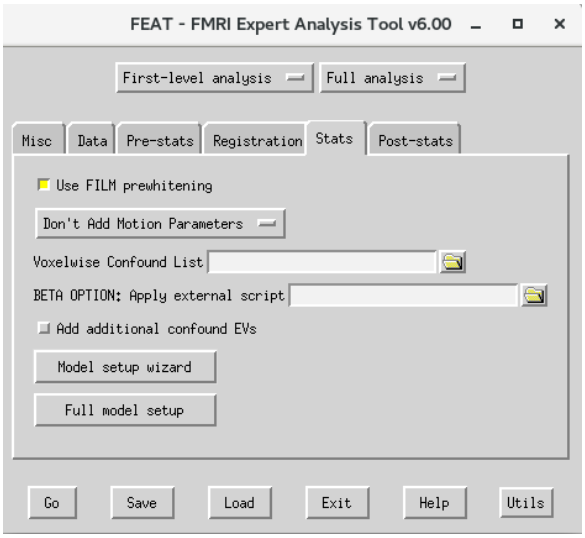

Fig. 13 FEAT Stats tab.

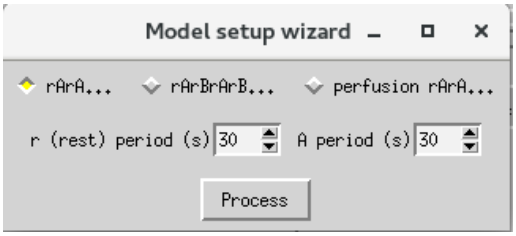

Fig. 14 Model Setup Wizard (includes rest and activity parameters).

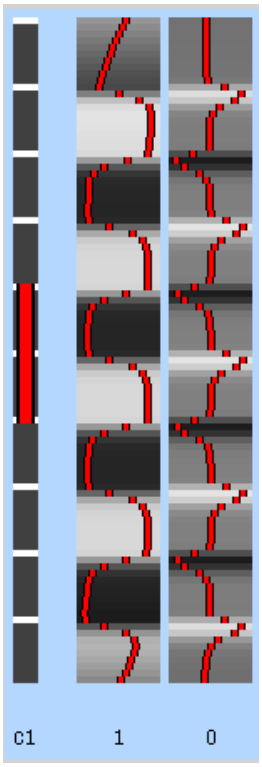

Fig. 15 Model generated through Model Setup Wizard (Fig.14) to fit the selected paradigm.

The final step of FEAT is the post-processing. In this step the clinician chooses the activation threshold values (Z threshold), used in comparing the different voxels to determine which ones are activated, while removing the signal from any voxels whose values are below the selected threshold, and the uncertainty threshold (P threshold), used for statistical validation of our analysis (Figure 16). During this step, an initial value of 3.5 was used for Z threshold, and the resulting image was overlapped on the structural image and subsequently analyzed by a radiologist in *fsleyes*, the FSL tool for image visualization. In this visualization tool the Z threshold can be changed manually, providing a new threshold suitable for image processing. After that, the resulting fMRI output (from FEAT) is registered to the structural MRI used in the registration with the option *"High-res FEAT stats color rendering"* (Figures 16 and 17).

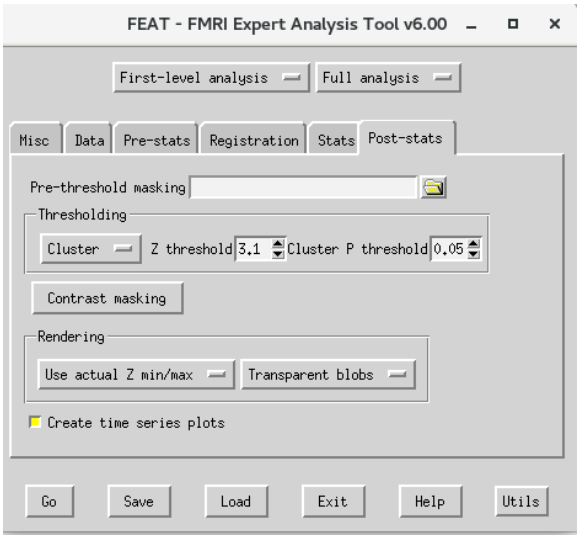

Fig. 16 FEAT Post-stats tab.

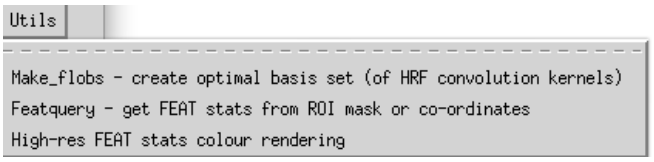

Fig. 17 FEAT Utils responsible for the image fusion.

6.2.2 – Image conversion with MATLAB

The TPS, unlike FSL, requires a DICOM format input image, not a NIFTI format (FSL output format). Therefore, a reconversion of the NIFTI images to DICOM is required. This reconversion was performed with the MATLAB software using the WriteDICOMImage function (created by Mark Geurts from the University of Wisconsin Board of Regents). The function saves a provided image array to a series of DICOM files and generates its DICOM header.

Before using the reconversion function, the NIFTI image and its metadata were imported by MATLAB using *niftiread* and *niftiinfo* commands, respectively. It is necessary to return the image to its initial orientation (changed by *mricron* in the first conversion from DICOM to NIFTI). This is achieved by flipping the image matrix once around every axis using the *flip* command[58].

Once the proper image orientation is established, the new data will be used by the WriteDICOMImage function to generate the DICOM image. During this step, the patient/volunteer Identification Number (ID) will be provided to the function to be included

in the image header. This will help the TPS to recognize the patient to whom the image belongs and facilitates the import of the DICOM image into the correct patient. Since the purpose of this image is to provide the correct anatomical localization of the activations for the contouring of the fOARs, no further information is required to be provided to the header, since the default values of the function have no impact in the image import and registration by the TPS.

Although the final image is an MRI, it was converted into a CT DICOM image in MATLAB because this seemed to cause less difficulties with the import of the image by the TPS and did not cause additional problems or had any impact with the registration or results of the image.

6.2.3 – Eclipse: Contouring of fOARs and treatment planning optimization

The contouring of the activations identified by the radiologists as control regions (or functional organs at risk) was performed in the Eclipse Treatment Planning System (Varian, version 13.5).

To import the converted DICOM images, the option "*import from CT"* from the program Import Setup Wizard was used, which identifies the patient ID of the files and provides the option to associate the patient/volunteer images with that ID. Once imported, the dosimetrist or physicist will perform the MRI registration with the planning CT. In this step the two sets of images are overlapped, and the dosimetrist manipulates the MRI image positioning to match the brain outline in both images, using identifiable characteristics such as brain grooves that might be perceptible in both images. After the images are registered any contour performed on the MRI can be automatically copied to the planning CT.
The contouring of the desired regions is made by creating a new control region structure and using the *brush* option to manually delineate the activation volumes, slice by slice (Figure 18).

Once the activation volumes, or structures (fOARs) have been created, the dosimetrist is able to see the doses in the original treatment plan that will affect them, as well as define constraints on those structures to optimize the treatment plan, generating a new

viable plan that minimizes the doses to those structures, while preserving the normal tissue and ensuring the prescribed dose is achieved in the PTV. The specific dose constraints used in the re-optimization of the patients' treatment plans are presented in the corresponding Results section (chapter 7).

Fig. 18 Example of "fOARs" contouring in the cerebellum and motor cortex (pink regions) performed with Eclipse Treatment Planning System.

6.2.4 – Eclipse: Volunteer treatment planning steps

The volunteers selected from the healthy group for this study cannot be subjected to a CT scan as it would expose them to unnecessary radiation dose. To circumvent the issue of not having a CT image to perform the treatment planning, the structural MRI that they were subjected to, before the fMRI acquisition, was converted with MATLAB to a CT DICOM image, using the same image conversion script as for the conversion of the fMRI data. This allows the TPS to recognize and import the MRI image series as a CT image series without complications.

Despite being converted to a CT, unlike an original CT, the pixel info on this 3D-image will not correspond to hounsfield units (HU), which are necessary for the treatment planning. Additional steps are then necessary to address this issue.

Firstly, it is necessary to acquire the mean HUs for each structure of the brain to be able to replicate them in the converted CT. This was done by selecting a patient that already

has a treatment plan created with an original CT, selecting its treatment plan and opening the contouring option. By selecting the desired structures and using the *measure* functionality, selecting *histogram*, which by drawing a ROI inside the desired structure and selecting *show statistics,* finally displays the mean HUs for that structure. Table 2 presents the mean HU values obtained from the previous method and used for the converted CTs of the volunteers.

Due to the Eclipse TPS not being able to recognize automatically any structures from the converted CT as it would with a normal CT, a different approach for their delineation was used. The MRI converted CT images were imported to the program iPLAN RT IMAGE 4.1.2. Within that program, the delineation of the brain structures was performed by using the option *Object Creation*, then *Cranial Treatment*, followed by *New*, where the structures to be delineated could be selected. Afterwards, by selecting *Auto Segmentation* option, the program automatically delineates the desired structures which were saved onto the imported image.

After the delineation of the structures is done, the image needs to be exported from the program iPLAN back to Eclipse. This was achieved by selecting the option *Data transfer* from Origin Server, selecting, from the patients' database of IPlan, the desired patient that was previously edited in iPLAN. Finally, we selected the option "*Export to Eclipse*" to export the images to Eclipse as desired. The actual import of the images to Eclipse was finally concluded using the *DICOM Media File Brainlab tool* from the import setup wizard of the program. For the fMRI, the same steps for the patients were used. Once in Eclipse, the HU values in Table 2 were attributed to the brain structures.

Table 2 Mean HUs used in the volunteer's image's delineated structures

Brain and fOARS	42
Brainstem	38
Chiasm	30
Eyes	22
Hippocampus	37
Lens	100
Normal Tissue	0
Optic Nerve	36
Optic Tract	35
Pituitary Gland	36

The treatment plans for the volunteers were elaborated using the standard procedures as for patients with similar pathologies, choosing a lower prescription dose given the relatively small size of the simulated meningiomas. For the re-optimization with the fOARs, the criterion used was to lower the dose to the fOARs as much as possible, while keeping the correct dose coverage to the PTV.

7 – Experimental Results

7.1 – FSL FWHM parameter

During image processing with FSL there are many parameters that can be selected and modified by the user. Of all, the *Full Width Half Maximum* (FWHM) is the parameter that had the greatest impact on the apparent volume of the activated regions before the selection of the final threshold used by the radiologist (Fig.1). The FWHM parameter influences spatial smoothing by defining the distance between half values at which a data average from nearby voxels will occur, and higher FWHM values increase the signal to noise ratio of the image. The final value selected for this study was 5 mm because it allows us to have a high signal to noise ratio while still allowing the cerebellum to show an activated area which, in some cases, can be averaged bellow the selected threshold.

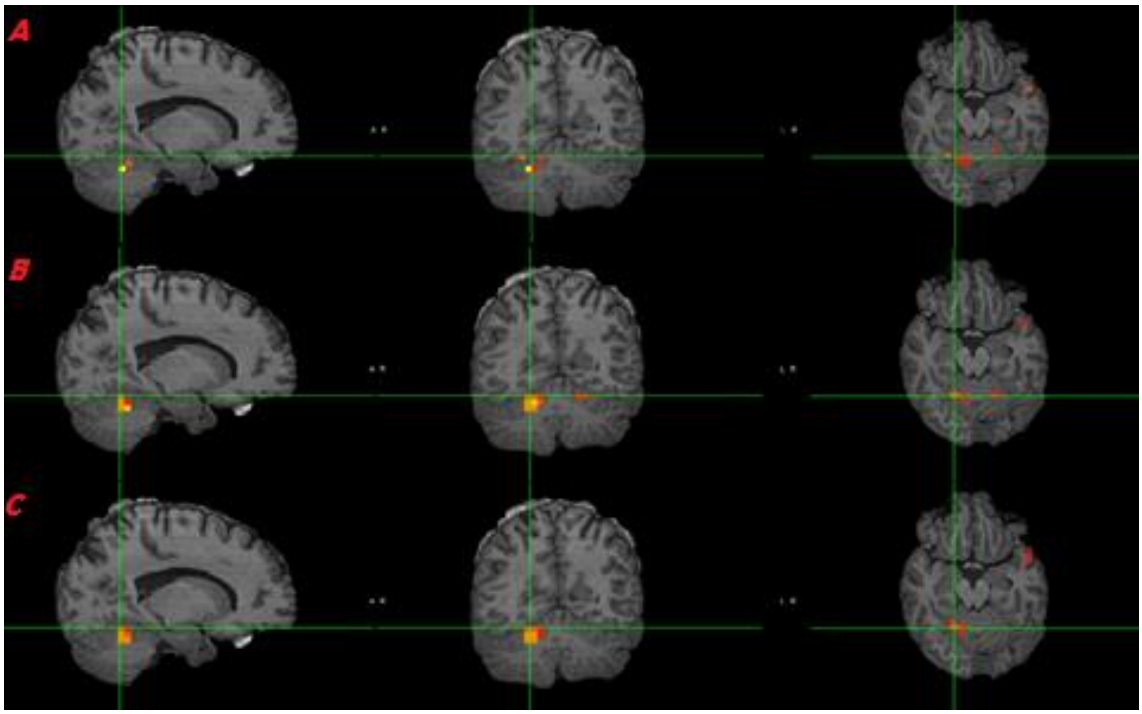

Fig. 19 Example of processing results using different FWHM values. A) FWHM of 2mm; B) FWHM of 5 mm; C) FWHM of 8 mm.

7.2 – Results from treatment plan optimization

Table 3 contains the different optimization parameters common to all treatment plans created for the different subject group, patients and volunteers.

Table 3 Optimization parameters for all treatment planning

	Total prescribed dose	Number of fractions	Dose per fraction	Treatment machine	Treatment technique	Maximum dose limit on PTV	Minimum dose limit on PTV	Minimum percentage volume of PTV covered with 100% of total prescribed dose
Patients	54 Gy	27	2 Gy	TRUEBEAM	VMAT	107% of total prescribed dose	95% of total prescribed dose	95%
Volunteers	25 Gy	5	5 Gy					

Results for patients 1-3 are displayed on Tables 4-12, while the results for the 15 volunteers are presented in Tables 13-54. For each patient and volunteer, we present mean, maximum and minimum doses to the PTV and to the fOARs (“Active_cortex” and “active_cerebellum”) on both treatment plans (“Original plan” and “reoptimized plan”) and the percent differences between them.

During the analysis of the original and re-optimized treatment plans created for patients it was concluded that the fOARs created using the fMRI data on patient 3 were too far from the PTV to have an impact on the created plan. Hence, only patient 1 and patient 2 had a re-optimized plan. With the new plan, a 43.12 % reduction in the mean dose in the cerebellum functional areas was achieved for patient 1, and a 6.784 % reduction in the mean dose in the cerebellum and a 46.32 % reduction in the mean dose in the motor cortex was achieved for patient 2.

As for the volunteers, the new re-optimized plans allowed us to achieve a reduction in the mean dose in the functional areas between 2.13 and 50.77 % for the cerebellum and between 3.57 and 82.42 % for the motor cortex, depending on the distance from those fOARs to PTV. As with patients, in some cases the re-optimized plan had no beneficial impact on dose reduction in the functional areas of volunteers.

All of these reductions were achieved without compromising the viability of the original radiosurgical treatment plan. Information on the remaining outlined structures (brainstem, chiasm, eyes, hippocampus, lens, optic nerve, optic tract and pituitary gland) can be found in Appendix A.

Figures 20, 23 and 27 show an example of the geometry of the treatment fields and the isodoses obtained, as well as the location of the fOARs created in the motor cortex and cerebellum. An example of a 3D representation of the field geometry and the location and proximity of both the PTV and the fOAR can be seen in figure 26. The overall visualization of the total dose distribution in the treatment plan before and after plan optimization with the new fOARs is represented in figures 21, 24 and 28. Another visualization of the impact of re-optimization on dose distribution above 7 Gy is shown in figures 22, 25 and 29.

Patient 1

Optimization parameters from adding the fMRI data:

1. Maximum dose in the activated region in the cerebellum: 4 Gy in 0% of activated volume
2. Maximum dose in activated region in the motor cortex: 2 Gy in 0% of activated volume

Table 4 Comparison between PTV doses in the original and re-optimized plans for Patient 1

PTV (Volume: 32.9 cm^3)	Mean dose (Gy)	Maximum dose (Gy)	Minimum dose (Gy)
Original plan	58.576	63.112	44.856
Reoptimized plan	59.808	65.240	41.272
Differences (Gy)	1.232	2.128	3.584
Percent differences (%)	2.103	3.372	-7.99

Table 5 Comparison between Motor cortex doses in the original and re-optimized plans for Patient 1

Active_Cortex (Volume: 10.7 cm^3)	Mean dose (Gy)	Maximum dose (Gy)	Minimum dose (Gy)
Original plan	0.560	1.064	0.336
Reoptimized plan	0.560	1.120	0.336
Differences (Gy)	0	0.056	0
Percent differences (%)	0	5.26	0

Table 6 Comparison between Cerebellum doses in the original and re-optimized plans for Patient 1

Active_Cerebellum (Volume: 1.2 cm3)	Mean dose (Gy)	Maximum dose (Gy)	Minimum dose (Gy)
Original plan	6.104	13.776	0.560
Reoptimized plan	3.472	7.672	0.504
Differences (Gy)	-2.632	-6.104	-0.056
Percent differences (%)	-43.12	-44.308	-10.0

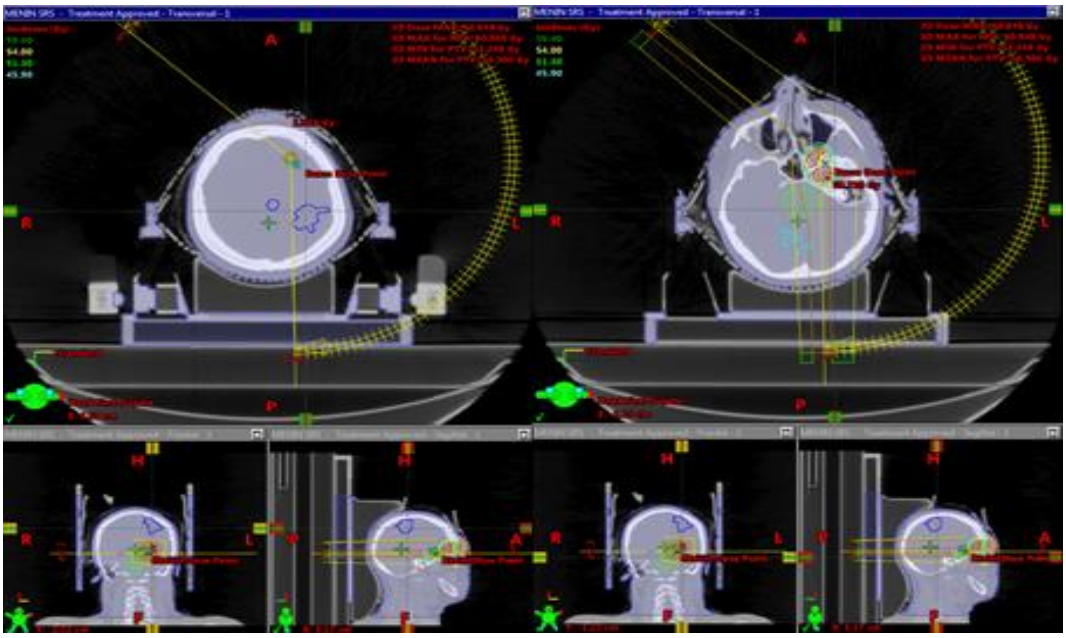

Fig. 20 General visualization of the treatment fields geometry, the isodoses in PTV and the position of the motor cortex (left) and cerebellum (right) of patient 1.

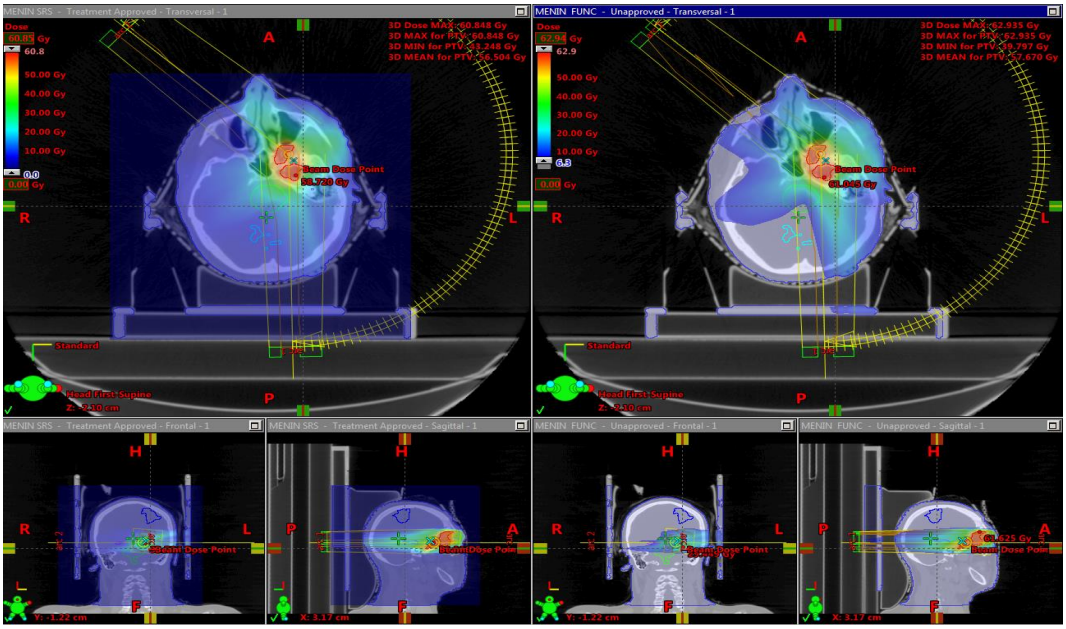

Fig. 21 General visualization of the total dose distribution in the original treatment plan (left) and in the re-optimized treatment plan (right) of patient 1.

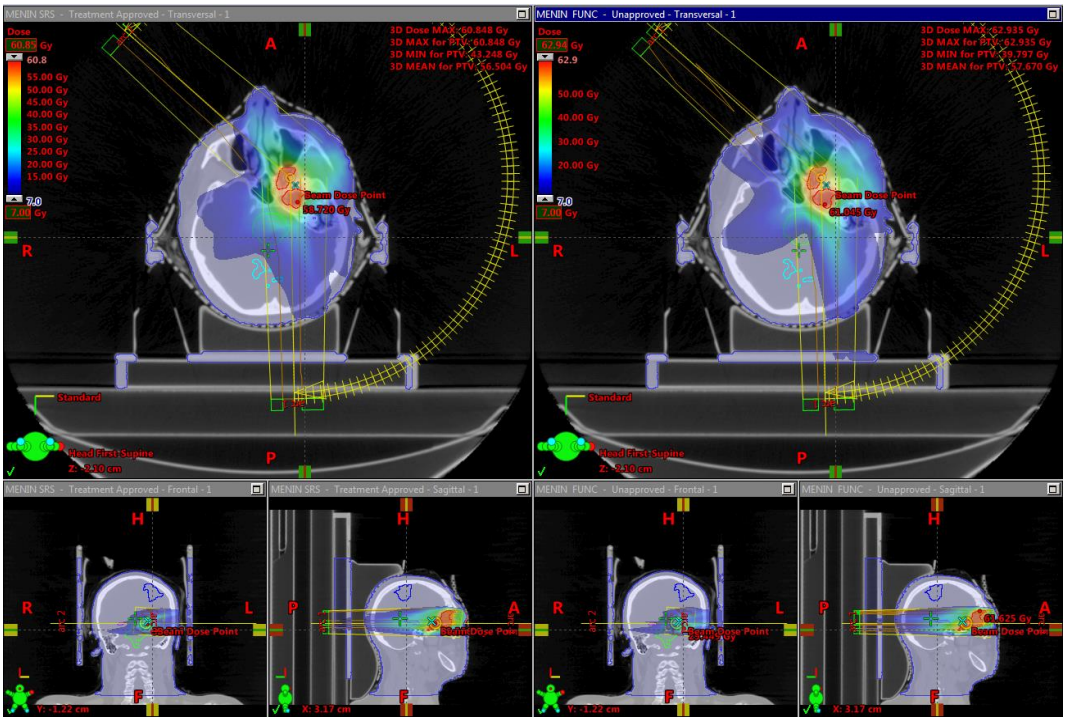

Fig. 22 General visualization of the dose distribution above 7 Gy in the original treatment plan (left) and in the re-optimized treatment plan (right) of patient 1.

Patient 2

<u>Optimization parameters from adding the fMRI data:</u>

1. Maximum dose in the activated region in the cerebellum: 7 Gy in 0% of activated volume
2. Maximum dose in activated region in the motor cortex: 7 Gy in 40% of activated volume

Table 7 Comparison between PTV doses in the original and re-optimized plans for Patient 2

PTV (Volume: 180.9 cm^3)	Mean dose (Gy)	Maximum dose (Gy)	Minimum dose (Gy)
Original plan	54.535	60.314	45.578
Reoptimized plan	54.641	59.653	46.230
Differences (Gy)	0.106	-0.661	0.652
Percent differences (%)	0.194	-1.096	1.431

Table 8 Comparison between Motor Cortex doses in the original and re-optimized plans for Patient 2

Active_Cortex (Volume: 42.7 cm^3)	Mean dose (Gy)	Maximum dose (Gy)	Minimum dose (Gy)
Original plan	14,663	29,402	2,180
Reoptimized plan	7,871	31,594	1,624
Differences (Gy)	-6,792	2,192	-0,556
Percent differences (%)	-46,321	7,46	-25,50

Table 9 Comparison between Cerebellum doses in the original and re-optmized plans for Patient 2

Active_Cerebellum (Volume: 6.2 cm^3)	Mean dose (Gy)	Maximum dose (Gy)	Minimum dose (Gy)
Original plan	3.965	10.948	1.344
Reoptimized plan	3.696	6,770	1.232
Differences (Gy)	-0.269	-4.178	-0.112
Percent differences (%)	-6.9	-38.16	-8.3

Patient 3

Optimization parameters from adding the fMRI data:

No re-optimization was done to the original treatment plan of this patient due to the fact that the control regions were located too far away from the PTV.

Table 10 PTV doses in the original plan for Patient 3

PTV (Volume: 6.7 cm^3)	Mean dose (Gy)	Maximum dose (Gy)	Minimum dose (Gy)
Original plan	54.540	58.735	50.780

Table 11 Motor cortex doses in the original plan for Patient 3

Active_Cortex (Volume: 14.9 cm^3)	Mean dose (Gy)	Maximum dose (Gy)	Minimum dose (Gy)
Original plan	0.112	0.429	0.062

Table 12 Cerebellum doses in the original plan for Patient 3

Active_Cerebellum (Volume: 4 cm^3)	Mean dose (Gy)	Maximum dose (Gy)	Minimum dose (Gy)
Original plan	3.874	8.069	0.456

Volunteer 1

Table 13 Comparison between PTV doses in the original and re-optimized plans for Volunteer 1

PTV (Volume: 1.4 cm^3)	Mean dose (Gy)	Maximum dose (Gy)	Minimum dose (Gy)
Original plan	26.284	29.416	23.600
Reoptimized plan	26.598	28.625	23.319
Differences (Gy)	0.314	-0.791	-0.281
Percent differences (%)	1.20	-2.688	-1.19

Table 14 Comparison between Motor cortex doses in the original and re-optimized plans for Volunteer 1

Active_Cortex (Volume: 0.8 cm^3)	Mean dose (Gy)	Maximum dose (Gy)	Minimum dose (Gy)
Original plan	0.032	0.041	0.018
Reoptimized plan	0.034	0.043	0.020
Differences (Gy)	0.002	0.002	0.002
Percent differences (%)	6.3	4.9	11.1

Table 15 Comparison between Cerebellum doses in the original and re-optimized plans for Volunteer 1

Active_Cerebellum (Volume: 0.1 cm^3)	Mean dose (Gy)	Maximum dose (Gy)	Minimum dose (Gy)
Original plan	14.410	18.584	10.978
Reoptimized plan	7.093	14.444	4.446
Differences (Gy)	-7.317	-4.140	-6.532
Percent differences (%)	-50.77	-22.28	-59.50

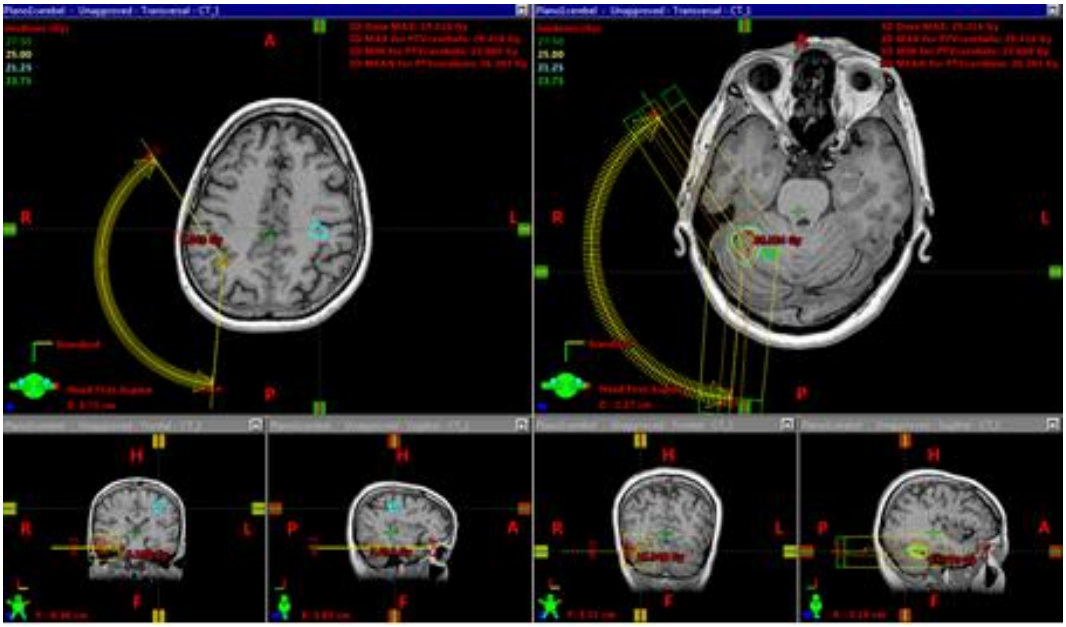

Fig. 23 General visualization of the treatment fields geometry, the isodoses in PTV and the position of the motor cortex (left) and cerebellum (right) of volunteer 1.

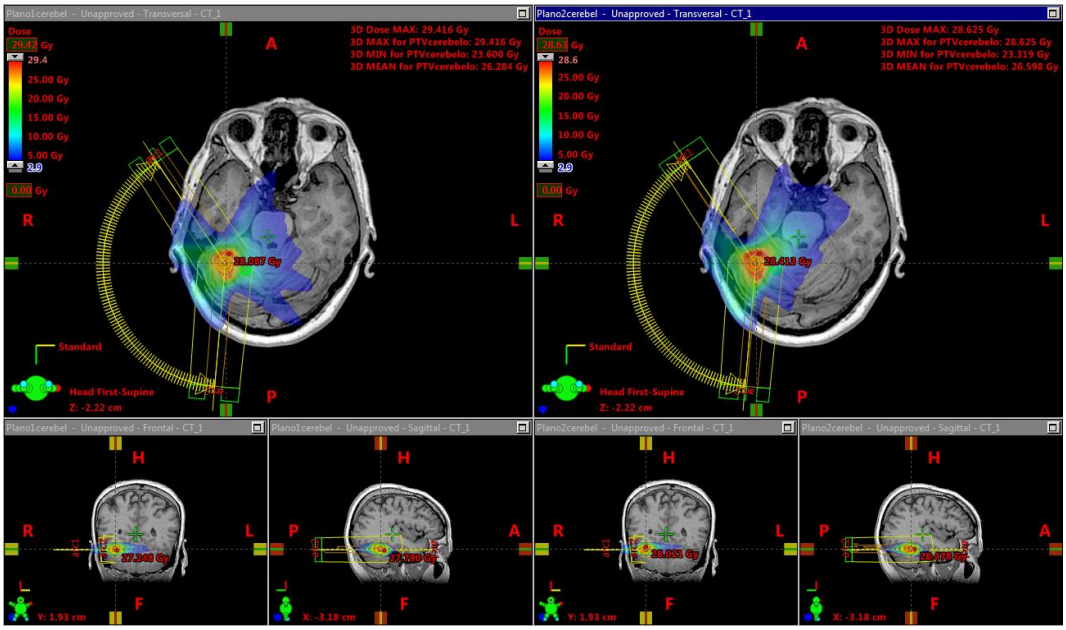

Fig. 24 General visualization of the total dose distribution in the original treatment plan (left) and in the re-optimized treatment plan (right) of volunteer 1.

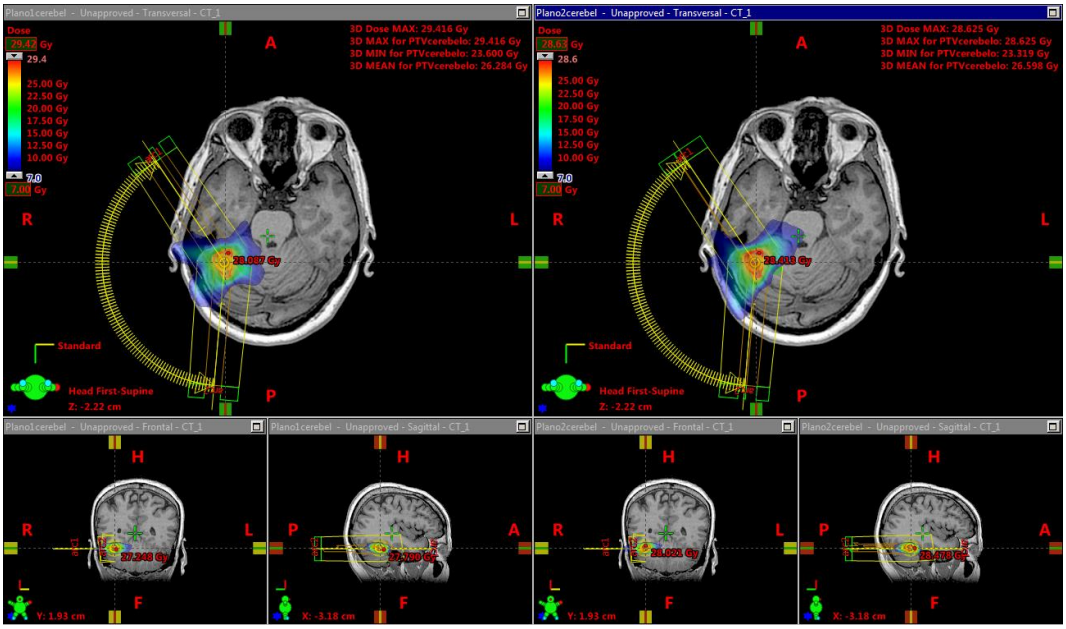

Fig. 25 General visualization of the dose distribution above 7 Gy in the original treatment plan (left) and in the re-optimized treatment plan (right) of volunteer 1.

Volunteer 2

Table 16 Comparison between PTV doses in the original and re-optimized plans for Volunteer 2

PTV (Volume: 10.6 cm^3)	Mean dose (Gy)	Maximum dose (Gy)	Minimum dose (Gy)
Original plan	26.259	28.315	23.361
Reoptimized plan	26.381	28.959	21.034
Differences (Gy)	0.122	0.644	-2.327
Percent differences (%)	0.465	2.274	-9.961

Table 17 Comparison between Motor Cortex doses in the original and re-optimized plans for Volunteer 2

Active_Cortex (Volume: 6.9 cm^3)	Mean dose (Gy)	Maximum dose (Gy)	Minimum dose (Gy)
Original plan	5.669	25.210	0.120
Reoptimized plan	4.020	24.040	0.116
Differences (Gy)	-1.649	-1.170	-0.004
Percent differences (%)	-29.09	4.641	3.33

Table 18 Comparison between Cerebellum doses in the original and re-optimized plans for Volunteer 2

Active_Cerebellum (Volume: 1.3 cm^3)	Mean dose (Gy)	Maximum dose (Gy)	Minimum dose (Gy)
Original plan	0.040	0.051	0.029
Reoptimized plan	0.039	0.050	0.028
Differences (Gy)	-0.001	-0.001	-0.001
Percent differences (%)	-2.5	-2.0	-3.4

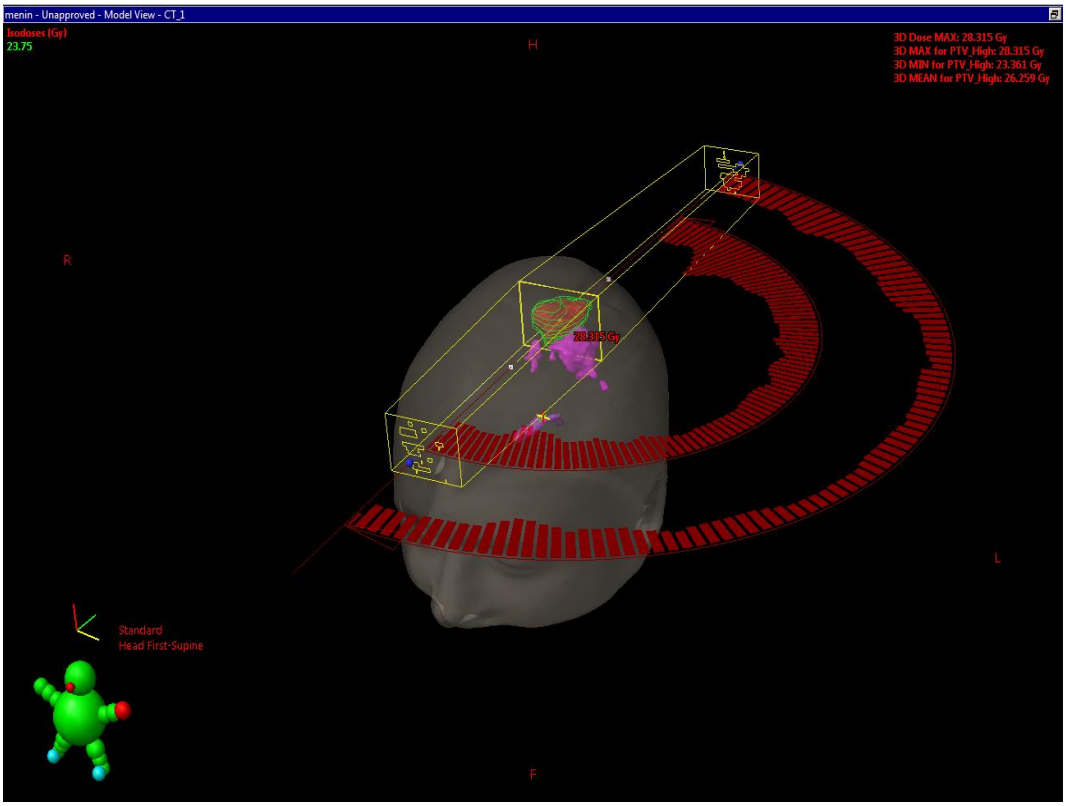

Fig. 26 3D visualization of the treatment fields geometry of volunteer 2.

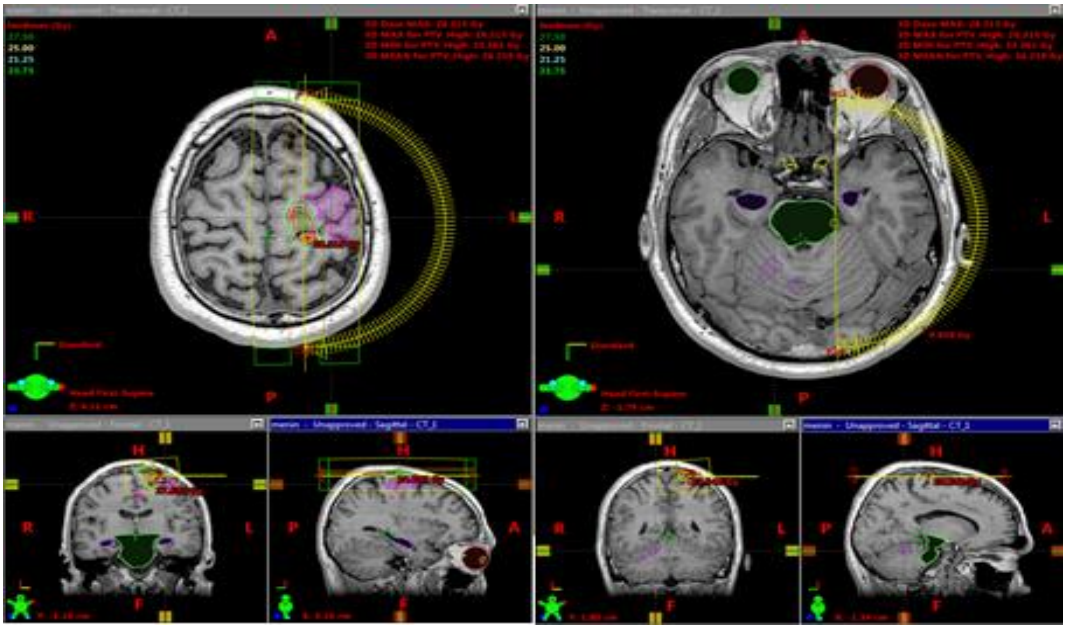

Fig. 27 General visualization of the treatment fields geometry, the isodoses in PTV and the position of the motor cortex (left) and cerebellum (right) of volunteer 2.

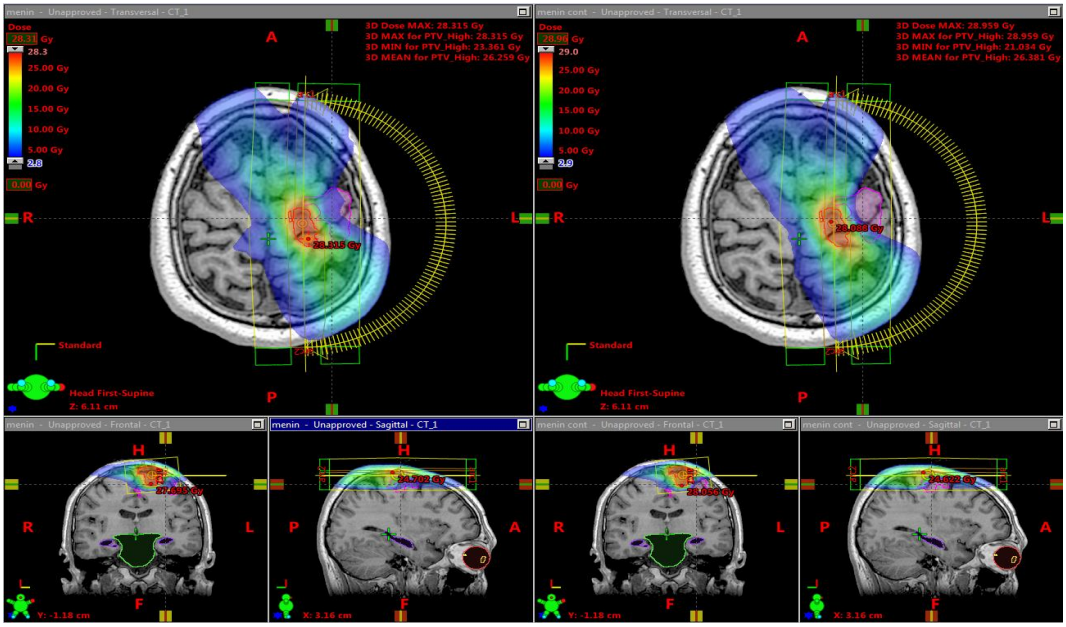

Fig. 28 General visualization of the total dose distribution in the original treatment plan (left) and in the re-optimized treatment plan (right) of volunteer 2.

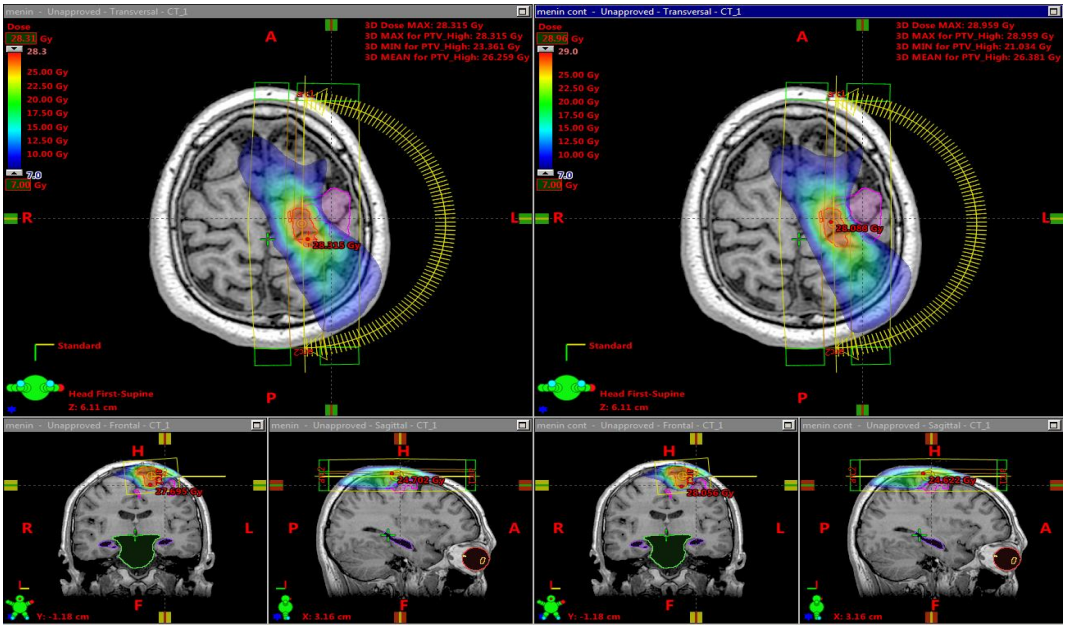

Fig. 29 General visualization of the dose distribution above 7 Gy in the original treatment plan (left) and in the re-optimized treatment plan (right) of volunteer 2.

Volunteer 3

Table 19 Comparison between PTV doses in the original and re-optimized plans for Volunteer 3

PTV (Volume: 7 cm^3)	Mean dose (Gy)	Maximum dose (Gy)	Minimum dose (Gy)
Original plan	26.469	29.947	23.753
Reoptimized plan	26.326	28.950	24.170
Differences (Gy)	-0.143	-0.997	0.417
Percent differences (%)	-0.54	-3.329	1.76

Table 20 Comparison between Motor Cortex doses in the original and re-optimized plans for Volunteer 3

Active_Cortex (Volume: 3.3 cm^3)	Mean dose (Gy)	Maximum dose (Gy)	Minimum dose (Gy)
Original plan	0.963	2.420	0.082
Reoptimized plan	1.161	2.256	0.101
Differences (Gy)	0.198	-0.164	0.019
Percent differences (%)	20.6	-6.8	23.2

Table 21 Comparison between Cerebellum doses in the original and re-optimized plans for Volunteer 3

Active_Cerebellum (Volume: 0.1 cm^3)	Mean dose (Gy)	Maximum dose (Gy)	Minimum dose (Gy)
Original plan	0.051	0.056	0.046
Reoptimized plan	0.066	0.072	0.061
Differences (Gy)	0.015	0.016	0.015
Percent differences (%)	29.4	28.6	32.6

Volunteer 4

Table 22 Comparison between PTV doses in the original and re-optimized plans for Volunteer 4

PTV (Volume: 37 cm^3)	Mean dose (Gy)	Maximum dose (Gy)	Minimum dose (Gy)
Original plan	26.225	29.525	22.975
Reoptimized plan	26.125	29.600	23.250
Differences (Gy)	-0.100	0.075	0.275
Percent differences (%)	-0.381	0.254	1.20

Table 23 Comparison between Motor Cortex doses in the original and re-optimized plans for Volunteer 4

Active_Cortex (Volume: 26 cm^3)	Mean dose (Gy)	Maximum dose (Gy)	Minimum dose (Gy)
Original plan	3.500	16.275	0.325
Reoptimized plan	2.725	18.250	0.325
Differences (Gy)	-0.775	1.975	0
Percent differences (%)	-22.14	12.14	0

Table 24 Comparison between Cerebellum doses in the original and re-optimized plans for Volunteer 4

Active_Cerebellum (Volume: 5 cm^3)	Mean dose (Gy)	Maximum dose (Gy)	Minimum dose (Gy)
Original plan	0.225	0.550	0.125
Reoptimized plan	0.225	0.550	0.125
Differences (Gy)	0	0	0
Percent differences (%)	0	0	0

Volunteer 5

Table 25 Comparison between PTV doses in the original and re-optimized plans for Volunteer 5

PTV (Volume: 59.3 cm^3)	Mean dose (Gy)	Maximum dose (Gy)	Minimum dose (Gy)
Original plan	26.375	28.325	23.675
Reoptimized plan	26.575	30.000	23.100
Differences (Gy)	0.200	1.675	-0.575
Percent differences (%)	0.758	5.91	-2.429

Table 26 Comparison between Motor Cortex doses in the original and re-optimized plans for Volunteer 5

Active_Cortex (Volume: 34 cm^3)	Mean dose (Gy)	Maximum dose (Gy)	Minimum dose (Gy)
Original plan	6.650	23.800	0.450
Reoptimized plan	3.700	23.475	0.425
Differences (Gy)	-2.950	-0.325	-0.025
Percent differences (%)	-44.36	-1.37	-5.6

Table 27 Comparison between Cerebellum doses in the original and re-optimized plans for Volunteer 5

Active_Cerebellum (Volume: 4.7 cm^3)	Mean dose (Gy)	Maximum dose (Gy)	Minimum dose (Gy)
Original plan	0.300	1.775	0.200
Reoptimized plan	0.275	0.975	0.200
Differences (Gy)	-0.025	-0.800	0
Percent differences (%)	-8.3	-45.1	0

Volunteer 6

Table 28 Comparison between PTV doses in the original and re-optimized plans for Volunteer 6

PTV (Volume: 59.3 cm^3)	Mean dose (Gy)	Maximum dose (Gy)	Minimum dose (Gy)
Original plan	26.377	28.323	23.687
Reoptimized plan	26.570	30.001	23.110
Differences (Gy)	0.193	1.678	-0.577
Percent differences (%)	0.732	5.93	-2.436

Table 29 Comparison between Motor cortex doses in the original and re-optimized plans for Volunteer 6

Active_Cortex (Volume: 34 cm^3)	Mean dose (Gy)	Maximum dose (Gy)	Minimum dose (Gy)
Original plan	6.660	23.794	0.453
Reoptimized plan	3.707	23.475	0.430
Differences (Gy)	-2.953	-0.319	-0.023
Percent differences (%)	-44.34	-1.34	-5.1

Table 30 Comparison between Cerebellum doses in the original and re-optimized plans for Volunteer 6

Active_Cerebellum (Volume: 4.7 cm^3)	Mean dose (Gy)	Maximum dose (Gy)	Minimum dose (Gy)
Original plan	0.296	1.786	0.192
Reoptimized plan	0.284	0.981	0.204
Differences (Gy)	-0.012	-0.805	0.012
Percent differences (%)	-4.1	-45.07	6.1

Volunteer 7

Table 31 Comparison between PTV doses in the original and re-optimized plans for Volunteer 7

PTV (Volume: 3.7 cm^3)	Mean dose (Gy)	Maximum dose (Gy)	Minimum dose (Gy)
Original plan	26.120	27.349	24.126
Reoptimized plan	26.054	27.721	24.038
Differences (Gy)	-0.066	0.372	-0.080
Percent differences (%)	-0.253	1.36	-0.365

Table 32 Comparison between Motor cortex doses in the original and re-optimized plans for Volunteer 7

Active_Cortex (Volume: 3.9 cm^3)	Mean dose (Gy)	Maximum dose (Gy)	Minimum dose (Gy)
Original plan	0.686	1.069	0.163
Reoptimized plan	0.691	1.154	0.184
Differences (Gy)	0.005	0.085	0.0210
Percent differences (%)	0.7	7.9	12.9

Volunteer 8

Table 33 Comparison between PTV doses in the original and re-optimized plans for Volunteer 8

PTV (Volume: 5.7 cm³)	Mean dose (Gy)	Maximum dose (Gy)	Minimum dose (Gy)
Original plan	26.678	29.576	21.557
Reoptimized plan	26.635	29.660	22.748
Differences (Gy)	-0.043	0.084	1.191
Percent differences (%)	-0.16	0.284	5.53

Table 34 Comparison between Motor cortex doses in the original and re-optimized plans for Volunteer 8

Active_Cortex (Volume: 1.7 cm³)	Mean dose (Gy)	Maximum dose (Gy)	Minimum dose (Gy)
Original plan	12.789	23.018	4.405
Reoptimized plan	7.786	23.638	1.686
Differences (Gy)	-5.003	0.620	-2.719
Percent differences (%)	-39.120	2.694	-61.7

Volunteer 9

Table 35 Comparison between PTV doses in the original and re-optimized plans for Volunteer 9

PTV (Volume: 6.6 cm³)	Mean dose (Gy)	Maximum dose (Gy)	Minimum dose (Gy)
Original plan	25.915	27.391	23.798
Reoptimized plan	26.065	28.016	23.648
Differences (Gy)	0.150	0.625	-0.150
Percent differences (%)	0.58	2.282	-0.63

Table 36 Comparison between Motor cortex doses in the original and re-optimized plans for Volunteer 9

Active_Cortex (Volume: 3.5 cm³)	Mean dose (Gy)	Maximum dose (Gy)	Minimum dose (Gy)
Original plan	6.769	20.435	2.321
Reoptimized plan	2.510	17.859	0.834
Differences (Gy)	-4.259	-2.576	-1.487
Percent differences (%)	-62.9	-12.61	-64.1

Table 37 Comparison between Cerebellum doses in the original and re-optimized plans for Volunteer 9

Active_Cerebellum (Volume: 0.6 cm^3)	Mean dose (Gy)	Maximum dose (Gy)	Minimum dose (Gy)
Original plan	0.044	0.055	0.036
Reoptimized plan	0.045	0.059	0.036
Differences (Gy)	0.001	0.004	0
Percent differences (%)	2.3	7.3	0

Volunteer 10

Table 38 Comparison between PTV doses in the original and re-optimized plans for Volunteer 10

PTV (Volume: 9.6 cm^3)	Mean dose (Gy)	Maximum dose (Gy)	Minimum dose (Gy)
Original plan	26.783	31.420	23.413
Reoptimized plan	27.025	31.790	23.133
Differences (Gy)	0.242	0.370	-0.280
Percent differences (%)	0.90	1.18	-1.20

Table 39 Comparison between Motor cortex doses in the original and re-optimized plans for Volunteer 10

Active_Cortex (Volume: 4.1 cm^3)	Mean dose (Gy)	Maximum dose (Gy)	Minimum dose (Gy)
Original plan	11.906	24.863	1.5030
Reoptimized plan	3.360	24.349	0.876
Differences (Gy)	-8.546	-0.514	-0.627
Percent differences (%)	-71.78	-2.067	-41.78

Table 40 Comparison between Cerebellum doses in the original and re-optimized plans for Volunteer 10

Active_Cerebellum (Volume: 0.1 cm^3)	Mean dose (Gy)	Maximum dose (Gy)	Minimum dose (Gy)
Original plan	0.070	0.077	0.064
Reoptimized plan	0.071	0.079	0.065
Differences (Gy)	0.001	0.002	0.001
Percent differences (%)	1.4	2.6	1.6

Volunteer 11

Table 41 Comparison between PTV doses in the original and re-optimized plans for Volunteer 11

PTV (Volume: 2.3 cm³)	Mean dose (Gy)	Maximum dose (Gy)	Minimum dose (Gy)
Original plan	26.388	28.162	22.872
Reoptimized plan	26.302	28.372	22.947
Differences (Gy)	-0.086	0.210	0.075
Percent differences (%)	-0.326	0.75	0.328

Table 42 Comparison between Motor cortex doses in the original and re-optimized plans for Volunteer 11

Active_Cortex (Volume: 4.1 cm³)	Mean dose (Gy)	Maximum dose (Gy)	Minimum dose (Gy)
Original plan	0.028	0.041	0.018
Reoptimized plan	0.027	0.039	0.018
Differences (Gy)	-0.001	-0.002	0
Percent differences (%)	-3.6	-4.9	0

Table 43 Comparison between Cerebellum doses in the original and re-optimized plans for Volunteer 11

Active_Cerebellum (Volume: 0.1 cm³)	Mean dose (Gy)	Maximum dose (Gy)	Minimum dose (Gy)
Original plan	11.709	16.545	3.6940
Reoptimized plan	6.414	9.300	4.496
Differences (Gy)	-5.295	-7.245	0.802
Percent differences (%)	-45.222	-43.790	21.71

Volunteer 12

Table 44 Comparison between PTV doses in the original and re-optimized plans for Volunteer 12

PTV (Volume: 1.2 cm³)	Mean dose (Gy)	Maximum dose (Gy)	Minimum dose (Gy)
Original plan	26.503	29.162	23.678
Reoptimized plan	27.006	30.698	22.849
Differences (Gy)	0.503	1.536	-0.829
Percent differences (%)	1.898	5.27	-3.501

Table 45 Comparison between Motor cortex doses in the original and re-optimized plans for Volunteer 12

Active_Cortex (Volume: 9.6 cm^3)	Mean dose (Gy)	Maximum dose (Gy)	Minimum dose (Gy)
Original plan	0.287	10.236	0.039
Reoptimized plan	0.245	5.266	0.037
Differences (Gy)	-0.042	-4.970	-0.002
Percent differences (%)	-14.6	-48.55	-5.1

Table 46 Comparison between Cerebellum doses in the original and re-optimized plans for Volunteer 12

Active_Cerebellum (Volume: 0.2 cm^3)	Mean dose (Gy)	Maximum dose (Gy)	Minimum dose (Gy)
Original plan	0.053	0.064	0.044
Reoptimized plan	0.051	0.062	0.041
Differences (Gy)	-0.002	-0.002	-0.003
Percent differences (%)	-3.8	-3.1	-6.8

Volunteer 13

Table 47 Comparison between PTV doses in the original and re-optimized plans for Volunteer 13

PTV (Volume: 1 cm^3)	Mean dose (Gy)	Maximum dose (Gy)	Minimum dose (Gy)
Original plan	27.031	31.041	23.145
Reoptimized plan	26.304	29.474	23.586
Differences (Gy)	-0.727	-1.567	0.441
Percent differences (%)	-2.690	-5.05	1.91

Table 48 Comparison between Motor cortex doses in the original and re-optimized plans for Volunteer 13

Active_Cortex (Volume: 9.6 cm^3)	Mean dose (Gy)	Maximum dose (Gy)	Minimum dose (Gy)
Original plan	0.040	0.112	0.021
Reoptimized plan	0.040	0.109	0.021
Differences (Gy)	0	-0.003	0
Percent differences (%)	0	-2.8	0

Table 49 Comparison between Cerebellum doses in the original and re-optimized plans for Volunteer 13

Active_Cerebellum (Volume: 0.2 cm^3)	Mean dose (Gy)	Maximum dose (Gy)	Minimum dose (Gy)
Original plan	5.691	18.446	0.721
Reoptimized plan	4.980	10.919	0.917
Differences (Gy)	-0.711	-7.527	0.196
Percent differences (%)	-12.49	-40.806	27.2

Volunteer 14

Table 50 Comparison between PTV doses in the original and re-optimized plans for Volunteer 14

PTV (Volume: 3.4 cm^3)	Mean dose (Gy)	Maximum dose (Gy)	Minimum dose (Gy)
Original plan	26.895	30.978	23.735
Reoptimized plan	26.398	29.035	23.640
Differences (Gy)	-0.497	-1.943	-0.095
Percent differences (%)	-1.85	-6.27	-0.400

Table 51 Comparison between Motor cortex doses in the original and re-optimized plans for Volunteer 14

Active_Cortex (Volume: 0.8 cm^3)	Mean dose (Gy)	Maximum dose (Gy)	Minimum dose (Gy)
Original plan	8.185	16.711	1.8340
Reoptimized plan	6.748	17.812	1.666
Differences (Gy)	-1.437	1.101	-0.168
Percent differences (%)	-17.56	6.59	-9.2

Table 52 Comparison between Cerebellum doses in the original and re-optimized plans for Volunteer 14

Active_Cerebellum (Volume: 0.1 cm^3)	Mean dose (Gy)	Maximum dose (Gy)	Minimum dose (Gy)
Original plan	0.047	0.052	0.043
Reoptimized plan	0.046	0.050	0.042
Differences (Gy)	-0.001	-0.002	-0.001
Percent differences (%)	-2.1	-3.8	-2.3

Volunteer 15

Table 53 Comparison between PTV doses in the original and re-optimized plans for Volunteer 15

PTV (Volume: 35.7 cm^3)	Mean dose (Gy)	Maximum dose (Gy)	Minimum dose (Gy)
Original plan	26.324	30.819	23.717
Reoptimized plan	26.298	30.503	23.428
Differences (Gy)	-0.026	-0.316	-0.289
Percent differences (%)	-0.098	-1.03	-1.22

Table 54 Comparison between Motor cortex doses in the original and re-optimized plans for Volunteer 15

Activ_cortex (Volume: 5.4 cm^3)	Mean dose (Gy)	Maximum dose (Gy)	Minimum dose (Gy)
Original plan	4.660	11.553	0.575
Reoptimized plan	0.819	6.981	0.289
Differences (Gy)	-3.841	-4.572	-0.286
Percent differences (%)	-82.4	-39.57	-49.7

Table 55 Comparison between Cerebellum doses in the original and re-optimized plans for Volunteer 15

Activ_cerebellum (Volume: 0.7 cm^3)	Mean dose (Gy)	Maximum dose (Gy)	Minimum dose (Gy)
Original plan	0.119	0.164	0.093
Reoptimized plan	0.117	0.160	0.092
Differences (Gy)	-0.002	-0.004	-0.001
Percent differences (%)	-1.7	-2.4	-1.1

Summary of Results

Figure 30 summarizes the motor cortex and cerebellum mean doses in relation to the total prescribed dose, obtained in the original and re-optimized plans of all patients and volunteers.

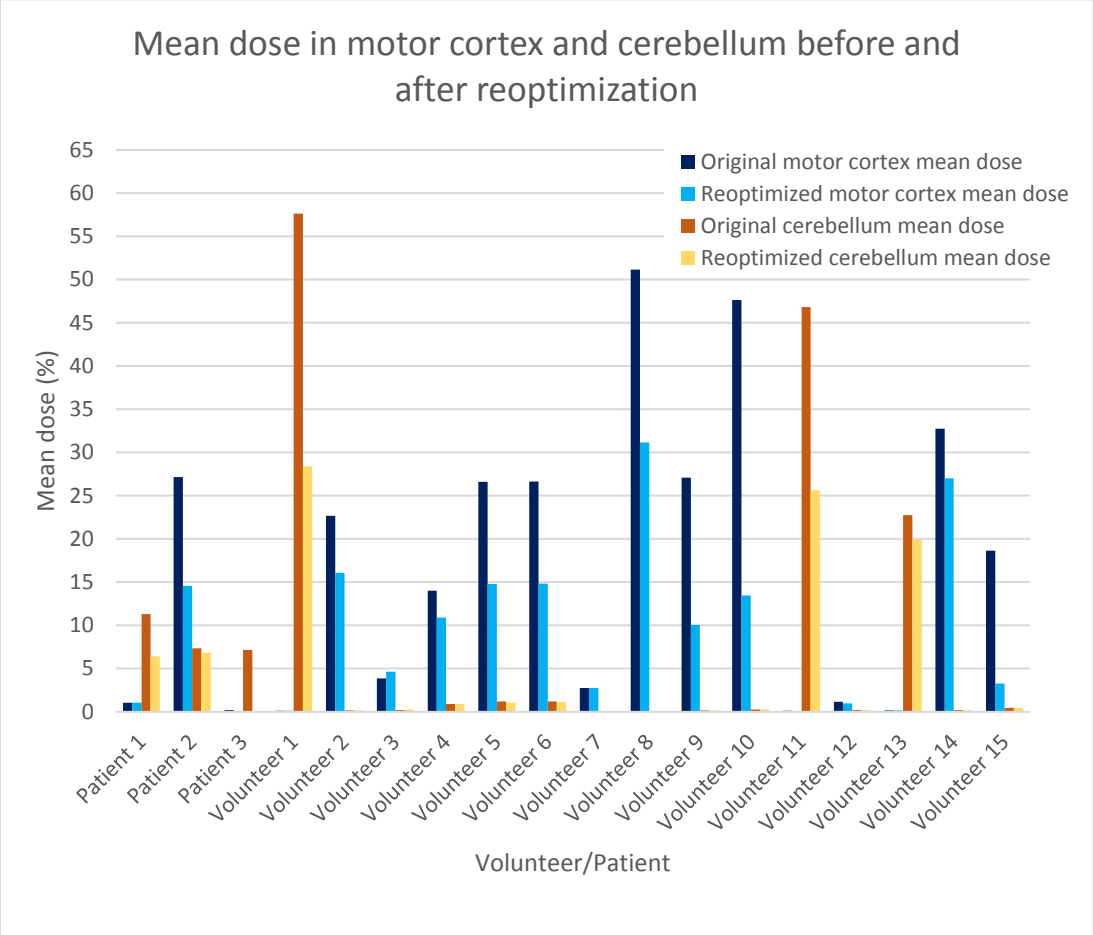

Fig. 30 Statistical representation of the mean dose in motor cortex and cerebellum in the original and re-optimized plans of all patients and volunteers.

8 - Discussion

8.1 – The paradigm for the study

The selection of the paradigm for this study aimed to obtain, with reproducibility, activations in cerebral regions close to the location of the benign tumor to be treated. For the MRI equipment available at IPO and the pathologies for the study, the paradigm selected was the motor task of continuous opening and closing of the hand.
Prior to the MRI acquisition, every volunteer participating in the study was carefully briefed about the paradigm to prevent the problem of the volunteer not knowing what to do during image acquisition.

When performing a study with volunteers, one should always consider the possibility of one or more of them performing the task incorrectly. If it was visually noticeable that the task was not being followed the data would be dismissed from the study.
By analyzing the resulting data from fMRI, visualizing the location of the activation region and basing on the good cooperation of the volunteers, it can be concluded that the paradigms were successfully performed.

One of the limitations of using a motor task as a paradigm is that it depends on the subject who performs it. To adjust to this limitation, in the selection of volunteers and patients who participated in this study their ability to cooperate and perform tasks was considered. Additionally, the paradigm was designed to be simple enough that everyone could accomplish it, because if the task was failed to be followed properly the resulting activation region would not be the desired one.

8.2 – fMRI acquisition sequence parameters

For our study, it was necessary to select the acquisition sequence and its parameters. The selected sequence was the EPI sequence which is the most commonly used sequence used for fMRI studies[59]. It was decided to perform it using the gradient-echo technique which, compared to the spin-echo technique, has higher BOLD sensitivity, imaging speed and versatility.

We used a 3T scanner, which represents an advantage in terms of image quality, because the higher the magnetic field intensity the higher the sensitivity, spatial resolution and SNR of the image[59]. For acquisition mode we chose a sequential slice acquisition over interleaved acquisition because the latter can be more vulnerable to the effects generated by head motion[59]. It was also decided that the acquisition would be performed head-to-foot over foot-to-head, where the latter is affected by excitation and saturation of in-flowing blood. The head-to-foot mode seemed to be the most favored of the two acquisition modes[59].

For full brain coverage we decided, as with typical fMRI acquisition for the same coverage, to use a repetition time (TR) of 3 s. To maximize BOLD contrast, we selected a typical time echo (TE) of 30 ms, suitable for a 3 T magnetic field. Another parameter that we decided to use with the typical value for 3 T fields was a matrix size of 64[59].

Lastly, the flip angle parameter we selected was 90º. This is the common choice for a TR of 3 s for 1.5 T field, while for 3 T with a TR of 2 s the commonly used angle is closer to 77º[59].

8.3 – Conversion and processing of the images

The files exported from the MRI machine are provided in DICOM format, which is not compatible with our chosen processing tool FSL. In the conversion from DICOM to NIFTI format the orientation of the images also needed to be considered, after an analysis of a simple file conversion that displayed incorrect orientation after imported to FSL. We decided to use the *mricron* tool to perform file conversion because it automatically identifies the orientation of DICOM files and proceeds with proper reorientation when converting the files to NIFTI format. After conversion, the files were imported and analyzed, comparing their new orientation with the desired one and confirmed that it was the correct one.

Once the files were properly converted and imported to FSL we started following the steps mentioned in chapter 6.2.1. During the BET step we needed to manually change many of the parameters shown in figure 9, such as the fractional intensity threshold and the threshold gradient, to obtain adequate brain extraction from the structural MRI to be used as the base for registration of the activations. Limitation of this step that we came across was that it was not possible to use fixed values of the parameters for every patient

and volunteer of the study because, in most cases, the brain was not extracted as a whole, missing parts of the cerebellum or the edges of the brain closer to the bone. This limitation led us to perform multiple brain extractions with different parameters for each case, until an acceptable image was achieved. However, this means that the parameters chosen to achieve the most acceptable image for registration were based on our empirical analysis of the images.

During the FEAT step we had to consider many parameters for processing the fMRI data. For the pre-processing parameters (figure 11) we started by selecting the default motion correction of FSL, *MCFLIRT*. Considering that each fMRI 4D image series is composed of 41 volumes (each composed of 100 images), this motion correction tool performs a comparison between the middle volume and the adjacent volume and creates a transformation to match the adjacent to the middle volume. The transformation created will then be used to estimate a transformation between the middle volume and the volumes beyond the adjacent one to match every volume of the data to the middle volume. For the slice timing correction parameter, we choose the *regular up* for slices that were acquired sequentially. The spatial smoothing parameter used was the one that showed the greatest impact on the resulting images (example in Figure 18). As previously referred in chapter 7, this parameter defines a distance between half values and performs a data averaging in the nearby voxels. This will increase the image signal-to-noise ratio (SNR) because any present signal will be averaged and summed, while the noise, expectedly random, will be canceled. We wanted to keep the spatial smoothing value high enough to increase our SNR, but the tradeoff is that higher values will perform spatial smoothing in larger areas of the brain, reducing the spatial resolution. The value we decided to use in this parameter was 5 mm to guarantee that minor activations in the cerebellum could still be properly localized and identified.

The next parameters considered were the registration parameters (Figure 12). These parameters have a high impact on the total processing time. At this stage the acquired BET image was used as main structural image, where activations will be registered. After experimenting with the different options and comparing them, we chose a normal search in 6 degrees of freedom (DoF) for the main structural and did not change the default standard space search. The processing time for the selected parameters was on average 5 min for each time FEAT was performed.

In the Stats parameters of the processing (Figure 13) we used the model setup wizard of the tool (Figure 14) to define the activation and rest periods of the signal being processed, to match the selected paradigm (Figure 6). This step defines which activations from the fMRI data occurred during the activation period and which ones occurred during the rest period.

In the final step of the processing are the Post-stats parameters. With the help of a radiologist we defined a threshold value for the Z-score, individually suited for each fMRI series processed. This parameter is responsible for determining which voxels were activated during the paradigm. When selecting a threshold value for Z, voxels with a score equal or above the threshold will be considered "fMRI-activated", while activations on voxels with a score below the threshold will be eliminated. A limitation for the selection of this parameter is that it cannot be a fixed parameter for every image series processed, because the intensity of the activations depends on multiple variables for people undergoing fMRI. Their dominant hand versus the hand used in the study, their age and the intensity of the task performed are examples of variables that may affect the activation intensity. Another limitation is that the selected Z threshold was based on the radiologist's empirical analysis, where in some cases small increases or decreases in the selected value had no major impact on the activations.

In order to be able to utilize the resulting images from fMRI processing it was necessary to reconvert them from NIFTI to DICOM, the compatible format for the treatment planning system. Just as we initially needed to change both the image format and orientation to match the FSL visualization, we had to re-orient the image to the initial orientation. We used MATLAB to perform this re-orientation and reconversion. For this study, the images processed by the FSL achieve their purpose regardless of the type of image TPS recognizes during import. With that in mind, we used a default CT header template and converted the images to CT-like images (changing the header information without changing the actual image data). This manipulation allowed us to import the fMRI images into TPS with no errors. Additionally, this conversion has no impact on the results obtained because the imported images were used exclusively for the creation and delineation of the new functional OARs in the treatment plan.

8.4 – Experimental Results

We have integrated the fMRI data, obtained in the course of the present thesis, into our radiosurgery treatment planning. With this data, new functional OARs were delineated using activation maps fused with a structural MRI that was registered to the patient's CT, prior to the treatment planning step. Using an inverse planning algorithm, a first plan was created with maximum allowed doses assigned to the target and critical volumes, excluding the new fOARs, following the rigorous clinical goals of radiosurgery. A copy of this first plan was subsequently reoptimized to consider the new fOARs as a critical region to be preserved. In the initial phase of the study the optimization parameter we selected to reduce the dose in the fOARs to a maximum dose limit was different for each patient: 4 Gy for the entire activated cerebellum volume and 2 Gy for the entire activated motor cortex for patient 1; 7 Gy for the entire activated cerebellum volume and for 40% of the activated motor cortex volume, respectively, for patient 2. Later in the study we decided for volunteers should use optimization parameters that would ensure the proper PTV dose coverage and reduce the dose in the fOARs as much as possible, without affecting the radiosurgery treatment.

During patient planning, only patient 1 and 2 treatment plans were re-optimized because patient 3 fOARs were too far away from PTV to have any impact in the plan re-optimization. After that re-optimization, the mean doses delivered to patient 1 fOARs of patient 1 decreased up to 43.12% in the cerebellum while no reduction occurred in the motor cortex because the doses were already below the maximum optimization and had no impact in the new plan. For patient 2, the mean doses in fOARs reduced up to 6.784% in the cerebellum and up to 46.32 % in the motor cortex. After the integration of the fMRI data in the treatment plan of the volunteers, the mean doses delivered to these critical regions decreased between 2.13 up to 50.77% in the cerebellum and between 3.57 and 82.42% in the motor cortex. These results can be compared with the range of results for mean dose reductions in the motor cortex between 12.5% and 63% obtained in the studies referred in chapter 1.1[16]

Because we did not exclusively delineate critical regions (motor cortex and cerebellum activations) close to the PTV and included other possible cases for the localization of the pathologies under study (mainly meningiomas), there are some volunteer cases where the activated regions did not have a dose reduction, not being affected by the treatment

fields, or had a negative impact in re-optimization. For example, in volunteer 3 (Tables 19 and 20) optimization showed a dose increase in the critical regions.
However, in critical regions near PTV, the dose reductions that can be achieved with the integration of fMRI data in the radiosurgery planning may be sufficient to reduce the probability of radiation induced complications, as intended in the optimization of all treatment plans.

8.5 – Integration of fMRI data in radiosurgery treatment planning

The fMRI images we processed were imported to the TPS with no complications, ensuring that images were properly reconverted. The fusion between the fMRI data and the structural MRI facilitated the dosimetrist's work in the registration of the image imported with the CT where the areas of interest for the treatment are delineated. This registration was performed manually by the dosimetrist using the structural MRI as a reference. For the delineation of fOARs, we had to manually contour them slice by slice because the TPS does not automatically identify the functional regions, and manual contouring ensures a proper fOAR delineation in all slices.

We were able to implement the fMRI data in plan optimization and to achieve mean dose reductions in the critical regions studied. There were some limitations and difficulties regarding the fMRI images used in the integration, like spatial accuracy and registration of the activations with the structural MRI, as well as the choice of Z threshold used in the processing of these images being of empirical nature of the professionals who helped with this step. The determination and quantification of the benefits for the patients from these dose reductions is also difficult to establish. However, despite these limitations, the simplification of integration of fMRI data in the treatment planning and the impact on the doses to critical regions in the treatment of benign tumors has shown to have potential benefits for patients undergoing radiosurgical treatment.

8.6 – Future perspectives for the study

The design of the paradigm selected for this study was limited by the equipment available at IPO facilities, which only allowed us to perform simple motor task paradigms. From the analysis to the results obtained, in some clinical cases presented, a different choice of paradigm (for example, speech, visual or memory) could allow activations closer to the tumor lesions. In the future it would be of interest to include other benign pathologies

in this study, designing and performing paradigms that produce activations in locations better suited for these benign pathologies, possibly achieving better results and drawing new conclusions on the importance of the integration of fMRI in radiosurgery treatment planning for benign tumors.

Another goal that can be considered for the future of this study is the optimization of the reconversion code in MATLAB to include the original header of the fMRI DICOM file to enable its utilization in the reconversion of files that require their header.

Further studies on dose tolerance in functional areas would be of great interest to determine proper optimization parameters for dose constraints in the fOARs treatment plan.

9 – Conclusion

This present dissertation aimed to integrate functional neuroimaging into LINAC radiosurgery treatment planning in a Radiotherapy department already performing routine radiosurgery treatments, as well as to create guidelines with all the necessary steps for the processing of fMRI data using FSL.

The data processed with FSL were imported without complication to TPS and it permitted the fMRI data of the motor task to be used in the delineation of new critical regions for treatment plan optimization. The results of this optimization showed a reduction in the mean doses in the fOARs from 2.13 to 50.77 % in the cerebellum and from 3.57 to 82.42% in the motor cortex. It can be concluded from the obtained results that the functional neuroimaging data was successfully integrated in the radiosurgery treatment planning after the correct processing of the functional images and proved to be beneficial in the treatment of the patients, allowing a better preservation of the critical regions.

From the results of this dissertation it can be also concluded that the integration of fMRI in the treatment planning of benign tumors shows potential to improve the quality of life of patients undergoing radiosurgery and deserves further research on the subject.

References

1- Pauling, L. and Coryell, C. (1936). The Magnetic Properties and Structure of Hemoglobin, Oxyhemoglobin and Carbonmonoxyhemoglobin. *Proceedings of the National Academy of Sciences*, 22(4), pp.210-216.

2- Ogawa, S., Lee, T., Kay, A. and Tank, D. (1990). Brain magnetic resonance imaging with contrast dependent on blood oxygenation. *Proceedings of the National Academy of Sciences*, 87(24), pp.9868-9872.

3- Belliveau, J., Kennedy, D., McKinstry, R., Buchbinder, B., Weisskoff, R., Cohen, M., Vevea, J., Brady, T. and Rosen, B. (1991). Functional mapping of the human visual cortex by magnetic resonance imaging. *Science*, 254(5032), pp.716-719.

4- S. Ogawa et al., "Intrinsic signal changes accompanying sensory stimulation: functional brain mapping with magnetic resonance imaging.", *Proceedings of the National Academy of Sciences*, vol. 89, no. 13, pp. 5951-5955, 1992.

5- K. Kwong et al., "Dynamic magnetic resonance imaging of human brain activity during primary sensory stimulation.", *Proceedings of the National Academy of Sciences*, vol. 89, no. 12, pp. 5675-5679, 1992.

6- L. Leksell, "Stereotactic radiosurgery.", *Journal of Neurology, Neurosurgery & Psychiatry*, vol. 46, no. 9, pp. 797-803, 1983.

7- Leksell L., “The stereotaxic method and radiosurgery of the brain”, Acta Chir. Scand., pp.316-9, 1951.

8- T. Witt, D. Kondziolka, S. Baumann, D. Noll, S. Small and L. Lunsford, "Preoperative Cortical Localization with Functional MRI for Use in Stereotactic Radiosurgery", *Stereotactic and Functional Neurosurgery*, vol. 66, no. 1-3, pp. 24-29, 1996.

9- R. Garcia-Alvarez, G. Liney and A. Beavis, "Repeatability of functional MRI for conformal avoidance radiotherapy planning", *Journal of Magnetic Resonance Imaging*, vol. 23, no. 2, pp. 108-114, 2006.

10- J. Stancanello et al., "BOLD FMRI integration into radiosurgery treatment planning of cerebral vascular malformations", *Medical Physics*, vol. 34, no. 4, pp. 1176-1184, 2007.

11- E. Pantelis et al., "Integration of Functional MRI and White Matter Tractography in Stereotactic Radiosurgery Clinical Practice", *International Journal of Radiation Oncology*Biology*Physics*, vol. 78, no. 1, pp. 257-267, 2010.

12- Á. Kovács et al., "Integrating functional MRI information into conventional 3D radiotherapy planning of CNS tumors. Is it worth it?", *Journal of Neuro-Oncology*, vol. 105, no. 3, pp. 629-637, 2011.

13- A. Conti et al., "Integration of functional neuroimaging in CyberKnife radiosurgery: feasibility and dosimetric results", *Neurosurgical Focus*, vol. 34, no. 4, p. E5, 2013.

14- M. Wang et al., "Integration of BOLD-fMRI and DTI into radiation treatment planning for high-grade gliomas located near the primary motor cortexes and corticospinal tracts", *Radiation Oncology*, vol. 10, no. 1, 2015.

15- L. Sun et al., "Integration of Functional MRI and White Matter Tractography in CyberKnife Radiosurgery", *Technology in Cancer Research & Treatment*, vol. 16, no. 6, pp. 850-856, 2017.

16- E. De Martin et al., "Integration of Functional Magnetic Resonance Imaging and Magnetoencephalography Functional Maps Into a CyberKnife Planning System: Feasibility Study for Motor Activity Localization and Dose Planning", *World Neurosurgery*, vol. 108, pp. 756-762, 2017.

17- P. A. Rinck, *Magnetic Resonance in Medicine*, 4th edition: in chapter twenty An Excursion into the History of MR Imaging, Blackwell Science (2001)

18- R. R. Edelman, J. Hesselink, M. Zlatkin, R. Irwan, and M. Oudkerk, *Clinical Magnetic Resonance Imaging: in chapter 1 History of Magnetic Resonance*, 3rd ed., vol. 1, 3 vols. Saunders, 2006.

19- L. Shah, J. Anderson, J. Lee and R. Wiggins, "Functional Magnetic Resonance Imaging", *Seminars in Roentgenology*, vol. 45, no. 2, pp. 147-156, 2010.

20- Kim MJJ, Holodny AI, Hou BL, Peck KK, Moskowitz CS, Bogomolny DL, Gutin PH. “The Effect of Prior Surgery on Blood Oxygen Level-Dependent MR Imaging in the Preoperative Assessment of Brain Tumors”, *American journal of neuroradiology*, vol. 26, no.8, pp. 1980-85, 2005

21- E. Vlieger, C. Majoie, S. Leenstra and G. den Heeten, "Functional magnetic resonance imaging for neurosurgical planning in neurooncology", *European Radiology*, vol. 14, no. 7, pp. 1143-1153, 2004.

22- Stippich C, editors. Clinical Functional MRI: Presurgical functional neuroimaging. New York-Heidelber-Tokyo:Springer;2007.

23- Zhi-Pei Liang, Paul C. Lauterbur, *Principles of Magnetic Resonance Imaging – A Signal Processing Perspective*, IEEE Press (2000)

24- J. Bushberg, J. Seibert, E. Leidholdt, J. Boone, *The Essential Physics of Medical Imaging*, Lippincott Williams & Wilkins, 2002

25- P.Reimer, P. M. Parizel, F. A. Stichnoth, "*Clinical MR Imaging – A Pratical Approach", Springer, 2006.*

26- "*Ressonância Magnética: Princípios de formação da imagem e aplicações em imagem funcional*" *Revista Brasileira de Física Médica*, vol. 3, no. 1, pp. 117–129, 2009.

27- Huettel S.A, Song A.W, MaCarthy G. Functional Magnetic Resonance Imaging. Sinauer Associates. 2004.

28- Cohen MS (2000) Echo-Planar Imaging and Functional MRI. In: Moonen CTW, Bandettini PA (eds) Functional MRI. Springer-Verlag, Berlin Heidelberg, pp 137–148

29- Poustchi-amin M, Mirowitz SA, Brown JJ et-al. "Principles and applications of echo-planar imaging: a review for the general radiologist.", Radiographics, vol. 21, no. 3, pp. 767-779, 2001

30- https://www.radiologycafe.com/radiology-trainees/frcr-physics-notes/gradient-recalled-echo-sequence

31- P. Jezzard, P. M. Matthews, and S. M. Smith, Eds., Functional MRI: An Introduction to Methods, 1st ed. Oxford University Press, USA, 2002. 31

32- James, J. S., Rajesh, P., Chandran, A. V., and Kesavadas, C. "fMRI paradigm designing and post-processing tools.", *Indian Journal of Radiology and* Imaging, vol. 24, no. 1, pp. 13–21, 2014

33- J. Kornak, D. A. Hall and M. P. Haggard, "Spatially Extended fMRI Signal Response to Stimulus in Non-Functionally Relevant Regions of the Human Brain: Preliminary Results.", Open Neuroimaging Jounal, vol. 5, pp. 24-323, 2011.

34- Jaakko Malmivuo, Robert Plonsey, "Bioelectromagnetism – Principles and Applications of Bioelectric and Biomagnetic Fields", Oxford University Press, 1995

35- Jawabri KH, Sharma S. "Physiology, Cerebral Cortex Functions.", *StatPearls [Internet]. Treasure Island (FL): StatPearls Publishing*, 2019.

36- Arslan, Orhan E. Neuroanatomical basis of clinical neurology. 2nd edition CRC Press, 2014.

37- Standring, Susan, et al. "Gray's anatomy: the anatomical basis of clinical practice.", *American Journal of Neuroradiology*, vol. 26, no.10, pp. 2703, 2005

38- http://www.mayfieldclinic.com/pe-anatbrain.htm

39- Schlerf, John E., et al. "Laterality differences in cerebellar–motor cortex connectivity." *Cerebral cortex*, vol. 25, no. 7, pp.1827-1834, 2014

40- Daskalakis, Zafiris J., et al. "Exploring the connectivity between the cerebellum and motor cortex in humans." *The Journal of physiology*, vol. 557, no. 2, pp. 689-700, 2004

41- https://fulcrumconnection.com/blog/

42- Claus EB *et al*. “Epidemiology of intracranial meningioma.” *Neurosurgery* vol. 57, no. 6, pp. 1088–1095, 2005

43- Wiemels J, Wrensch M, Claus EB. “Epidemiology and etiology of meningioma”, *Journal of neuro-oncology*, vol. 99, no. 3, pp. 307-314, 2010.

44- Marosi C, Hassler M, Roessler K, Reni M, Sant M, Mazza E, Vecht C, “Meningioma.” *Critical reviews in oncology and hematology*, vol. 67, no. 2, pp. 153–171, 2008

45- Kumar, V, Abbas, AK, Fausto. “*Pathologic Basis of Disease”*, *V Kumar, AK Abbas, N Fausto (eds). Elsevier Saunders: Philadelphia, PA*, pp. 87-118, 2005.

46- Scheithauer BW, Kovacs KT, Laws Jr ER, Randall RV, “Pathology of invasive pituitary tumors with special reference to functional classification.” *Journal of neurosurgery*, vol. 65, no. 6, pp. 733–744, 1986

47- Asa, SL, Ezzat, S., “The cytogenesis and pathogenesis of pituitary adenomas.”, *Endocrine* reviews, vol. 19, no. 6, pp. 798-827, 1998

48- Chin, Lawrence S., and William F. Regine, eds. “*Principles and practice of stereotactic radiosurgery*.” Springer Science & Business Media, 2010.

49- Deodato F, Cilla S, Macchia G, Torre G, Caravatta L, Mariano G, et al. “Stereotactic Radiosurgery (SRS) with Volumetric Modulated Arc Therapy (VMAT): Interim Results of a Multi-arm Phase I Trial (DESTROY-2).” *Clinical Oncology*, vol. 26, no. 12, pp. 748–756, 2014.

50- ICRU report 91

51- Clark GM , Popple RA , Young PE , Fiveash JB . “Feasibility of single-isocenter volumetric modulated arc radiosurgery for treatment of multiple brain metastases.” *International Journal of Radiation Oncology* Biology* Physics*, vol.76, no.1, pp. 296–302, 2010.

52- https://www.varian.com/pt-pt/oncology/treatment-techniques/external-beam-radiation/vmat

53- Wolff, Hendrik A., et al. "Single fraction radiosurgery using Rapid Arc for treatment of intracranial targets." *Radiation Oncology*, vol. 5, no. 1, pp. 77, 2010.

54- https://www.brainlab.com/radiosurgery-products/exactrac/

55- http://www3.gehealthcare.in/en/products/categories/magnetic-resonance-imaging/signa-hdxt-3-0t

56- https://fsl.fmrib.ox.ac.uk/fsl/fslwiki

57- S.M. Smith, M. Jenkinson, M.W. Woolrich, C.F. Beckmann, T.E.J. Behrens, H. Johansen-Berg, P.R. Bannister, M. De Luca, I. Drobnjak, D.E. Flitney, R. Niazy, J. Saunders, J. Vickers, Y. Zhang, N. De Stefano, J.M. Brady, and P.M. Matthews. “Advances in functional and structural MR image analysis and implementation as FSL.” *NeuroImage*, vol. 23, pp. S208-S219, 2004

58- https://www.mathworks.com/help/

59- Soares J. M., Magalhães R., Moreira P. S., Sousa A., Ganz E., Sampaio A., et al. “A hitchhiker’s guide to functional magnetic resonance imaging.” *Frontiers in Neuroscience*, vol. 10, pp. 515, 2016

Appendix A

Patient 1

Table A. 1 Comparison between Brain doses in the original and re-optimized plans for Patient 1

Brain (Volume: 962.9 cm^3)	Mean dose (Gy)	Maximum dose (Gy)	Minimum dose (Gy)
Original plan	6.160	60.704	0.280
Reoptimized plan	6.440	62.664	0.280
Differences (Gy)	0.280	1.960	0
Percent differences (%)	4.55	3.229	0

Table A. 2 Comparison between Brainstem doses in the original and re-optimized plans for Patient 1

Brainstem (Volume: 25.9 cm^3)	Mean dose (Gy)	Maximum dose (Gy)	Minimum dose (Gy)
Original plan	14.280	47.152	0.672
Reoptimized plan	12.880	46.872	0.672
Differences (Gy)	-1.400	-0.280	0
Percent differences (%)	-9.80	-0.59	0

Table A. 3 Comparison between Chiasm doses in the original and re-optimized plans for Patient 1

Chiasm (Volume: 0.1 cm^3)	Mean dose (Gy)	Maximum dose (Gy)	Minimum dose (Gy)
Original plan	23.184	41.832	13.552
Reoptimized plan	23.128	42.000	13.048
Differences (Gy)	-0.056	0.168	-0.504
Percent differences (%)	-0.242	0.402	-3.719

Table A. 4 Comparison between Left Eye doses in the original and re-optimized plans for Patient 1

Left Eye (Volume: 12.5 cm^3)	Mean dose (Gy)	Maximum dose (Gy)	Minimum dose (Gy)
Original plan	34.496	57.008	0
Reoptimized plan	37.296	59.360	0
Differences (Gy)	2.800	2.352	0
Percent differences (%)	8.12	4.126	0

Table A. 5 Comparison between Right Eye doses in the original and re-optimized plans for Patient 1

Right Eye (Volume: 11.8 cm^3)	Mean dose (Gy)	Maximum dose (Gy)	Minimum dose (Gy)
Original plan	3.472	9.016	0
Reoptimized plan	3.920	9.240	0
Differences (Gy)	0.448	0.224	0
Percent differences (%)	12.9	2.48	0

Table A. 6 Comparison between Hippocampus doses in the original and re-optimized plans for Patient 1

Hippocampus (Volume: 4.1 cm^3)	Mean dose (Gy)	Maximum dose (Gy)	Minimum dose (Gy)
Original plan	28.168	51.072	13.832
Reoptimized plan	27.608	48.272	15.960
Differences (Gy)	-0.560	-2.800	2.128
Percent differences (%)	-1.988	-5.48	15.38

Table A. 7 Comparison between Right Optic Nerve doses in the original and re-optimized plans for Patient 1

Right Optic Nerve (Volume: 1.4 cm^3)	Mean dose (Gy)	Maximum dose (Gy)	Minimum dose (Gy)
Original plan	11.536	21.672	4.256
Reoptimized plan	14.000	23.968	4.816
Differences (Gy)	2.464	2.296	0.560
Percent differences (%)	21.36	10.59	13.16

Table A. 8 Comparison between Pituitary Gland doses in the original and re-optimized plans for Patient 1

Pituitary Gland (Volume: 0.5 cm^3)	Mean dose (Gy)	Maximum dose (Gy)	Minimum dose (Gy)
Original plan	26.824	58.632	12.880
Reoptimized plan	25.760	56.728	12.600
Differences (Gy)	-1.064	-1.904	-0.280
Percent differences (%)	-3.967	-3.247	-2.17

Patient 2

Table A. 9 Comparison between Brain doses in the original and re-optimized plans for Patient 2

Brain (Volume: 1240.5 cm^3)	Mean dose (Gy)	Maximum dose (Gy)	Minimum dose (Gy)
Original plan	17.690	58.616	0.532
Reoptimized plan	16.599	59.003	0.505
Differences (Gy)	-1.091	0.387	-0.027
Percent differences (%)	-6.17	0.66	-5.1

Table A. 10 Comparison between Brainstem doses in the original and re-optimized plans for Patient 2

Brainstem (Volume: 32.5 cm^3)	Mean dose (Gy)	Maximum dose (Gy)	Minimum dose (Gy)
Original plan	7.150	21.219	0.684
Reoptimized plan	6.405	20.429	0.657
Differences (Gy)	-0.745	-0.790	-0.027
Percent differences (%)	-10.42	-3.723	-3.9

Table A. 11 Comparison between Chiasm doses in the original and re-optimized plans for Patient 2

Chiasm (Volume: 0.2 cm^3)	Mean dose (Gy)	Maximum dose (Gy)	Minimum dose (Gy)
Original plan	15.844	18.947	13.833
Reoptimized plan	15.599	20.015	11.987
Differences (Gy)	-0.245	1.068	-1.846
Percent differences (%)	-1.55	5.64	-13.34

Table A. 12 Comparison between Left Eye doses in the original and re-optimized plans for Patient 2

Left Eye (Volume: 9.8 cm^3)	Mean dose (Gy)	Maximum dose (Gy)	Minimum dose (Gy)
Original plan	12.463	23.864	0
Reoptimized plan	12.564	24.077	0
Differences (Gy)	0.101	0.213	0
Percent differences (%)	0.81	0.89	0

Table A. 13 Comparison between Right Eye doses in the original and re-optimized plans for Patient 2

Right Eye (Volume: 10.3 cm^3)	Mean dose (Gy)	Maximum dose (Gy)	Minimum dose (Gy)
Original plan	11.458	23.931	0
Reoptimized plan	11.036	24.432	0
Differences (Gy)	-0.422	0.501	0
Percent differences (%)	-3.68	2.094	0

Table A. 14 Comparison between Hippocampus doses in the original and re-optimized plans for Patient 2

Hippocampus (Volume: 7.1 cm^3)	Mean dose (Gy)	Maximum dose (Gy)	Minimum dose (Gy)
Original plan	6.694	15.386	3.553
Reoptimized plan	6.631	16.259	3.388
Differences (Gy)	-0.063	0.873	-0.165
Percent differences (%)	-0.94	5.67	-4.64

Table A. 15 Comparison between Left Optic Nerve doses in the original and re-optimized plans for Patient 2

Left Optic Nerve (Volume: 0.9 cm^3)	Mean dose (Gy)	Maximum dose (Gy)	Minimum dose (Gy)
Original plan	34.911	47.037	17.026
Reoptimized plan	34.898	47.044	18.347
Differences (Gy)	-0.013	0.007	1.321
Percent differences (%)	-0.04	0.01	7.76

Table A. 16 Comparison between Right Optic Nerve doses in the original and re-optimized plans for Patient 2

Right Optic Nerve (Volume: 0.8 cm^3)	Mean dose (Gy)	Maximum dose (Gy)	Minimum dose (Gy)
Original plan	32.550	40.863	17.643
Reoptimized plan	32.775	40.750	15.969
Differences (Gy)	0.225	-0.113	-1.674
Percent differences (%)	0.69	-0.277	-9.49

Table A. 17 Comparison between Pituitary Gland doses in the original and re-optimized plans for Patient 2

Pituitary Gland (Volume: 0.9 cm^3)	Mean dose (Gy)	Maximum dose (Gy)	Minimum dose (Gy)
Original plan	12.386	17.668	8.883
Reoptimized plan	12.696	17.933	8.986
Differences (Gy)	0.310	0.265	0.103
Percent differences (%)	2.50	1.50	1.16

Patient 3

Table A. 18 Brain doses in the original for Patient 3

Brain (Volume: 1233 cm^3)	Mean dose (Gy)	Maximum dose (Gy)	Minimum dose (Gy)
Original plan	2.099	53.204	0.057

Table A. 19 Brainstem doses in the original plan for Patient 3

Brainstem (Volume: 29.2 cm^3)	Mean dose (Gy)	Maximum dose (Gy)	Minimum dose (Gy)
Original plan	9.847	52.255	0.375

Table A. 20 Chiasm doses in the original plan for Patient 3

Chiasm (Volume: 0.3 cm^3)	Mean dose (Gy)	Maximum dose (Gy)	Minimum dose (Gy)
Original plan	35.187	51.217	17.365

Table A. 21 Left Eye doses in the original plan for Patient 3

Left Eye (Volume: 11 cm^3)	Mean dose (Gy)	Maximum dose (Gy)	Minimum dose (Gy)
Original plan	1.503	2.971	0.081

Table A. 22 Right Eye doses in the original plan for Patient 3

Right Eye (Volume: 11.5 cm^3)	Mean dose (Gy)	Maximum dose (Gy)	Minimum dose (Gy)
Original plan	1.456	2.947	0.621

Table A. 23 Hippocampus doses in the original plan for Patient 3

Hippocampus (Volume: 6.5 cm^3)	Mean dose (Gy)	Maximum dose (Gy)	Minimum dose (Gy)
Original plan	5.469	20.644	0.683

Table A. 24 Left Optic Nerve doses in the original plan for Patient 3

Left Optic Nerve (Volume: 1.5 cm^3)	Mean dose (Gy)	Maximum dose (Gy)	Minimum dose (Gy)
Original plan	7.877	45.169	1.397

Table A. 25 Right Optic Nerve doses in the original plan for Patient 3

Right Optic Nerve (Volume: 1.5 cm^3)	Mean dose (Gy)	Maximum dose (Gy)	Minimum dose (Gy)
Original plan	6.96	46.254	1.443

Volunteer 1

Table A. 26 Comparison between Brain doses in the original and re-optimized plans for Volunteer 1

Brain (Volume: 2891 cm^3)	Mean dose (Gy)	Maximum dose (Gy)	Minimum dose (Gy)
Original plan	0.424	28.258	0.003
Reoptimized plan	0.452	27.944	0.003
Differences (Gy)	0.028	-0.314	0
Percent differences (%)	7	-1.11	0

Table A. 27 Comparison between Brainstem doses in the original and re-optimized plans for Volunteer 1

Brainstem (Volume: 24.8 cm^3)	Mean dose (Gy)	Maximum dose (Gy)	Minimum dose (Gy)
Original plan	1.593	7.409	0.079
Reoptimized plan	2.151	10.551	0.083
Differences (Gy)	0.558	3.142	0.004
Percent differences (%)	35.03	42.41	5

Table A. 28 Comparison between Chiasm doses in the original and re-optimized plans for Volunteer 1

Chiasm (Volume: 0.2 cm^3)	Mean dose (Gy)	Maximum dose (Gy)	Minimum dose (Gy)
Original plan	2.323	3.637	1.521
Reoptimized plan	2.690	3.255	1.723
Differences (Gy)	0.367	-0.382	0.202
Percent differences (%)	15.8	-10.5	13.3

Table A. 29 Comparison between Left Eye doses in the original and re-optimized plans for Volunteer 1

Left Eye (Volume: 9.9 cm^3)	Mean dose (Gy)	Maximum dose (Gy)	Minimum dose (Gy)
Original plan	0.561	1.512	0.078
Reoptimized plan	0.638	1.775	0.088
Differences (Gy)	0.077	0.263	0.010
Percent differences (%)	13.7	17.4	13

Table A. 30 Comparison between Right Eye doses in the original and re-optimized plans for Volunteer 1

Right Eye (Volume: 9.1 cm^3)	Mean dose (Gy)	Maximum dose (Gy)	Minimum dose (Gy)
Original plan	0.397	1.288	0.038
Reoptimized plan	0.482	1.957	0.044
Differences (Gy)	0.085	0.669	0.006
Percent differences (%)	21.4	51.9	16

Table A. 31 Comparison between Hippocampus doses in the original and re-optimized plans for Volunteer 1

Hippocampus (Volume: 4.9 cm^3)	Mean dose (Gy)	Maximum dose (Gy)	Minimum dose (Gy)
Original plan	1.138	6.137	0.125
Reoptimized plan	1.535	6.631	0.132
Differences (Gy)	0.397	0.494	0.007
Percent differences (%)	34.9	8.0	6

Table A. 32 Comparison between Left Optic Nerve doses in the original and re-optimized plans for Volunteer 1

Left Optic Nerve (Volume: 0.2 cm^3)	Mean dose (Gy)	Maximum dose (Gy)	Minimum dose (Gy)
Original plan	1.538	2.090	0.723
Reoptimized plan	2.097	3.144	0.689
Differences (Gy)	0.559	1.054	-0.034
Percent differences (%)	36.35	50.4	-5

Table A. 33 Comparison between Right Optic Nerve doses in the original and re-optimized plans for Volunteer 1

Right Optic Nerve (Volume: 0.2 cm^3)	Mean dose (Gy)	Maximum dose (Gy)	Minimum dose (Gy)
Original plan	2.374	3.711	0.935
Reoptimized plan	2.466	3.136	1.363
Differences (Gy)	0.092	-0.575	0.428
Percent differences (%)	0.69	-0.277	-9.49

Table A. 34 Comparison between Pituitary Gland doses in the original and re-optimized plans for Volunteer 1

Pituitary Gland (Volume: 0.4 cm^3)	Mean dose (Gy)	Maximum dose (Gy)	Minimum dose (Gy)
Original plan	2.084	3.132	1.131
Reoptimized plan	2.318	3.788	1.097
Differences (Gy)	0.234	0.656	-0.034
Percent differences (%)	2.50	1.50	1.16

Volunteer 2

Table A. 35 Comparison between Brain doses in the original and re-optimized plans for Volunteer 2

Brain (Volume: 1287 cm^3)	Mean dose (Gy)	Maximum dose (Gy)	Minimum dose (Gy)
Original plan	0.590	25.315	0.008
Reoptimized plan	0.575	28.959	0.007
Differences (Gy)	-0.015	3.644	-0.001
Percent differences (%)	-2.5	14.39	-13

Table A. 36 Comparison between Brainstem doses in the original and re-optimized plans for Volunteer 2

Brainstem (Volume: 30.8 cm^3)	Mean dose (Gy)	Maximum dose (Gy)	Minimum dose (Gy)
Original plan	0.043	0.081	0.014
Reoptimized plan	0.042	0.080	0.014
Differences (Gy)	-0.001	-0.001	0
Percent differences (%)	-2	-1	0

Table A. 37 Comparison between Chiasm doses in the original and re-optimized plans for Volunteer 2

Chiasm (Volume: 0.2 cm^3)	Mean dose (Gy)	Maximum dose (Gy)	Minimum dose (Gy)
Original plan	0.047	0.054	0.041
Reoptimized plan	0.047	0.053	0.040
Differences (Gy)	0	-0.001	-0.001
Percent differences (%)	0	-2	-2

Table A. 38 Comparison between Left Eye doses in the original and re-optimized plans for Volunteer 2

Left Eye (Volume: 11.8 cm^3)	Mean dose (Gy)	Maximum dose (Gy)	Minimum dose (Gy)
Original plan	0.016	0.025	0
Reoptimized plan	0.016	0.025	0
Differences (Gy)	0	0	0
Percent differences (%)	0	0	0

Table A. 39 Comparison between Right Eye doses in the original and re-optimized plans for Volunteer 2

Right Eye (Volume: 11.8 cm^3)	Mean dose (Gy)	Maximum dose (Gy)	Minimum dose (Gy)
Original plan	0.007	0.022	0
Reoptimized plan	0.007	0.021	0
Differences (Gy)	0	-0.001	0
Percent differences (%)	0	-5	0

Table A. 40 Comparison between Hippocampus doses in the original and re-optimized plans for Volunteer 2

Hippocampus (Volume: 6.4 cm^3)	Mean dose (Gy)	Maximum dose (Gy)	Minimum dose (Gy)
Original plan	0.053	0.092	0.034
Reoptimized plan	0.052	0.089	0.034
Differences (Gy)	-0.001	-0.003	0
Percent differences (%)	-2	-3	0

Table A. 41 Comparison between Left Optic Nerve doses in the original and re-optimized plans for Volunteer 2

Left Optic Nerve (Volume: 0.3 cm^3)	Mean dose (Gy)	Maximum dose (Gy)	Minimum dose (Gy)
Original plan	0.030	0.045	0.018
Reoptimized plan	0.030	0.044	0.018
Differences (Gy)	0	-0.001	0
Percent differences (%)	0	-2	0

Table A. 42 Comparison between Right Optic Nerve doses in the original and re-optimized plans for Volunteer 2

Right Optic Nerve (Volume: 0.3 cm^3)	Mean dose (Gy)	Maximum dose (Gy)	Minimum dose (Gy)
Original plan	0.035	0.048	0.015
Reoptimized plan	0.034	0.047	0.015
Differences (Gy)	-0.001	-0.001	0
Percent differences (%)	-3	-2	0

Table A. 43 Comparison between Pituitary Gland doses in the original and re-optimized plans for Volunteer 2

Pituitary Gland (Volume: 0.4 cm^3)	Mean dose (Gy)	Maximum dose (Gy)	Minimum dose (Gy)
Original plan	0.037	0.05	0.032
Reoptimized plan	0.036	0.05	0.031
Differences (Gy)	-0.001	0	-0.001
Percent differences (%)	-3	0	-3

Volunteer 3

Table A. 44 Comparison between Brain doses in the original and re-optimized plans for Volunteer 3

Brain (Volume: 1208 cm^3)	Mean dose (Gy)	Maximum dose (Gy)	Minimum dose (Gy)
Original plan	0.876	29.947	0.016
Reoptimized plan	1.075	28.745	0.021
Differences (Gy)	0.199	-1.202	0.005
Percent differences (%)	22.7	-4.014	31

Table A. 45 Comparison between Brainstem doses in the original and re-optimized plans for Volunteer 3

Brainstem (Volume: 25.5 cm^3)	Mean dose (Gy)	Maximum dose (Gy)	Minimum dose (Gy)
Original plan	0.057	0.103	0.02
Reoptimized plan	0.071	0.133	0.025
Differences (Gy)	0.014	0.030	0.005
Percent differences (%)	25	29	25

Table A. 46 Comparison between Chiasm doses in the original and re-optimized plans for Volunteer 3

Chiasm (Volume: 0.2 cm^3)	Mean dose (Gy)	Maximum dose (Gy)	Minimum dose (Gy)
Original plan	0.072	0.081	0.063
Reoptimized plan	0.085	0.096	0.075
Differences (Gy)	0.013	0.015	0.012
Percent differences (%)	18	19	19

Table A. 47 Comparison between Left Eye doses in the original and re-optimized plans for Volunteer 3

Left Eye (Volume: 9.4 cm^3)	Mean dose (Gy)	Maximum dose (Gy)	Minimum dose (Gy)
Original plan	0.041	0.063	0
Reoptimized plan	0.044	0.066	0
Differences (Gy)	0.003	0.003	0
Percent differences (%)	7	5	0

Table A. 48 Comparison between Right Eye doses in the original and re-optimized plans for Volunteer 3

Right Eye (Volume: 9.5 cm^3)	Mean dose (Gy)	Maximum dose (Gy)	Minimum dose (Gy)
Original plan	0.041	0.072	0
Reoptimized plan	0.045	0.083	0
Differences (Gy)	0.004	0.011	0
Percent differences (%)	10	15	0

Table A. 49 Comparison between Hippocampus doses in the original and re-optimized plans for Volunteer 3

Hippocampus (Volume: 5.1 cm^3)	Mean dose (Gy)	Maximum dose (Gy)	Minimum dose (Gy)
Original plan	0.077	0.156	0.054
Reoptimized plan	0.096	0.203	0.064
Differences (Gy)	0.019	0.047	0.010
Percent differences (%)	25	30	19

Table A. 50 Comparison between Left Optic Nerve doses in the original and re-optimized plans for Volunteer 3

Left Optic Nerve (Volume: 0.2 cm^3)	Mean dose (Gy)	Maximum dose (Gy)	Minimum dose (Gy)
Original plan	0.057	0.068	0.046
Reoptimized plan	0.064	0.08	0.05
Differences (Gy)	0.007	0.012	0.004
Percent differences (%)	12	18	9

Table A. 51 Comparison between Right Optic Nerve doses in the original and re-optimized plans for Volunteer 3

Right Optic Nerve (Volume: 0.2 cm^3)	Mean dose (Gy)	Maximum dose (Gy)	Minimum dose (Gy)
Original plan	0.054	0.069	0.043
Reoptimized plan	0.062	0.080	0.047
Differences (Gy)	0.008	0.011	0.004
Percent differences (%)	15	16	9

Table A. 52 Comparison between Pituitary Gland doses in the original and re-optimized plans for Volunteer 3

Pituitary Gland (Volume: 0.4 cm^3)	Mean dose (Gy)	Maximum dose (Gy)	Minimum dose (Gy)
Original plan	0.055	0.074	0.049
Reoptimized plan	0.066	0.088	0.059
Differences (Gy)	0.011	0.014	0.010
Percent differences (%)	20	19	20

Volunteer 4

Table A. 53 Comparison between Brain doses in the original and re-optimized plans for Volunteer 4

Brain (Volume: 1246.4 cm^3)	Mean dose (Gy)	Maximum dose (Gy)	Minimum dose (Gy)
Original plan	4.150	29.525	0.075
Reoptimized plan	4.125	29.400	0.075
Differences (Gy)	-0.025	-0.125	0
Percent differences (%)	-0.6	-0.423	0

Table A. 54 Comparison between Brainstem doses in the original and re-optimized plans for Volunteer 4

Brainstem (Volume: 25 cm^3)	Mean dose (Gy)	Maximum dose (Gy)	Minimum dose (Gy)
Original plan	0.475	2.875	0.100
Reoptimized plan	0.475	2.85	0.100
Differences (Gy)	0	-0.025	0
Percent differences (%)	0	-0.9	0

Table A. 55 Comparison between Chiasm doses in the original and re-optimized plans for Volunteer 4

Chiasm (Volume: 0.2 cm^3)	Mean dose (Gy)	Maximum dose (Gy)	Minimum dose (Gy)
Original plan	0.500	0.575	0.400
Reoptimized plan	0.500	0.575	0.400
Differences (Gy)	0	0	0
Percent differences (%)	0	0	0

Table A. 56 Comparison between Left Eye doses in the original and re-optimized plans for Volunteer 4

Left Eye (Volume: 9.9 cm^3)	Mean dose (Gy)	Maximum dose (Gy)	Minimum dose (Gy)
Original plan	0.275	0.475	0
Reoptimized plan	0.275	0.450	0
Differences (Gy)	0	-0.025	0
Percent differences (%)	0	-5	0

Table A. 57 Comparison between Right Eye doses in the original and re-optimized plans for Volunteer 4

Right Eye (Volume: 9.8 cm^3)	Mean dose (Gy)	Maximum dose (Gy)	Minimum dose (Gy)
Original plan	0.200	0.300	0
Reoptimized plan	0.200	0.275	0
Differences (Gy)	0	-0.025	0
Percent differences (%)	0	-8	0

Table A. 58 Comparison between Hippocampus doses in the original and re-optimized plans for Volunteer 4

Hippocampus (Volume: 5.1 cm^3)	Mean dose (Gy)	Maximum dose (Gy)	Minimum dose (Gy)
Original plan	0.775	3.875	0.275
Reoptimized plan	0.775	3.800	0.275
Differences (Gy)	0	-0.075	0
Percent differences (%)	0	-1.94	0

Table A. 59 Comparison between Left Optic Nerve doses in the original and re-optimized plans for Volunteer 4

Left Optic Nerve (Volume: 0.2 cm^3)	Mean dose (Gy)	Maximum dose (Gy)	Minimum dose (Gy)
Original plan	0.400	0.475	0.325
Reoptimized plan	0.400	0.475	0.325
Differences (Gy)	0	0	0
Percent differences (%)	0	0	0

Table A. 60 Comparison between Right Optic Nerve doses in the original and re-optimized plans for Volunteer 4

Right Optic Nerve (Volume: 0.2 cm^3)	Mean dose (Gy)	Maximum dose (Gy)	Minimum dose (Gy)
Original plan	0.325	0.4	0.225
Reoptimized plan	0.300	0.4	0.225
Differences (Gy)	-0.025	0	0
Percent differences (%)	-8	0	0

Table A. 61 Comparison between Pituitary Gland doses in the original and re-optimized plans for Volunteer 4

Pituitary Gland (Volume: 0.4 cm^3)	Mean dose (Gy)	Maximum dose (Gy)	Minimum dose (Gy)
Original plan	0.350	0.475	0.300
Reoptimized plan	0.350	0.475	0.300
Differences (Gy)	0	0	0
Percent differences (%)	0	0	0

Volunteer 5

Table A. 62 Comparison between Brain doses in the original and re-optimized plans for Volunteer 5

Brain (Volume: 1254.9 cm^3)	Mean dose (Gy)	Maximum dose (Gy)	Minimum dose (Gy)
Original plan	4.500	28.325	0.100
Reoptimized plan	4.525	30.000	0.100
Differences (Gy)	0.025	1.675	0
Percent differences (%)	0.6	5.91	0

Table A. 63 Comparison between Brainstem doses in the original and re-optimized plans for Volunteer 5

Brainstem (Volume: 29.6 cm^3)	Mean dose (Gy)	Maximum dose (Gy)	Minimum dose (Gy)
Original plan	0.375	1.650	0.125
Reoptimized plan	0.375	2.075	0.125
Differences (Gy)	0	0.425	0
Percent differences (%)	0	25.8	0

Table A. 64 Comparison between Chiasm doses in the original and re-optimized plans for Volunteer 5

Chiasm (Volume: 0.2 cm^3)	Mean dose (Gy)	Maximum dose (Gy)	Minimum dose (Gy)
Original plan	0.375	0.450	0.325
Reoptimized plan	0.400	0.475	0.350
Differences (Gy)	0.025	0.025	0.025
Percent differences (%)	7	6	8

Table A. 65 Comparison between Left Eye doses in the original and re-optimized plans for Volunteer 5

Left Eye (Volume: 9.6 cm^3)	Mean dose (Gy)	Maximum dose (Gy)	Minimum dose (Gy)
Original plan	0.175	0.250	0
Reoptimized plan	0.425	0.250	0
Differences (Gy)	0.250	0	0
Percent differences (%)	143	0	0

Table A. 66 Comparison between Right Eye doses in the original and re-optimized plans for Volunteer 5

Right Eye (Volume: 9.6 cm^3)	Mean dose (Gy)	Maximum dose (Gy)	Minimum dose (Gy)
Original plan	0.150	0.225	0
Reoptimized plan	0.150	0.225	0
Differences (Gy)	0	0	0
Percent differences (%)	0	0	0

Table A. 67 Comparison between Hippocampus doses in the original and re-optimized plans for Volunteer 5

Hippocampus (Volume: 5.8 cm^3)	Mean dose (Gy)	Maximum dose (Gy)	Minimum dose (Gy)
Original plan	0.575	2.725	0.275
Reoptimized plan	0.675	4.125	0.300
Differences (Gy)	0.100	1.400	0.025
Percent differences (%)	17.4	51.4	9

Table A. 68 Comparison between Left Optic Nerve doses in the original and re-optimized plans for Volunteer 5

Left Optic Nerve (Volume: 0.2 cm^3)	Mean dose (Gy)	Maximum dose (Gy)	Minimum dose (Gy)
Original plan	0.275	0.350	0.200
Reoptimized plan	0.275	0.375	0.200
Differences (Gy)	0	0.025	0
Percent differences (%)	0	7	0

Table A. 69 Comparison between Right Optic Nerve doses in the original and re-optimized plans for Volunteer 5

Right Optic Nerve (Volume: 0.2 cm^3)	Mean dose (Gy)	Maximum dose (Gy)	Minimum dose (Gy)
Original plan	0.250	0.350	0.175
Reoptimized plan	0.275	0.375	0.200
Differences (Gy)	0.025	0.025	0.025
Percent differences (%)	10	7	14

Table A. 70 Comparison between Pituitary Gland doses in the original and re-optimized plans for Volunteer 5

Pituitary Gland (Volume: 0.4 cm^3)	Mean dose (Gy)	Maximum dose (Gy)	Minimum dose (Gy)
Original plan	0.275	0.400	0.250
Reoptimized plan	0.300	0.425	0.275
Differences (Gy)	0.025	0.025	0.025
Percent differences (%)	9	6	10

Volunteer 6

Table A. 71 Comparison between Brain doses in the original and re-optimized plans for Volunteer 6

Brain (Volume: 1254.9 cm^3)	Mean dose (Gy)	Maximum dose (Gy)	Minimum dose (Gy)
Original plan	4.494	28.323	0.111
Reoptimized plan	4.525	30.001	0.107
Differences (Gy)	0.031	1.678	-0.004
Percent differences (%)	0.7	5.92	-4

Table A. 72 Comparison between Brainstem doses in the original and re-optimized plans for Volunteer 6

Brainstem (Volume: 29.6 cm^3)	Mean dose (Gy)	Maximum dose (Gy)	Minimum dose (Gy)
Original plan	0.370	1.653	0.117
Reoptimized plan	0.380	2.084	0.117
Differences (Gy)	0.010	0.431	0
Percent differences (%)	2.7	26.1	0

Table A. 73 Comparison between Chiasm doses in the original and re-optimized plans for Volunteer 6

Chiasm (Volume: 0.2 cm^3)	Mean dose (Gy)	Maximum dose (Gy)	Minimum dose (Gy)
Original plan	0.383	0.448	0.323
Reoptimized plan	0.408	0.472	0.349
Differences (Gy)	0.025	0.024	0.026
Percent differences (%)	7	5	8

Table A. 74 Comparison between Left Eye doses in the original and re-optimized plans for Volunteer 6

Left Eye (Volume: 9.6 cm^3)	Mean dose (Gy)	Maximum dose (Gy)	Minimum dose (Gy)
Original plan	0.168	0.249	0
Reoptimized plan	0.170	0.253	0
Differences (Gy)	0.002	0.004	0
Percent differences (%)	1	2	0

Table A. 75 Comparison between Right Eye doses in the original and re-optimized plans for Volunteer 6

Right Eye (Volume: 9.6 cm^3)	Mean dose (Gy)	Maximum dose (Gy)	Minimum dose (Gy)
Original plan	0.142	0.219	0
Reoptimized plan	0.155	0.222	0
Differences (Gy)	0	0	0
Percent differences (%)	9	1	0

Table A. 76 Comparison between Hippocampus doses in the original and re-optimized plans for Volunteer 6

Hippocampus (Volume: 5.8 cm^3)	Mean dose (Gy)	Maximum dose (Gy)	Minimum dose (Gy)
Original plan	0.586	2.726	0.283
Reoptimized plan	0.683	4.116	0.312
Differences (Gy)	0.097	1.390	0.029
Percent differences (%)	16.6	51.0	10

Table A. 77 Comparison between Left Optic Nerve doses in the original and re-optimized plans for Volunteer 6

Left Optic Nerve (Volume: 0.2 cm^3)	Mean dose (Gy)	Maximum dose (Gy)	Minimum dose (Gy)
Original plan	0.278	0.353	0.202
Reoptimized plan	0.286	0.368	0.204
Differences (Gy)	0.008	0.015	0.002
Percent differences (%)	2.9	4.2	1

Table A. 78 Comparison between Right Optic Nerve doses in the original and re-optimized plans for Volunteer 6

Right Optic Nerve (Volume: 0.2 cm^3)	Mean dose (Gy)	Maximum dose (Gy)	Minimum dose (Gy)
Original plan	0.246	0.343	0.172
Reoptimized plan	0.269	0.370	0.191
Differences (Gy)	0.023	0.027	0.019
Percent differences (%)	9	8	11

Table A. 79 Comparison between Pituitary Gland doses in the original and re-optimized plans for Volunteer 6

Pituitary Gland (Volume: 0.4 cm^3)	Mean dose (Gy)	Maximum dose (Gy)	Minimum dose (Gy)
Original plan	0.284	0.390	0.258
Reoptimized plan	0.298	0.415	0.273
Differences (Gy)	0.014	0.025	0.015
Percent differences (%)	5	6	6

Volunteer 7

Table A. 80 Comparison between Brain doses in the original and re-optimized plans for Volunteer 7

Brain (Volume: 1192.4 cm^3)	Mean dose (Gy)	Maximum dose (Gy)	Minimum dose (Gy)
Original plan	0.771	27.349	0.009
Reoptimized plan	0.786	27.721	0.010
Differences (Gy)	0.015	0.372	0.001
Percent differences (%)	1.9	1.36	11

Table A. 81 Comparison between Brainstem doses in the original and re-optimized plans for Volunteer 7

Brainstem (Volume: 27.3 cm^3)	Mean dose (Gy)	Maximum dose (Gy)	Minimum dose (Gy)
Original plan	0.037	0.068	0.037
Reoptimized plan	0.039	0.07	0.013
Differences (Gy)	0	0	0
Percent differences (%)	5	3	-65

Table A. 82 Comparison between Chiasm doses in the original and re-optimized plans for Volunteer 7

Chiasm (Volume: 0.2 cm^3)	Mean dose (Gy)	Maximum dose (Gy)	Minimum dose (Gy)
Original plan	0.055	0.061	0.049
Reoptimized plan	0.053	0.059	0.047
Differences (Gy)	0	0	0
Percent differences (%)	-4	-3	-4

Table A. 83 Comparison between Left Eye doses in the original and re-optimized plans for Volunteer 7

Left Eye (Volume: 8.8 cm^3)	Mean dose (Gy)	Maximum dose (Gy)	Minimum dose (Gy)
Original plan	0.039	0.057	0
Reoptimized plan	0.039	0.057	0
Differences (Gy)	0	0	0
Percent differences (%)	0	0	0

Table A. 84 Comparison between Right Eye doses in the original and re-optimized plans for Volunteer 7

Right Eye (Volume: 8.7 cm^3)	Mean dose (Gy)	Maximum dose (Gy)	Minimum dose (Gy)
Original plan	0.042	0.061	0
Reoptimized plan	0.034	0.065	0
Differences (Gy)	0	0	0
Percent differences (%)	-19	7	0

Table A. 85 Comparison between Hippocampus doses in the original and re-optimized plans for Volunteer 7

Hippocampus (Volume: 5.5 cm^3)	Mean dose (Gy)	Maximum dose (Gy)	Minimum dose (Gy)
Original plan	0.047	0.064	0.038
Reoptimized plan	0.049	0.071	0.035
Differences (Gy)	0	0	0
Percent differences (%)	16.6	51.0	10

Table A. 86 Comparison between Left Optic Nerve doses in the original and re-optimized plans for Volunteer 7

Left Optic Nerve (Volume: 0.2 cm^3)	Mean dose (Gy)	Maximum dose (Gy)	Minimum dose (Gy)
Original plan	0.046	0.054	0.04
Reoptimized plan	0.046	0.053	0.04
Differences (Gy)	0	0	0
Percent differences (%)	0	-2	0

Table A. 87 Comparison between Right Optic Nerve doses in the original and re-optimized plans for Volunteer 7

Right Optic Nerve (Volume: 0.2 cm^3)	Mean dose (Gy)	Maximum dose (Gy)	Minimum dose (Gy)
Original plan	0.049	0.055	0.043
Reoptimized plan	0.043	0.052	0.034
Differences (Gy)	0	0	0
Percent differences (%)	-12	-5	-21

Table A. 88 Comparison between Pituitary Gland doses in the original and re-optimized plans for Volunteer 7

Pituitary Gland (Volume: 0.4 cm^3)	Mean dose (Gy)	Maximum dose (Gy)	Minimum dose (Gy)
Original plan	0.042	0.056	0.036
Reoptimized plan	0.041	0.054	0.035
Differences (Gy)	0	0	0
Percent differences (%)	-2	-4	-3

Volunteer 8

Table A. 89 Comparison between Brain doses in the original and re-optimized plans for Volunteer 8

Brain (Volume: 1041.5 cm^3)	Mean dose (Gy)	Maximum dose (Gy)	Minimum dose (Gy)
Original plan	1.306	28.442	0.018
Reoptimized plan	1.304	28.322	0.016
Differences (Gy)	-0.002	-0.120	-0.002
Percent differences (%)	-0.2	-0.422	-11

Table A. 90 Comparison between Brainstem doses in the original and re-optimized plans for Volunteer 8

Brainstem (Volume: 23.7 cm^3)	Mean dose (Gy)	Maximum dose (Gy)	Minimum dose (Gy)
Original plan	0.077	0.156	0.031
Reoptimized plan	0.076	0.155	0.031
Differences (Gy)	-0.001	-0.001	0
Percent differences (%)	-1	-1	0

Table A. 91 Comparison between Chiasm doses in the original and re-optimized plans for Volunteer 8

Chiasm (Volume: 0.2 cm^3)	Mean dose (Gy)	Maximum dose (Gy)	Minimum dose (Gy)
Original plan	0.068	0.085	0.053
Reoptimized plan	0.065	0.082	0.051
Differences (Gy)	-0.003	-0.003	-0.002
Percent differences (%)	-4	-4	-4

Table A. 92 Comparison between Left Eye doses in the original and re-optimized plans for Volunteer 8

Left Eye (Volume: 9.1 cm^3)	Mean dose (Gy)	Maximum dose (Gy)	Minimum dose (Gy)
Original plan	0.018	0.034	0.012
Reoptimized plan	0.017	0.032	0.011
Differences (Gy)	-0.001	-0.002	-0.001
Percent differences (%)	-6	-6	-8

Table A. 93 Comparison between Right Eye doses in the original and re-optimized plans for Volunteer 8

Right Eye (Volume: 9.2 cm^3)	Mean dose (Gy)	Maximum dose (Gy)	Minimum dose (Gy)
Original plan	0.023	0.038	0
Reoptimized plan	0.021	0.040	0
Differences (Gy)	-0.002	0.002	0
Percent differences (%)	-9	5	0

Table A. 94 Comparison between Hippocampus doses in the original and re-optimized plans for Volunteer 8

Hippocampus (Volume: 4.8 cm^3)	Mean dose (Gy)	Maximum dose (Gy)	Minimum dose (Gy)
Original plan	0.101	0.207	0.052
Reoptimized plan	0.099	0.207	0.052
Differences (Gy)	-0.002	0	0
Percent differences (%)	-2	0	0

Table A. 95 Comparison between Left Optic Nerve doses in the original and re-optimized plans for Volunteer 8

Left Optic Nerve (Volume: 0.2 cm^3)	Mean dose (Gy)	Maximum dose (Gy)	Minimum dose (Gy)
Original plan	0.036	0.057	0.019
Reoptimized plan	0.035	0.056	0.019
Differences (Gy)	-0.001	-0.001	0
Percent differences (%)	-3	-2	0

Table A. 96 Comparison between Right Optic Nerve doses in the original and re-optimized plans for Volunteer 8

Right Optic Nerve (Volume: 0.2 cm^3)	Mean dose (Gy)	Maximum dose (Gy)	Minimum dose (Gy)
Original plan	0.045	0.064	0.028
Reoptimized plan	0.043	0.062	0.026
Differences (Gy)	-0.002	-0.002	-0.002
Percent differences (%)	-4	-3	-7

Table A. 97 Comparison between Pituitary Gland doses in the original and re-optimized plans for Volunteer 8

Pituitary Gland (Volume: 0.3 cm^3)	Mean dose (Gy)	Maximum dose (Gy)	Minimum dose (Gy)
Original plan	0.054	0.073	0.046
Reoptimized plan	0.052	0.070	0.045
Differences (Gy)	-0.002	-0.003	-0.001
Percent differences (%)	-4	-4	-2

Volunteer 9

Table A. 98 Comparison between Brain doses in the original and re-optimized plans for Volunteer 9

Brain (Volume: 1424.6 cm^3)	Mean dose (Gy)	Maximum dose (Gy)	Minimum dose (Gy)
Original plan	1.313	27.391	0.016
Reoptimized plan	1.230	28.016	0.017
Differences (Gy)	-0.083	0.625	0.001
Percent differences (%)	-6.3	2.282	6

Table A. 99 Comparison between Brainstem doses in the original and re-optimized plans for Volunteer 9

Brainstem (Volume: 26.7 cm^3)	Mean dose (Gy)	Maximum dose (Gy)	Minimum dose (Gy)
Original plan	0.059	0.117	0.018
Reoptimized plan	0.057	0.111	0.018
Differences (Gy)	-0.002	-0.006	0
Percent differences (%)	-3	-5	0

Table A. 100 Comparison between Chiasm doses in the original and re-optimized plans for Volunteer 9

Chiasm (Volume: 0.4 cm^3)	Mean dose (Gy)	Maximum dose (Gy)	Minimum dose (Gy)
Original plan	0.075	0.092	0.057
Reoptimized plan	0.066	0.085	0.046
Differences (Gy)	-0.009	-0.007	-0.011
Percent differences (%)	-12	-8	-19

Table A. 101 Comparison between Left Eye doses in the original and re-optimized plans for Volunteer 9

Left Eye (Volume: 6.8 cm^3)	Mean dose (Gy)	Maximum dose (Gy)	Minimum dose (Gy)
Original plan	0.036	0.053	0
Reoptimized plan	0.032	0.047	0
Differences (Gy)	-0.004	-0.006	0
Percent differences (%)	-11	-11	0

Table A. 102 Comparison between Right Eye doses in the original and re-optimized plans for Volunteer 9

Right Eye (Volume: 9.1 cm^3)	Mean dose (Gy)	Maximum dose (Gy)	Minimum dose (Gy)
Original plan	0.037	0.055	0.010
Reoptimized plan	0.025	0.039	0.014
Differences (Gy)	-0.012	-0.016	0.004
Percent differences (%)	-32	-29	40

Table A. 103 Comparison between Hippocampus doses in the original and re-optimized plans for Volunteer 9

Hippocampus (Volume: 5.1 cm^3)	Mean dose (Gy)	Maximum dose (Gy)	Minimum dose (Gy)
Original plan	0.075	0.103	0.060
Reoptimized plan	0.077	0.106	0.058
Differences (Gy)	0.002	0.003	-0.002
Percent differences (%)	3	3	-3

Table A. 104 Comparison between Left Optic Nerve doses in the original and re-optimized plans for Volunteer 9

Left Optic Nerve (Volume: 0.1 cm^3)	Mean dose (Gy)	Maximum dose (Gy)	Minimum dose (Gy)
Original plan	0.052	0.064	0.044
Reoptimized plan	0.047	0.058	0.039
Differences (Gy)	-0.005	-0.006	-0.005
Percent differences (%)	-10	-9	-11

Table A. 105 Comparison between Right Optic Nerve doses in the original and re-optimized plans for Volunteer 9

Right Optic Nerve (Volume: 0.2 cm^3)	Mean dose (Gy)	Maximum dose (Gy)	Minimum dose (Gy)
Original plan	0.053	0.062	0.044
Reoptimized plan	0.039	0.050	0.029
Differences (Gy)	-0.014	-0.012	-0.015
Percent differences (%)	-26	-19	-34

Volunteer 10

Table A. 106 Comparison between Brain doses in the original and re-optimized plans for Volunteer 10

Brain (Volume: 1268.6 cm^3)	Mean dose (Gy)	Maximum dose (Gy)	Minimum dose (Gy)
Original plan	1.298	29.574	0.028
Reoptimized plan	1.248	29.608	0.027
Differences (Gy)	-0.050	0.034	-0.001
Percent differences (%)	-3.85	0.11	-4

Table A. 107 Comparison between Brainstem doses in the original and re-optimized plans for Volunteer 10

Brainstem (Volume: 29.2 cm^3)	Mean dose (Gy)	Maximum dose (Gy)	Minimum dose (Gy)
Original plan	0.093	0.197	0.031
Reoptimized plan	0.088	0.183	0.029
Differences (Gy)	-0.005	-0.014	-0.002
Percent differences (%)	-5	-7	-6

Table A. 108 Comparison between Chiasm doses in the original and re-optimized plans for Volunteer 10

Chiasm (Volume: 0.3 cm^3)	Mean dose (Gy)	Maximum dose (Gy)	Minimum dose (Gy)
Original plan	0.100	0.119	0.083
Reoptimized plan	0.095	0.113	0.079
Differences (Gy)	-0.005	-0.006	-0.004
Percent differences (%)	-5	-5	-5

Table A. 109 Comparison between Left Eye doses in the original and re-optimized plans for Volunteer 10

Left Eye (Volume: 10.1 cm^3)	Mean dose (Gy)	Maximum dose (Gy)	Minimum dose (Gy)
Original plan	0.041	0.059	0.028
Reoptimized plan	0.035	0.051	0.024
Differences (Gy)	-0.006	-0.008	-0.004
Percent differences (%)	-15	-14	-14

Table A. 110 Comparison between Right Eye doses in the original and re-optimized plans for Volunteer 10

Right Eye (Volume: 9.8 cm^3)	Mean dose (Gy)	Maximum dose (Gy)	Minimum dose (Gy)
Original plan	0.042	0.064	0
Reoptimized plan	0.038	0.056	0
Differences (Gy)	-0.004	-0.008	0
Percent differences (%)	-10	-13	0

Table A. 111 Comparison between Hippocampus doses in the original and re-optimized plans for Volunteer 10

Hippocampus (Volume: 6.9 cm^3)	Mean dose (Gy)	Maximum dose (Gy)	Minimum dose (Gy)
Original plan	0.120	0.201	0.075
Reoptimized plan	0.118	0.194	0.074
Differences (Gy)	-0.002	-0.007	-0.001
Percent differences (%)	-2	-3.5	-1

Table A. 112 Comparison between Left Optic Nerve doses in the original and re-optimized plans for Volunteer 10

Left Optic Nerve (Volume: 0.2 cm^3)	Mean dose (Gy)	Maximum dose (Gy)	Minimum dose (Gy)
Original plan	0.069	0.093	0.047
Reoptimized plan	0.063	0.088	0.041
Differences (Gy)	-0.006	-0.005	-0.006
Percent differences (%)	-9	-5	-13

Table A. 113 Comparison between Right Optic Nerve doses in the original and re-optimized plans for Volunteer 10

Right Optic Nerve (Volume: 0.2 cm^3)	Mean dose (Gy)	Maximum dose (Gy)	Minimum dose (Gy)
Original plan	0.068	0.091	0.051
Reoptimized plan	0.063	0.086	0.045
Differences (Gy)	-0.005	-0.005	-0.006
Percent differences (%)	-7	-5	-12

Table A. 114 Comparison between Pituitary Gland doses in the original and re-optimized plans for Volunteer 10

Pituitary Gland (Volume: 0.5 cm^3)	Mean dose (Gy)	Maximum dose (Gy)	Minimum dose (Gy)
Original plan	0.075	0.104	0.066
Reoptimized plan	0.071	0.099	0.063
Differences (Gy)	-0.004	-0.005	-0.003
Percent differences (%)	-5	-5	-5

Volunteer 11

Table A. 115 Comparison between Brain doses in the original and re-optimized plans for Volunteer 11

Brain (Volume: 1268.6 cm^3)	Mean dose (Gy)	Maximum dose (Gy)	Minimum dose (Gy)
Original plan	0.697	28.162	0.008
Reoptimized plan	0.690	28.372	0.007
Differences (Gy)	-0.007	0.210	-0.001
Percent differences (%)	-1.0	0.75	-13

Table A. 116 Comparison between Brainstem doses in the original and re-optimized plans for Volunteer 11

Brainstem (Volume: 29.2 cm^3)	Mean dose (Gy)	Maximum dose (Gy)	Minimum dose (Gy)
Original plan	0.501	2.078	0.083
Reoptimized plan	0.477	2.317	0.078
Differences (Gy)	-0.024	0.239	-0.005
Percent differences (%)	-5	11.5	-6

Table A. 117 Comparison between Chiasm doses in the original and re-optimized plans for Volunteer 11

Chiasm (Volume: 0.3 cm^3)	Mean dose (Gy)	Maximum dose (Gy)	Minimum dose (Gy)
Original plan	0.521	1.533	0.214
Reoptimized plan	0.508	1.525	0.239
Differences (Gy)	-0.013	-0.008	0.025
Percent differences (%)	-2.5	-0.5	12

Table A. 118 Comparison between Left Eye doses in the original and re-optimized plans for Volunteer 11

Left Eye (Volume: 10.1 cm^3)	Mean dose (Gy)	Maximum dose (Gy)	Minimum dose (Gy)
Original plan	0.296	0.885	0.080
Reoptimized plan	0.277	0.817	0.091
Differences (Gy)	-0.019	-0.068	0.011
Percent differences (%)	-6	-7.7	14

Table A. 119 Comparison between Right Eye doses in the original and re-optimized plans for Volunteer 11

Right Eye (Volume: 9.8 cm^3)	Mean dose (Gy)	Maximum dose (Gy)	Minimum dose (Gy)
Original plan	0.026	0.077	0
Reoptimized plan	0.026	0.075	0
Differences (Gy)	0	-0.002	0
Percent differences (%)	-10	-13	0

Table A. 120 Comparison between Hippocampus doses in the original and re-optimized plans for Volunteer 11

Hippocampus (Volume: 6.9 cm^3)	Mean dose (Gy)	Maximum dose (Gy)	Minimum dose (Gy)
Original plan	0.427	3.407	0.094
Reoptimized plan	0.418	3.535	0.092
Differences (Gy)	-0.009	0.128	-0.002
Percent differences (%)	-2.1	3.76	-2

Table A. 121 Comparison between Left Optic Nerve doses in the original and re-optimized plans for Volunteer 11

Left Optic Nerve (Volume: 0.2 cm^3)	Mean dose (Gy)	Maximum dose (Gy)	Minimum dose (Gy)
Original plan	0.326	0.426	0.257
Reoptimized plan	0.348	0.476	0.263
Differences (Gy)	0.022	0.050	0.006
Percent differences (%)	7	11.7	2.3

Table A. 122 Comparison between Right Optic Nerve doses in the original and re-optimized plans for Volunteer 11

Right Optic Nerve (Volume: 0.2 cm^3)	Mean dose (Gy)	Maximum dose (Gy)	Minimum dose (Gy)
Original plan	0.989	2.075	0.037
Reoptimized plan	1.065	2.111	0.038
Differences (Gy)	0.076	0.036	0.001
Percent differences (%)	7.7	1.7	3

Table A. 123 Comparison between Pituitary Gland doses in the original and re-optimized plans for Volunteer 11

Pituitary Gland (Volume: 0.5 cm^3)	Mean dose (Gy)	Maximum dose (Gy)	Minimum dose (Gy)
Original plan	0.658	2.104	0.147
Reoptimized plan	0.670	2.176	0.330
Differences (Gy)	0.012	0.072	0.183
Percent differences (%)	1.8	3.42	124

Volunteer 12

Table A. 124 Comparison between Brain doses in the original and re-optimized plans for Volunteer 12

Brain (Volume: 1046.5 cm^3)	Mean dose (Gy)	Maximum dose (Gy)	Minimum dose (Gy)
Original plan	0.708	27.917	0.020
Reoptimized plan	0.677	28.844	0.018
Differences (Gy)	-0.031	0.927	-0.002
Percent differences (%)	-4.4	3.321	-10

Table A. 125 Comparison between Brainstem doses in the original and re-optimized plans for Volunteer 12

Brainstem (Volume: 26.2 cm^3)	Mean dose (Gy)	Maximum dose (Gy)	Minimum dose (Gy)
Original plan	0.087	0.429	0.022
Reoptimized plan	0.084	0.454	0.020
Differences (Gy)	-0.003	0.025	-0.002
Percent differences (%)	-3	6	-9

Table A. 126 Comparison between Chiasm doses in the original and re-optimized plans for Volunteer 12

Chiasm (Volume: 0.2 cm^3)	Mean dose (Gy)	Maximum dose (Gy)	Minimum dose (Gy)
Original plan	0.084	0.104	0.067
Reoptimized plan	0.077	0.097	0.062
Differences (Gy)	-0.007	-0.007	-0.005
Percent differences (%)	-8	-7	-7

Table A. 127 Comparison between Left Eye doses in the original and re-optimized plans for Volunteer 12

Left Eye (Volume: 10.3 cm^3)	Mean dose (Gy)	Maximum dose (Gy)	Minimum dose (Gy)
Original plan	0.040	0.069	0
Reoptimized plan	0.039	0.069	0
Differences (Gy)	-0.001	0	0
Percent differences (%)	-3	0	0

Table A. 128 Comparison between Right Eye doses in the original and re-optimized plans for Volunteer 12

Right Eye (Volume: 9.3 cm^3)	Mean dose (Gy)	Maximum dose (Gy)	Minimum dose (Gy)
Original plan	0.036	0.058	0
Reoptimized plan	0.034	0.055	0
Differences (Gy)	-0.002	-0.003	0
Percent differences (%)	-6	-5	0

Table A. 129 Comparison between Hippocampus doses in the original and re-optimized plans for Volunteer 12

Hippocampus (Volume: 6.9 cm^3)	Mean dose (Gy)	Maximum dose (Gy)	Minimum dose (Gy)
Original plan	0.218	1.807	0.055
Reoptimized plan	0.203	1.946	0.050
Differences (Gy)	-0.015	0.139	-0.005
Percent differences (%)	-7	7.7	-9

Table A. 130 Comparison between Left Optic Nerve doses in the original and re-optimized plans for Volunteer 12

Left Optic Nerve (Volume: 0.2 cm^3)	Mean dose (Gy)	Maximum dose (Gy)	Minimum dose (Gy)
Original plan	0.062	0.082	0.047
Reoptimized plan	0.060	0.078	0.045
Differences (Gy)	-0.002	-0.004	-0.002
Percent differences (%)	-3	-5	-4

Table A. 131 Comparison between Right Optic Nerve doses in the original and re-optimized plans for Volunteer 12

Right Optic Nerve (Volume: 0.2 cm^3)	Mean dose (Gy)	Maximum dose (Gy)	Minimum dose (Gy)
Original plan	0.054	0.074	0.041
Reoptimized plan	0.051	0.069	0.038
Differences (Gy)	-0.003	-0.005	-0.003
Percent differences (%)	-6	-7	-7

Table A. 132 Comparison between Pituitary Gland doses in the original and re-optimized plans for Volunteer 12

Pituitary Gland (Volume: 0.5 cm^3)	Mean dose (Gy)	Maximum dose (Gy)	Minimum dose (Gy)
Original plan	0.061	0.084	0.053
Reoptimized plan	0.057	0.078	0.049
Differences (Gy)	-0.004	-0.006	-0.004
Percent differences (%)	-7	-7	-8

Volunteer 13

Table A. 133 Comparison between Brain doses in the original and re-optimized plans for Volunteer 13

Brain (Volume: 1046.5 cm^3)	Mean dose (Gy)	Maximum dose (Gy)	Minimum dose (Gy)
Original plan	0.804	28.338	0.016
Reoptimized plan	0.794	23.038	0.015
Differences (Gy)	-0.010	-5.300	-0.001
Percent differences (%)	-1.2	-18.703	-6

Table A. 134 Comparison between Brainstem doses in the original and re-optimized plans for Volunteer 13

Brainstem (Volume: 26.2 cm^3)	Mean dose (Gy)	Maximum dose (Gy)	Minimum dose (Gy)
Original plan	3.078	14.547	0.113
Reoptimized plan	3.270	16.534	0.111
Differences (Gy)	0.192	1.987	-0.002
Percent differences (%)	6.2	13.66	-2

Table A. 135 Comparison between Chiasm doses in the original and re-optimized plans for Volunteer 13

Chiasm (Volume: 0.2 cm^3)	Mean dose (Gy)	Maximum dose (Gy)	Minimum dose (Gy)
Original plan	2.502	3.904	0.636
Reoptimized plan	1.328	3.048	0.276
Differences (Gy)	-1.174	-0.856	-0.360
Percent differences (%)	-46.92	-21.93	-57

Table A. 136 Comparison between Left Eye doses in the original and re-optimized plans for Volunteer 13

Left Eye (Volume: 10.3 cm^3)	Mean dose (Gy)	Maximum dose (Gy)	Minimum dose (Gy)
Original plan	0.925	2.298	0
Reoptimized plan	0.685	1.737	0
Differences (Gy)	-0.240	-0.561	0
Percent differences (%)	-25.9	-24.41	0

Table A. 137 Comparison between Right Eye doses in the original and re-optimized plans for Volunteer 13

Right Eye (Volume: 9.3 cm^3)	Mean dose (Gy)	Maximum dose (Gy)	Minimum dose (Gy)
Original plan	0.029	0.045	0
Reoptimized plan	0.026	0.040	0
Differences (Gy)	-0.003	-0.005	0
Percent differences (%)	-10	-11	0

Table A. 138 Comparison between Hippocampus doses in the original and re-optimized plans for Volunteer 13

Hippocampus (Volume: 4.5 cm^3)	Mean dose (Gy)	Maximum dose (Gy)	Minimum dose (Gy)
Original plan	1.510	4.663	0.168
Reoptimized plan	1.406	5.009	0.167
Differences (Gy)	-0.104	0.346	-0.001
Percent differences (%)	-6.9	7.4	-1

Table A. 139 Comparison between Left Optic Nerve doses in the original and re-optimized plans for Volunteer 13

Left Optic Nerve (Volume: 0.2 cm^3)	Mean dose (Gy)	Maximum dose (Gy)	Minimum dose (Gy)
Original plan	2.295	4.151	1.375
Reoptimized plan	1.731	2.882	1.058
Differences (Gy)	-0.564	-1.269	-0.317
Percent differences (%)	-24.58	-30.57	-23.1

Table A. 140 Comparison between Right Optic Nerve doses in the original and re-optimized plans for Volunteer 13

Right Optic Nerve (Volume: 0.2 cm^3)	Mean dose (Gy)	Maximum dose (Gy)	Minimum dose (Gy)
Original plan	0.133	0.921	0.037
Reoptimized plan	0.093	0.305	0.033
Differences (Gy)	-0.040	-0.616	-0.004
Percent differences (%)	-30	-66.9	-11

Table A. 141 Comparison between Pituitary Gland doses in the original and re-optimized plans for Volunteer 13

Pituitary Gland (Volume: 0.4 cm^3)	Mean dose (Gy)	Maximum dose (Gy)	Minimum dose (Gy)
Original plan	3.268	4.472	1.117
Reoptimized plan	2.380	3.679	0.552
Differences (Gy)	-0.888	-0.793	-0.565
Percent differences (%)	-27.17	-17.73	-50.6

Volunteer 14

Table A. 142 Comparison between Brain doses in the original and re-optimized plans for Volunteer 14

Brain (Volume: 2891 cm^3)	Mean dose (Gy)	Maximum dose (Gy)	Minimum dose (Gy)
Original plan	0.660	28.816	0
Reoptimized plan	0.658	27.991	0
Differences (Gy)	-0.002	-0.825	0
Percent differences (%)	-0.3	-2.863	0

Table A. 143 Comparison between Brainstem doses in the original and re-optimized plans for Volunteer 14

Brainstem (Volume: 24.8 cm^3)	Mean dose (Gy)	Maximum dose (Gy)	Minimum dose (Gy)
Original plan	0.059	0.112	0.019
Reoptimized plan	0.059	0.111	0.019
Differences (Gy)	0	-0.001	0
Percent differences (%)	0	-1	0

Table A. 144 Comparison between Chiasm doses in the original and re-optimized plans for Volunteer 14

Chiasm (Volume: 0.2 cm^3)	Mean dose (Gy)	Maximum dose (Gy)	Minimum dose (Gy)
Original plan	0.066	0.076	0.056
Reoptimized plan	0.067	0.077	0.056
Differences (Gy)	0.001	0.001	0
Percent differences (%)	2	1	0

Table A. 145 Comparison between Left Eye doses in the original and re-optimized plans for Volunteer 14

Left Eye (Volume: 9.9 cm^3)	Mean dose (Gy)	Maximum dose (Gy)	Minimum dose (Gy)
Original plan	0.029	0.044	0.020
Reoptimized plan	0.030	0.045	0.020
Differences (Gy)	0.001	0.001	0
Percent differences (%)	3	2	0

Table A. 146 Comparison between Right Eye doses in the original and re-optimized plans for Volunteer 14

Right Eye (Volume: 9.1 cm^3)	Mean dose (Gy)	Maximum dose (Gy)	Minimum dose (Gy)
Original plan	0.036	0.053	0.019
Reoptimized plan	0.037	0.055	0.019
Differences (Gy)	0.001	0.002	0
Percent differences (%)	3	4	0

Table A. 147 Comparison between Hippocampus doses in the original and re-optimized plans for Volunteer 14

Hippocampus (Volume: 4.9 cm^3)	Mean dose (Gy)	Maximum dose (Gy)	Minimum dose (Gy)
Original plan	0.077	0.122	0.053
Reoptimized plan	0.076	0.119	0.052
Differences (Gy)	-0.001	-0.003	-0.001
Percent differences (%)	-1	-2	-2

Table A. 148 Comparison between Left Optic Nerve doses in the original and re-optimized plans for Volunteer 14

Left Optic Nerve (Volume: 0.2 cm^3)	Mean dose (Gy)	Maximum dose (Gy)	Minimum dose (Gy)
Original plan	0.045	0.062	0.031
Reoptimized plan	0.046	0.063	0.033
Differences (Gy)	0.001	0.001	0.002
Percent differences (%)	2	2	6

Table A. 149 Comparison between Right Optic Nerve doses in the original and re-optimized plans for Volunteer 14

Right Optic Nerve (Volume: 0.2 cm^3)	Mean dose (Gy)	Maximum dose (Gy)	Minimum dose (Gy)
Original plan	0.050	0.062	0.040
Reoptimized plan	0.051	0.063	0.041
Differences (Gy)	0.001	0.001	0.001
Percent differences (%)	2	2	3

Table A. 150 Comparison between Pituitary Gland doses in the original and re-optimized plans for Volunteer 14

Pituitary Gland (Volume: 0.4 cm^3)	Mean dose (Gy)	Maximum dose (Gy)	Minimum dose (Gy)
Original plan	3.268	4.472	1.117
Reoptimized plan	0.049	0.071	0.043
Differences (Gy)	-3.219	-4.401	-1.074
Percent differences (%)	-98.5	-98.4	-96.2

Volunteer 15

Table A. 151 Comparison between Brain doses in the original and re-optimized plans for Volunteer 15

Brain (Volume: 1131.2 cm^3)	Mean dose (Gy)	Maximum dose (Gy)	Minimum dose (Gy)
Original plan	1.433	27.911	0.025
Reoptimized plan	1.295	27.460	0.021
Differences (Gy)	-0.138	-0.451	-0.004
Percent differences (%)	-9.6	-1.62	-16

Table A. 152 Comparison between Brainstem doses in the original and re-optimized plans for Volunteer 15

Brainstem (Volume: 28 cm^3)	Mean dose (Gy)	Maximum dose (Gy)	Minimum dose (Gy)
Original plan	0.109	0.205	0.047
Reoptimized plan	0.102	0.194	0.046
Differences (Gy)	-0.007	-0.011	-0.001
Percent differences (%)	-6	-5.4	-2

Table A. 153 Comparison between Chiasm doses in the original and re-optimized plans for Volunteer 15

Chiasm (Volume: 0.2 cm^3)	Mean dose (Gy)	Maximum dose (Gy)	Minimum dose (Gy)
Original plan	0.094	0.106	0.079
Reoptimized plan	0.085	0.099	0.072
Differences (Gy)	-0.009	-0.007	-0.007
Percent differences (%)	-9.6	-6.6	-8.9

Table A. 154 Comparison between Left Eye doses in the original and re-optimized plans for Volunteer 15

Left Eye (Volume: 10.5 cm^3)	Mean dose (Gy)	Maximum dose (Gy)	Minimum dose (Gy)
Original plan	0.023	0.039	0.005
Reoptimized plan	0.023	0.036	0.005
Differences (Gy)	0	-0.003	0
Percent differences (%)	0	-8	0

Table A. 155 Comparison between Right Eye doses in the original and re-optimized plans for Volunteer 15

Right Eye (Volume: 9.8 cm^3)	Mean dose (Gy)	Maximum dose (Gy)	Minimum dose (Gy)
Original plan	0.025	0.039	0
Reoptimized plan	0.022	0.036	0
Differences (Gy)	-0.003	-0.003	0
Percent differences (%)	-12	-8	0

Table A. 156 Comparison between Hippocampus doses in the original and re-optimized plans for Volunteer 15

Hippocampus (Volume: 5.2 cm^3)	Mean dose (Gy)	Maximum dose (Gy)	Minimum dose (Gy)
Original plan	0.137	0.251	0.086
Reoptimized plan	0.129	0.244	0.076
Differences (Gy)	-0.008	-0.007	-0.010
Percent differences (%)	-5.8	-2.8	-12

Table A. 157 Comparison between Left Optic Nerve doses in the original and re-optimized plans for Volunteer 15

Left Optic Nerve (Volume: 0.2 cm^3)	Mean dose (Gy)	Maximum dose (Gy)	Minimum dose (Gy)
Original plan	0.056	0.081	0.028
Reoptimized plan	0.050	0.072	0.027
Differences (Gy)	-0.006	-0.009	-0.001
Percent differences (%)	-11	-11	-4

Table A. 158 Comparison between Right Optic Nerve doses in the original and re-optimized plans for Volunteer 15

Right Optic Nerve (Volume: 0.2 cm^3)	Mean dose (Gy)	Maximum dose (Gy)	Minimum dose (Gy)
Original plan	0.060	0.085	0.031
Reoptimized plan	0.055	0.078	0.027
Differences (Gy)	-0.005	-0.007	-0.004
Percent differences (%)	-8	-8	-13

Table A. 159 Comparison between Pituitary Gland doses in the original and re-optimized plans for Volunteer 15

Pituitary Gland (Volume: 0.5 cm^3)	Mean dose (Gy)	Maximum dose (Gy)	Minimum dose (Gy)
Original plan	0.078	0.101	0.069
Reoptimized plan	0.071	0.092	0.063
Differences (Gy)	-0.007	-0.009	-0.006
Percent differences (%)	-9	-8.9	-8.7